FRACTURE MODELING AND FAULT ZONE CHARACTERISTICS APPLIED TO RESERVOIR CHARACTERIZATION OF THE RULISON GAS FIELD, GARFIELD COUNTY, COLORADO

by

Jeffrey W. Jackson

A thesis submitted to the Faculty and Board of Trustees of the Colorado School of Mines in partial fulfillment of the requirements for the degree of Master of Science in Geology.

Golden, Colorado
Date 8/24/2007

Signed: ___________
Jeffrey W. Jackson

Approved: ___________
Dr. Bruce Trudgill
Thesis Advisor

Golden, Colorado
Date 8/27/07

____
Dr. John D. Humphrey
Acting Department Head
Department of Geology
and Geological Engineering

ABSTRACT

Structural modeling is a potentially valuable reservoir characterization tool. A good structural model is grounded in geologic data but incorporates many aspects from other disciplines. This thesis presents a structural model that incorporates geologic well data, three dimensional seismic data, geomechanical analysis, and well production data to characterize the Cretaceous stratigraphic interval of the Rulison Field area in the Piceance Basin of northwestern Colorado. The structural evolution of the Rulison Field was derived from the interpretation of three dimensional seismic. Shale Gouge Ratios along the seismically mapped fault surfaces have been calculated based on available well data. Incorporation of geomechanical stresses allows the dilation tendency of faults and fractures within the field to be calculated and analyzed. The mapped faults and horizons were used to create an elastic dislocation model of the reservoir. This elastic dislocation model yields a 3-D fracture model, which predicts qualitative fracture densities and shear failure types from the known geomechanical properties of the reservoir interval.

Ultimately, this model highlights compartmentalization within key reservoir intervals in the Rulison Field. It also confirms that the fault zones are pathways for fluid migration through their dilation, and that predicted 3-D fractures can be correlated to areas of known fracture production. On a larger scale, the interpreted tectonic history of early Cretaceous extension followed by Laramide aged inversion is a new interpretation of the structural evolution of the Piceance Basin within this important time interval. Thus, the structural model could be used to better optimize drilling locations and

therefore production from within Rulison Field; and therefore, this model clearly shows the benefits of structural modeling and its application to reservoir characterization.

TABLE OF CONTENTS

ABSTRACT iii

LIST OF FIGURES viii

LIST OF TABLES xv

ACKNOWLEDGMENTS xvi

CHAPTER 1 INTROCUCTION 1

1.1 General Introduction 1

1.2 Research Objectives 2

1.3 Previous Work 2

CHAPTER 2 BASIN GEOLOGY 4

2.1 Study Area and Data Set 4

2.2 Regional Stratigraphic Setting 6

2.3 Regional Structural Setting 13

CHAPTER 3 SEISMIC DATA ANALYSIS 19

3.1 Methodology 19

3.2 Seismic Data Analysis Results 21

3.3 Coherency Analysis 27

CHAPTER 4 STRATIGRAPHIC AND WELL LOG ANALYSIS 29

4.1 Methodology 29

4.2 Depth Conversion 32

4.3 Shale Volume Determination and Pseudo-Wells 33

4.4 Shale Gouge Ratio 39

CHAPTER 5 FIELD STRESS ANALYSIS 51
5.1 Methodology 51
5.2 Stress Field Analysis...52
5.3. Dilation Tendency...58
CHAPTER 6 ELASTIC DISCLOCATION MODELING 63
6.1 Methodology 63
6.2 Results..64
6.2.1 Elastic Dislocation Inputs 67
6.2.2 Maximum Coulomb Shear Stress 67
6.2.3 3-D Subseismic Fracture Model and Faults Stress Analysis 70
CHAPTER 7 DISCUSSION...85
7.1 Structural Evolution of the Rulison Field Study Area.....................................85
7.2 Fault Zone Characteristics 93
7.3 Compartmentalization and Fluid Migration..99
7.4 3-D Fracture Model...102
7.5 Hydrocarbon Significance of Study...107
CHAPTER 8 CONCLUSIONS AND RECOMMENDATIONS....................................117
8.1 Conclusions..117
8.2 Recommendations for Future Research..118
REFERENCES 120
APPENDICES 124
APPENDIXA ....CD
APPENDIX B ....CD

APPENDIX C 126

C.1 Nomenclature of the Depth Conversion Equations 126

C.2 Nomenclature of the Volume Shale Equation 126

C.3 Nomenclature of the Shale Gouge Ratio Equation 127

C.4 Nomenclature of the Dilation Tendency Equation 127

LIST OF FIGURES

Figure 2.1 - Location of Piceance Basin in northwest Colorado and the location of Rulison Field within the basin, modified after Jansen, 2005 4

Figure 2.2 - Location of the Seitel (2003) seismic volume (dark blue), as well as the Reservoir Characterization Project Surveys (light blue), the MWX site (red) for reference, and the wells used for stratigraphic modeling 7

Figure 2.3 – Generalized stratigraphic column of the Piceance Basin near Rulison field, modified after Lorenz and Finley (1991)..8

Figure 2.4 – Interpreted paleogeographic settings of the Mancos Shale, Iles Formation and the Williams Fork during the Late Cretaceous. Deposition occurred into an aging Cordilleran Foreland Basin and was controlled by the Sevier Orogenic Belt to the west and the Cretaceous Interior Seaway in the east, from Cumella and Ostby (2003) who modified from Blakey (2003) 9

Figure 2.5 – Location of major structural uplifts that bound the Piceance Basin, modified after Jensen (2005)...13

Figure 2.6 – Locations of major foreland basin features of the Cordillera. The Red box roughly indicates the location of the Piceance Basin, modified from Currie (2002) 15

Figure 2.7 – Anticlines, synclines, and other structural features that are present in the Piceance Basin, from Hoak and Klawitter (1997). The red oval is the location of the study area 16

Figure 2.8 – Illustration of interpreted faults from 2D seismic lines that propagate up from the basement in the eastern and central Piceance Basin, from Hoak and Klawitter (1997)..17

Figure 3.1 – The same seismic line showing the difference between the interpretations viewed at 1:1 and 5:1 scales. The upper left is the 5:1 scale view of line 90 and the bottom is the 1:1 view of line 90. In the 5:1 image the interpreted faults appear to be near vertical while in the 1:1 interpretation the faults have a lower much lower dip angle. However, in the 5:1 the regional structures are easier to see...22

Figure 3.2 – Seismic line 90. This line cuts through the southern end of the survey. Each of the four interpreted horizons is shown as well as the regional fault interpretation. Pink is the UMV Shale, yellow is the Cameo Coal, light blue is the Rollins Sandstone, and light green is the Dakota horizon...23

Figure 3.3 – Seismic trace 120. This trace cuts through the western end of the survey. Each of the four interpreted horizons is shown as well as the regional fault interpretation. Pink is the UMV Shale, yellow is the Cameo Coal, light blue is the Rollins Sandstone, and light green is the Dakota horizon. The dashed lines are projections of the various faults cutting across the data in strike view 24

Figure 3.4 – Time structure map of the Cameo Coal horizon pick. The horizon gently dips to the northeast 25

Figure 3.5 – Rose diagram showing the strikes of the regional faults at each horizon 26

Figure 3.6 – Illustration of the difference between coherent and incoherent seismic wavelets. When the returning expected wavelet is not where it is predicted then the returning wavelets are considered to be incoherent..27

Figure 3.7 – Coherency time slices showing where regional faults are located. The black areas are places where the returning traces are incoherent, while the white areas are where the data is coherent. Continuous linear areas of incoherency are interpreted as faults...28

Figure 4.1 – Map showing what wells were used for determining the depth function used to convert the seismic picks, as well as the wells used in the cross section. Two wells were used in the MWX study area but are so close to each other that they overlap on this map at this scale. Two wells are also not shown on this map because they are several miles outside of the study area...34

Figure 4.2 – Plot of Velocity Average versus depth. Erroneous data were removed and not included in determining the depth conversion function...35

Figure 4.3 – Plot of Time versus Depth. These values came from averaging the different Vav's and Depths for each horizon. Then the averaged Vav for each horizon was converted to time using the average depth for that horizon..36

Figure 4.4 – Pseudo interval creation process was applied to each of the six wells and was used to infer a stratigraphy below the Rollins Sandstone in Rulison 38

Figure 4.5 – Smoothing process applied to the shale volume logs (Vsh) of the six wells. This process preserves intervals of the logs that are dominantly one lithology while it underestimates intervals of rapidly changing lithology. The cutoffs used in assigning lithology type can be seen in Table 4.1. Yellow = sand, orange = shaley sand, and gray = shale 40

Figure 4.6 – A cross section through the study area. Logs shown are the Gamma Ray (GR) the Shale Volume (VSH_JWJ) and the Smoothed Shale Volume (VSH__JWJ_SMOOTHED). Picked tops are shown as well. Colored tops are also mapped in the Seitel (2003) survey. Blue is the UMV Shale Green is the Cameo Coal and Red is the Rollins. Black picks are various stratigraphic markers used for the TrapTester modeling. (see also Figure 4.6a in Appendix A.)..43

Figure 4.7 – Interval from O'Connell F11X-34P well. This interval was attached to each of the six wells in the cross section of Figure 4.6 and 4.6a in Microsoft Excel. (see also Figure 4.7a in Appendix A.) 44

Figure 4.8 – Stratigraphic column that was used for input into TrapTester. See Figure 4.6 and 4.7 for reference to locations of picks in well logs 46

Figure 4.9 – Shale Gouge Ratio (SGR) is a representation of the percent of clay that is in a slipped interval of a fault plane. It is a measure of the thickness of a series of beds and their composition divided by the amount of throw that they have undergone..................47

Figure 4.10 – Shale Gouge Ratio (SGR) along three faults. There are portions of fault C that show the potential to be non sealing faults. These faults also bound the RCP study area. The wells the vertical banded lines with the shale volume log (Vsh) values represented as the bands. The gray surface is the UMV Shale and the blue surface is the Dakota Sandstone...48

Figure 4.11 – Shale Gouge Ratio (SGR) mapped out on all of the fault surfaces. There are areas of low SGR along some fault surfaces, while most of them tend to have higher SGR values. The vertical banded lines are the wells with the shale volume logs (Vsh) values represented as the bands 49

Figure 4.12 – A close up of the RCP study area representing the Shale Gouge Ratio (SGR) along the faults. Also, in the background is a fault that lies to the east of the RCP study area showing the potential to be non-sealing (green areas). The gray surface is the UMV Shale and the vertical banded lines are the wells with the shale volume logs (Vsh) values represented as the bands 50

Figure 5.1 – Minimum horizontal stress magnitudes (σh) from mini fracture tests done at Rulison. The gradient of the best fit line between 5,200 ft to 7,000 ft was used for modeling, image from Higgins (2006)...53

Figure 5.2 – Higgins (2006) modeling results of well RWF 542-20. The gradient used for σV (Overburden) was calculated from the slope of the Overburden line above 55

Figure 5.3 – Pore pressure estimates from mini fracture tests in Rulison. The pore pressure gradient comes from RWF 523-20 which is assumed to be representative for the rest of the wells in the area, from Higgins (2006) 56

Figure 5.4 – This figure shows how the Dilation Tendency (DT) at any point along a fault is calculated from the Mohr diagram, from Badley (2007) 59

Figure 5.5 – Strike view of faults with Dilation Tendency (DT) mapped out on them. There are portions along the faults that show the potential to be dilated. The greater the DT the more likely the fault will allow fluids to flow. These faults also bound the RCP study area. The gray surface is the UMV Shale and the blue surface is the Dakota Sandstone 60

Figure 5.6 – Dilation Tendency (DT) mapped out on all of the fault surfaces. There are areas of high DT along some fault surfaces, while other has low DT values....................61

Figure 5.7 – A close up of the RCP study area representing the Dilation Tendency (DT) along the faults. Also, in the background are faults that lie to the east of the RCP study area. The gray surface is the UMV Shale the blue surface is the Dakota Sandstone 62

Figure 6.1 – Illustration of Allen lines that have been projected from the Rollins Sandstone on to this fault surface. The amount of throw is determined by calculating the vertical separation between the hangingwall and footwall Allen lines.............................65

Figure 6.2 – Plan view of the Cameo Coal horizon (pink). The grid shown is the grid used for the elastic dislocation modeling. The brown planes intersecting the pink Cameo are faults. Each square in the grid is 500 ft by 500 ft. This same grid was used for all of the deformation surfaces 68

Figure 6.3 – Diagram representing how Maximum Coulomb Shear Stress (MCSS) is determined. This diagram also shows the relationship between MCSS, cohesive strength (C), and fracture density. Image modified from Badley, (2006) 69

Figure 6.4 – Top view of the modeled deformation surface at the Cameo Coal depth. The colors mapped out represent the amount of MCSS at that point on the surface. Solid white lines are where the faults cut the surface, dashed white lines are where a fault above or below is deforming the surface with out contacting the surface.........................71

Figure 6.5 – Top view of the modeled deformation surface at the Rollins Sandstone depth. The colors mapped out represent the amount of MCSS at that point on the surface. Solid white lines are where the faults cut the surface, dashed white lines are where a fault above or below is deforming the surface with out contacting the surface.........................72

Figure 6.6 – Top view of the modeled deformation surface at the Dakota Sandstone depth. The colors mapped out represent the amount of MCSS at that point on the surface. Solid white lines are where the faults cut the surface, dashed white lines are where a fault above or below is deforming the surface with out contacting the surface.........................73

Figure 6.7 – A Side view of an arbitrary deformation plane cut through the survey. This view shows the vertical planes deformation caused by the faults. The white lines are where the fault intersects the plane 74

Figure 6.8 – Top view of the modeled deformation surface at the UMV Shale depth. The colors mapped out represent the amount of MCSS at that point on the surface. Solid white lines are where the faults cut the surface, dashed white lines are where a fault above or below is deforming the surface with out contacting the surface 75

Figure 6.9 – Generalized example of how the FaultED module determines compressional and tension orientations from the fault panels 76

Figure 6.10 –Pseudo stress directions and vector attribute explanation. Green arrows are compressional stresses, red arrows are tensional stresses, light green plane is perpendicular to maximum stress direction, and light pink plane is perpendicular to minimum stress direction 77

Figure 6.11 – Top view of the various fracture types generated on the UMV Shale deformation surface. Areas of no color represent areas on the deformation surface where the stresses did not exceed the threshold limit 80

Figure 6.12 – Top view of the various fracture types generated on the Cameo Coal deformation surface. Areas of no color represent areas on the deformation surface where the stresses did not exceed the threshold limit. The white lines are faults 81

Figure 6.13 – Top view of the various fracture types generated on the Rollins Sandstone deformation surface. Areas of no color represent areas on the deformation surface where the stresses did not exceed the threshold limit. The white lines are faults 82

Figure 6.14 – Top view of the various fracture types generated on the Dakota Sandstone deformation surface. Areas of no color represent areas on the deformation surface where the stresses did not exceed the threshold limit. The white lines are faults 83

Figure 6.15 –Side view of the arbitrary plane through the model. Areas of no color represent areas on the deformation surface where the stresses did not exceed the threshold limit. The tan surfaces are faults 84

Figure 7.1 – A simplified representation of the two structural styles that are present in the Seitel (2003) survey 85

Figure 7.2 – Seismic line 90 showing the difference between inversion pop-up blocks as well as normal compressional pop-up blocks 86

Figure 7.3 – Seismic line 90 from Seitel (2003) survey showing the colored interpretation 89

Figure 7.4 –Step evolution through time of line 90 from the Seitel (2003) survey. Dakota Sandstone (Dk.) Williams Fork (W.F.) UMV Shale (UMV) Wasatch (Was.). Pink line in last slide is an unconformity. Red lines are faults 90

Figure 7.5 – Upper left is a top view of the Cameo Coal horizon. Bottom left is a north view of the model. Bottom right and upper right are close ups of the RCP block 92

Figure 7.6 – The Shale Gouge Ratios mapped out on the regional faults. The dark red and orange values indicate a high sealing potential. The green is areas of low sealing potential. The reservoir interval has a high capacity to be sealing with a few areas of potential non sealing or leakage..95

Figure 7.7 – The Shale Gouge Ratios mapped out in the RCP study area. The green areas within the reservoir interval are places where hydrocarbons may leak into the fault zone ... .96

Figure 7.8 – Dilation tendency mapped out on the lower hemisphere of a stereonet........98

Figure 7.9 – Rose diagram of fault strikes at each horizon mapped out on the dilation tendency stereonet hemisphere. The fault orientations suggest that they are dilated 98

Figure 7.10 – Micro seismic results of a hydraulic fracture job completed in well RWF-541-20. Riley (2007) hypothesized that a fault was acting as a barrier to the fractures in the Mesaverde (MV 1 and MV 2), modified from Riley (2007) 100

Figure 7.11 – The gas migration model of Cumella (2006). This model shows gas migrating from deeper in the basin along faults and fractures..101

Figure 7.12 – The Maximum Coulomb Shear Stress (MCSS) at the Cameo deformation surface near the RCP study area. Areas near Fault C have low MCSS values. These low MCSS areas relate to portions of the Fault C that have small throws 103

Figure 7.13 – Maximum Coulomb Shear Stress (MCSS) mapped out on the vertical plane cut through the survey. Deformation from the faults extends out from the various faults. The deformation event extends up to the UMV level where no faults are mapped seismically...104

Figure 7.14 – A view of the RCP study area with the MCSS mapped out on two deformation planes; the vertical plane and the Cameo horizontal plane. This image also shows the 3D halo affect of the deformation around the faults 105

Figure 7.15 – Failure types mapped out on the Cameo deformation plane. The failure planes have strikes similar to that of the faults 108

Figure 7.16 – Failure types mapped out on the vertical deformation plane near the RCP study area. The failure planes have strikes similar to that of the faults 109

Figure 7.17 – Normalized decline curve slope analysis. Curves with two separate slopes are suggestive of natural fracture production. Curves with linear slopes have little to no natural fracture production..112

Figure 7.18 – The Maximum Coulomb Shear Stress (MCSS) at the Cameo deformation surface near the RCP study area mapped out with the four wells used in the decline curve analysis..113

Figure 7.19 – The normalized decline curves with indicators of their respective EUR and MCSS values...114

Figure 7.20 – The Maximum Coulomb Shear Stress (MCSS) at the Cameo deformation surface near the RCP study area and the Estimated Ultimate Recovery (EUR) of wells drilled after 1/1/2000. The EUR is the numerous colored circles. The faults are the thin green lines. High EUR seems to be related to high MCSS..115

LIST OF TABLES

Table 4.1 – Shale volume (Vsh) cutoffs used for each lithology type..............................41

Table 5.1 – Stress Field Editor inputs used in modeling the stresses between the UMV Shale and the Dakota Sandstone, values were derived from Higgins (2006)....................57

Table 5.2 – Rock properties used for modeling between the UMV Shale and the Dakota Sandstone 57

Table 6.1 – The inputs used for each deformation surface. The values came from geomechanical modeling done by Higgins (2006) 66

Table 6.2 – The different total densities used for each deformation surface. The values came from well logs within the RCP study area...66

ACKNOWLEDGMENTS

I would like to thank my advisor Dr. Bruce Trudgill, for his help and support throughout my time as a graduate student. I would also like to thank my committee members, Dr. Tom Davis and Dr. Jennifer Miskimins, for their guidance and ideas. I especially appreciate Dr. Tom Davis allowing me to join up with the Reservoir Characterization Project at the Colorado School of Mines, and allowing me the opportunity to work along side its many gifted students.

I would like to acknowledge the sponsors of the Reservoir Characterization Project for sponsoring me and its many other students, your contributions of, data and guidance have made this thesis possible. I would also like to acknowledge Badley Geoscience Limited for donating the TrapTester software package.

Huge thanks to the many friends that I have acquired over these past few years here at CSM both in Geology, Geophysics, and Petroleum Engineering. There are so many that I can't even begin to name all of you. Special thanks go to my family, especially my mother, for all of their encouragement and praise over these many years.

Finally, I would like to send my thanks to Antero Resources whose financial assistance started this whole journey.

CHAPTER 1

INTRODUCTION

1.1 General Introduction

Unconventional gas plays are fast becoming a dominant source of energy for the United States. In response to this, exploration and production companies have begun to research ways to maximize gas production from these plays and to locate the best locations to drill for them. The tight gas sands of the Piceance Basin have long been known to be a significant source of energy for the United States. Fractures by natural and hydrologic means within the sands are the main source of permeability for the production of gas. Studies by Jansen (2005), Gomez et al. (2003), Cumella and Ostby (2003), Kuuskraa et al. (1997), Lorenz (1997), Hoak and Klawitter (1997), Grout and Verbeek (1992), and Lorenz and Finley (1991) have all tried to gain a better understanding of the way that fractures have controlled the production of gas in these tight gas sands.

This study is meant to complement their work by using conventional 3D seismic data coupled with fault zone properties to interpret the structural evolution of fractures in Rulison and Parachute fields of Western Colorado. This includes a 3-D sub-seismic model of fractures, fault zone properties, and their ability to trap or flow hydrocarbons.

Previous structural work within the field suggests that wrench faulting dominates the subsurface within Rulison field (Kuuskraa et al. 1997), the fault tips being the sweet gas spots within the field. A clearer understanding of how the fractures are distributed around the faults will lead to a more efficient method of production from Rulison Field.

1.2 Research Objectives

This study is intended to improve the understanding of faults and associated natural fracture properties within the Piceance Basin. This work was used to:

1. Create a sub-seismic 3-D fracture model.
2. Attempt to establish a relationship between fractures and the quality of well production.
3. Analyze the potential for fluid movement along faults and into fractures by studying fault zone attributes.
4. Analyze the fault network within the reservoir and understand how it affects the distribution of fractures.
5. Improve fracture prediction within the basin.

1.3 Previous Work

Multiple groups of workers, both those in the government and those in the oil and gas industry, have worked on the Piceance Basin and Rulison field. Below are brief summaries of their work:

Lorenz and Finley (1991) surmised that regional dilational fracturing in the basin is an example of load-parallel extension fracturing from conditions of high pore pressures and anisotropic horizontal stress. Cumella and Ostby (2003) showed the potential for lateral slip as well as normal and reverse movement along faults within the Rulison field.

Grout and Verbeek (1992) determined that in the Wolf Creek and Divide Creek anticlines, fluids moved through the Mesaverde primarily by matrix-dominated flow for the first 20-30 M.Y. after deposition. Later fluid flow occurred through a vertically continuous network of fractures. Hoak and Klawitter (1997) were able to link back fracture anomalies to basement related structures using relatively inexpensive sources of data. Lorenz (1997) studied how different fracture patterns could be present in the Piceance Basin even though a regionally uniform stress has been applied.

Jansen (2005) used 3-D seismic attributes to locate fault patterns within Rulison field and then assigned potential prospect areas along the faults where fracture anomalies might occur. Higgins (2006) used well log data to geomechanically model the stress magnitudes and directions that she saw during various micro-seismic jobs. She was also able to link her models back to various reservoir characteristics. Matesic (2007) used Formation Micro Image (FMI) logs to characterize the structural and stratigraphic features of the fluvial sandstones and shales of the lower Williams Fork Formation. He also looked at different fracture types and their orientations with in the reservoir. Riley (2007) showed that frac jobs had an asymmetric propagation. He proposed that either the sands being hydraulically fractured were not symmetric in shape compared to the location of the well; or there was a fault barrier inhibiting the growth of the hydraulic fracture job.

CHAPTER 2

BASIN GEOLOGY

2.1 Study Area and Data Set

The Piceance Basin is located in northwestern Colorado (Figure 2.1), and the Rulison field lies in the east central portion of the Piceance Basin along Interstate 70, about 8 mi (12.9 km) west of Rifle, Colorado. The field lies within an east to west trend of tight gas sand fields that produce a substantial amount of the total gas produced within the basin (Hemborg, 2000).

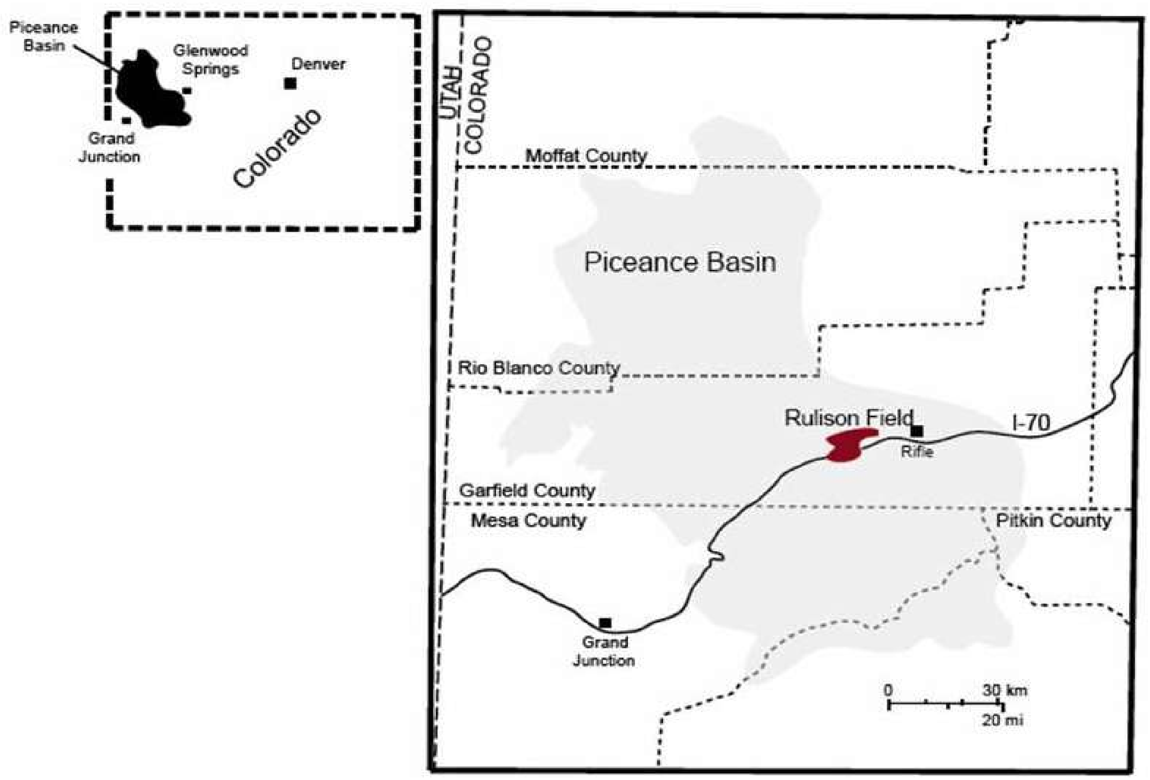

Figure 2.1 - Location of Piceance Basin in northwest Colorado and the location of Rulison Field within the basin, modified after Jansen, 2005.

There are multiple stratigraphic reservoirs that make up Rulison field, both marine and fluvial in origin. The marine reservoirs are relatively flat-lying shoreline and fluvial channel sandstones inter-bedded with various types of shales with a present day dip to the northeast of about 1 to 5 degrees. The sandstones within the reservoir have low permeability (microdarcy scale), and low porosity about 5 to 12 percent. These sands also have relatively high capillary pressures (Hemborg, 2000). The fluvial reservoir is composed of various stacked channel sands, splay sands, and point bar systems. The sands are highly discontinuous and lack connectivity over long distances. These fluvial sands also have low permeability and low porosity. However, it is to a lesser degree of quality then that of the marine sands.

The 3-D data set that will be used for this study was provided to the Reservoir Characterization Project (RCP) at Colorado School of Mines (CSM) by Seitel Data. WesternGeco shot the survey in 2001 with a 110 ft (33.5m) by 110 ft (33.5m) bin size and a 35 fold at full offset range (Jansen, 2005). The survey covers 36 mi^2 (93.2km^2) with a duel source spacing of 220 feet (67.1m) in an east to west orientation and a receiver orientation of north to south. Its location is shown in Figure 2.2. Seitel Data originally processed and interpreted the seismic data. The other 3-D seismic volume used for the study was the multi component time lapse survey shot by the RCP. There have been several additional surveys shot over the RCP study area. They were shot in 2003, 2004, and 2006. The RCP survey was shot with a 55 ft (16.7 m) by 55 ft (16.7 m) bin size (Kusuma, 2005). The survey covers about 2 mi^2 (5.18 km^2) with a source and receiver spacing of 110 feet (33.5 m) and its location is also shown in Figure 2.2. The Seitel survey covers portions of Rulison and Parachute fields.

Several well logs of varying vintages were incorporated into this work. The wells and their locations in the basin in relation to the Seitel data volume and the RCP volume are shown in Figure 2.2. These wells were used for various stratigraphic calculations related to the modeling study.

2.2 Regional Stratigraphic Setting

The Piceance Basin sediments range from Cretaceous to Eocene in age, and are overlain by Tertiary sediments. These basin sediments were deposited in two phases. The first phase of deposition occurred before the Laramide Uplift and is related to the early Cordilleran Foreland Basin system (Currie, 2002). The second phase of sedimentation within the basin occurred during, and subsequently after, the Laramide Uplift. The sediments deposited before the uplift constitute the targeted reservoir intervals for Rulison Field.

The target reservoir sediments were shed from the Sevier Orogenic front into an aging Cordilleran Foreland Basin. The Sevier Orogeny at the time of deposition was located to the west of the Piceance Basin in central Utah. Deposition of the reservoir interval was during the Middle Cretaceous. At this time the Cretaceous Interior Seaway covered most of the area and sediments were deposited in a combination of marine, shoreline, and fluvial environments (Hettinger and Kirschbaum, 2002). The formations of interest in ascending order are the Dakota Sandstone, Mancos Shale, and the Mesaverde Group all of which are Cretaceous in age. These formations can be seen in the generalized stratigraphic column in Figure 2.3.

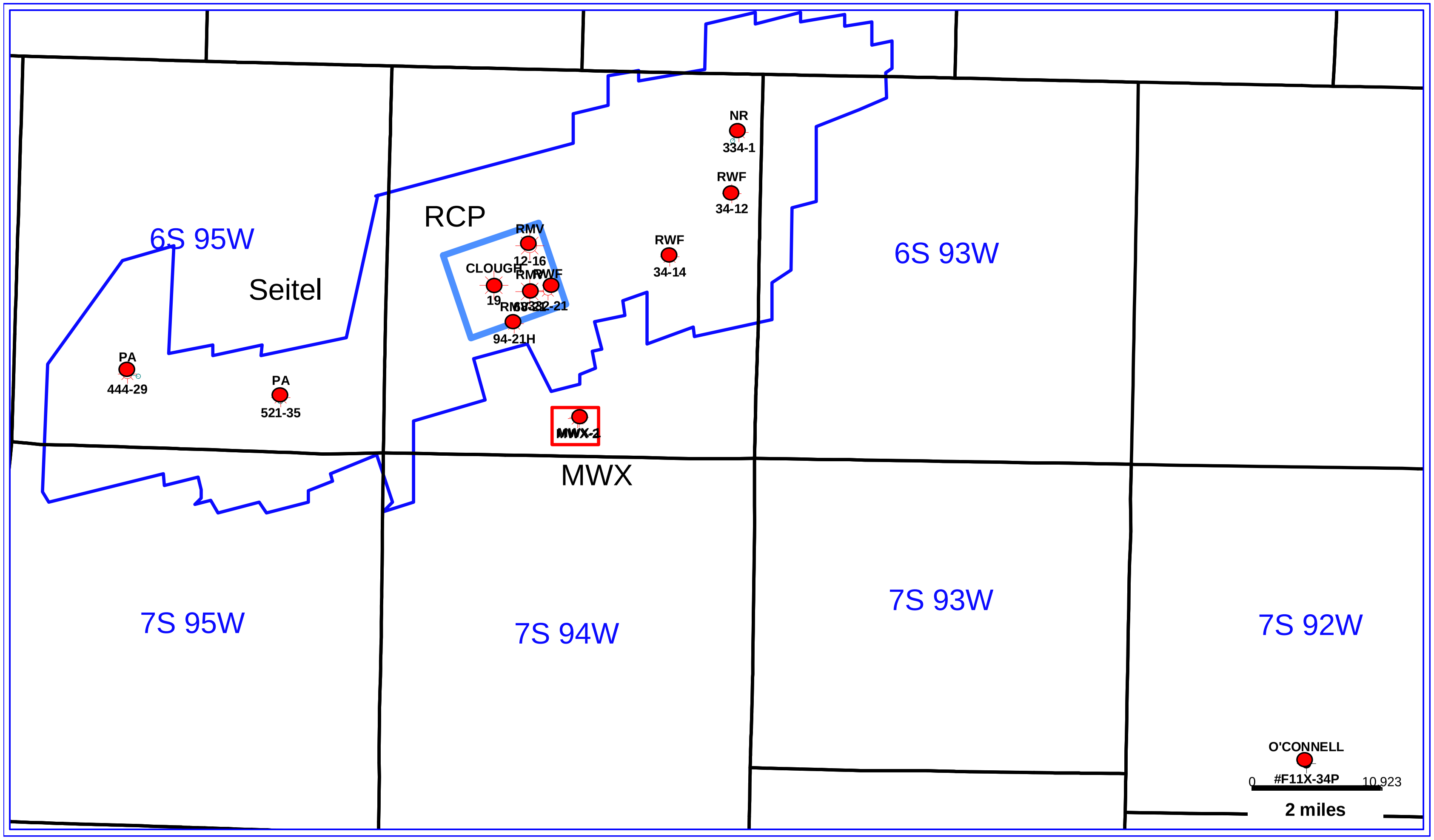

Figure 2.2 - Location of the Seitel (2003) seismic volume (dark blue), as well as the Reservoir Characterization Project Surveys (light blue), the MWX site (red) for reference, and the wells used for stratigraphic modeling.

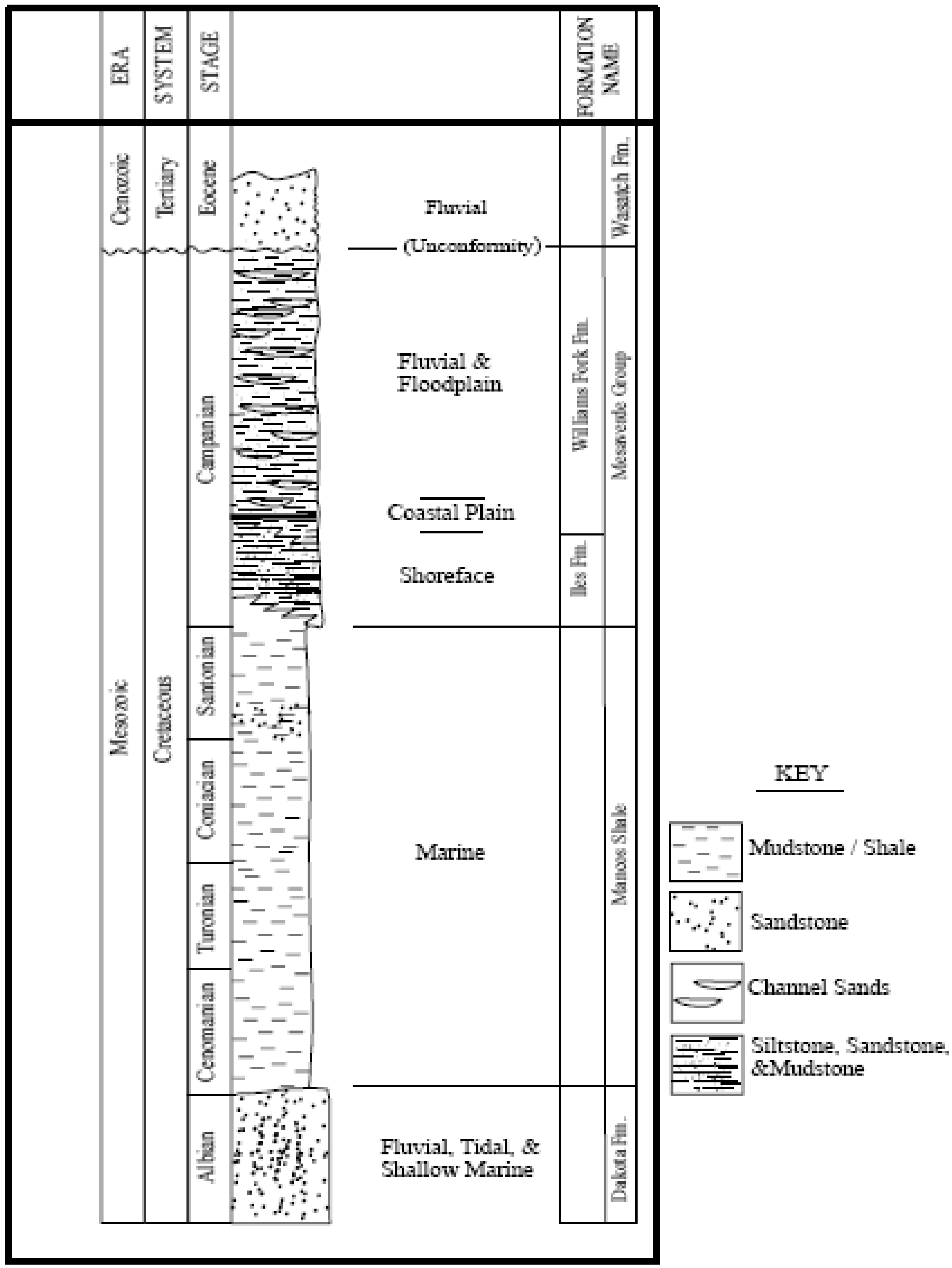

Figure 2.3 – Generalized stratigraphic column of the Piceance Basin near Rulison field, modified after Lorenz and Finley (1991).

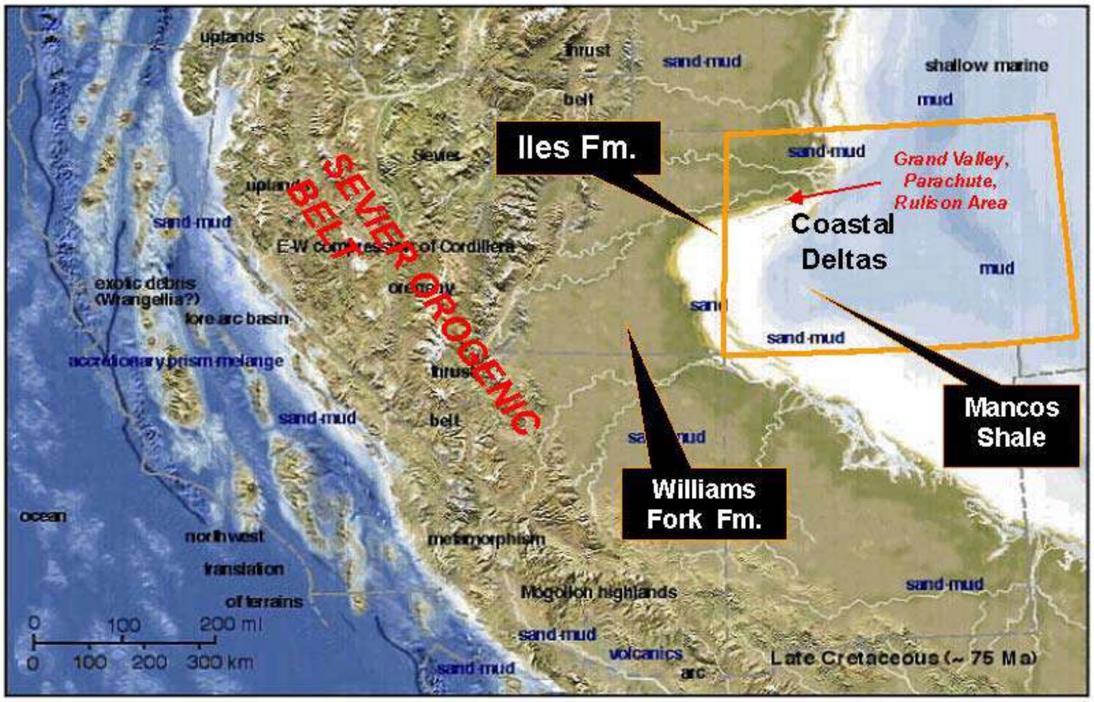

Figure 2.4 – Interpreted paleogeographic settings of the Mancos Shale, Iles Formation and the Williams Fork during the Late Cretaceous. Deposition occurred into an aging Cordilleran Foreland Basin and was controlled by the Sevier Orogenic Belt to the west and the Cretaceous Interior Seaway in the east, from Cumella and Ostby (2003) who modified from Blakey (2003).

The Mesaverde Group in the Piceance Basin consists of the Iles and the Williams Fork formations. Figure 2.4 shows Cumella and Ostby (2003) interpretation of the paleogeographic setting of each of the following formations, excluding the Dakota Sandstone.

The Dakota Sandstone Formation (Dakota) is composed of sandstones, conglomerates, and mudstones that were deposited in a combination of fluvial, tidal, and shallow marine systems (Ryer et al., 1987; Currie, 2002). These deposits were deposited in the Cordilleran Foreland Basin system (Currie, 2002). The Dakota crops out in various places in Utah and western Colorado, and can be characterized into two distinctive units. The lower portion of the Dakota was deposited in valleys that were incised into the underlying Cedar Mountain Formation (Ryer et al.; 1987, Currie, 2002). These deposits are dominantly fluvial in origin. The upper unit of the Dakota incises into the lower portion of the Dakota. Currie (2002), discusses how the Dakota is composed of alluvial, fluvial, and tidal deposits that consist of sandstones, mudstones, and conglomerates. The Dakota for this study is the lowest unit of interest and is the deepest mapped horizon in the seismic survey. There are other sandstones and mudstones below but they are not important for the Rulison area.

The Mancos Shale Formation (Mancos) is a very widespread formation that was deposited during the Late Cretaceous into the aging Cordilleran Foreland Basin. It is dominated by offshore and open marine mudrocks deposited in the Cretaceous Interior Seaway, Figure 2.4. Exposures in the southern Piceance Basin are 3,450 to 4,150 ft (1,051 to 1,264 m) thick (Hettinger and Kirschbaum 2002). While the Mancos is dominated by mudstones, there is a predominate hydrocarbon producing unit within the middle of the formation that has been documented by several authors, Kellogg, (1977), Cole et al (1997), and Hettinger and Kirschbaum, (2002), as the Mancos B Formation. These authors have described the Mancos B as being composed of thinly bedded and laminated fine grained siltstones and claystones. This unit is thought to be a prograding fore slope sets within the open marine environment of the Cretaceous Interior Seaway (Kellogg, 1977).

The Mesaverde Group lies conformably on top of the Mancos and is composed of two formations, the Iles Formation and the Williams Fork Formation. With the lower part of the Iles being a time transgressive contact with the interfingering of the members with the Mancos. Each of these formations is briefly described below.

The Iles Formation (Iles) is composed of three members known as the Corcoran, Cozzette and Rollins Sandstone Members. These sandstones are fine grained to coarse grained progradational shoreface deposits. Each of these members is separated by tongues of the Mancos Shale (Hettinger and Kirschbaum, 2002). These sandstones are believed to be marine regressive cycles of the Mancos Shale (Johnson, 1989) and range in thicknesses of 100 to 230 ft (30 to 70 m) each. These sandstones were deposited on the shoreline of the Cretaceous Interior Seaway (Hettinger and Kirschbaum 2002, Cumella and Ostby, 2003), (Figure 2.4). For this study the Rollins Sandstone Member (Rollins) is the main focus. This sandstone was singled out because it is the uppermost sand deposit that represents a change between a marine dominated environments and terrestrially dominated environments. Johnson (1989) and Hettinger and Kirschbaum, (2002), discuss the trend of the different members regressive shoreline limits and their lateral extents.

The Williams Fork Formation (Williams Fork) is composed of two distinct units. They are the lower costal plain deltaic deposits and upper more fluvial dominated deposits. The lower coastal plain deposits are locally known as the Cameo-Wheeler Coal Zone (Cameo). They consist of 50 to 450 ft (15 to 137 m) of fine grained sands and silts inter mixed with several thick mappable coals that overlie and intertounge with the Rollins Sandstone (Hettinger and Kirschbaum, 2002). These sandstones are considered by Cumella and Ostby (2003) to be point bar deposits from meandering streams. Several authors, Cumella and Ostby (2003), Cumella (2006), and Johnson (1989), also believe that the coals are the dominant source for the gas found in the Piceance Basin. Above the Cameo lies the fluvial portion of the Williams Fork. The lower and middle portions of this appear to be meandering point bar stream deposits that represent an overall increase in the gradient of the costal plain (Cumella and Ostby, 2003, Tayler et al, 1996). This would have changed the environment from dominantly coal bearing to more fluvial. These point bar sands are highly discontinuous. Within the upper part of the fluvial deposits in the Williams Fork are laterally extensive thick sandstones that are thought to be braided stream deposits. However, they are not well understood (Cumella and Ostby, 2003)

2.3 Regional Structural Setting

The current structural orientation of the Piceance Basin is a northwest to southeast trending basin of Late Cretaceous age that covers 6,000 mi^2 (15,540 km^2). The basin is asymmetrical with a sharply upturned eastern flank and a gently dipping western flank (Johnson, 1989), see Figure 2.5. To the east is the thrust fault of the Grand Hogback the western extent of the White River Uplift. The north is bounded by the Uinta Mountain Uplift and the Axial Basin Anticline. The basin is bounded along its western edge by the Douglas Creek Arch; this arch also separates the Piceance Creek basin from the Uinta basin. Lastly, the southern boundaries are the Gunnison, Uncompahgre, and Sawatch Uplifts. The current basin geometry is that of a Laramide structural basin bounded on all sides by basement-involved tectonic structures. Most of these features have undergone multiple periods of deformation from Precambrian through Neogene time (Hemborg, 2000). Within the basin lie many anticlines and synclines that all have a northwest to southeast trend.

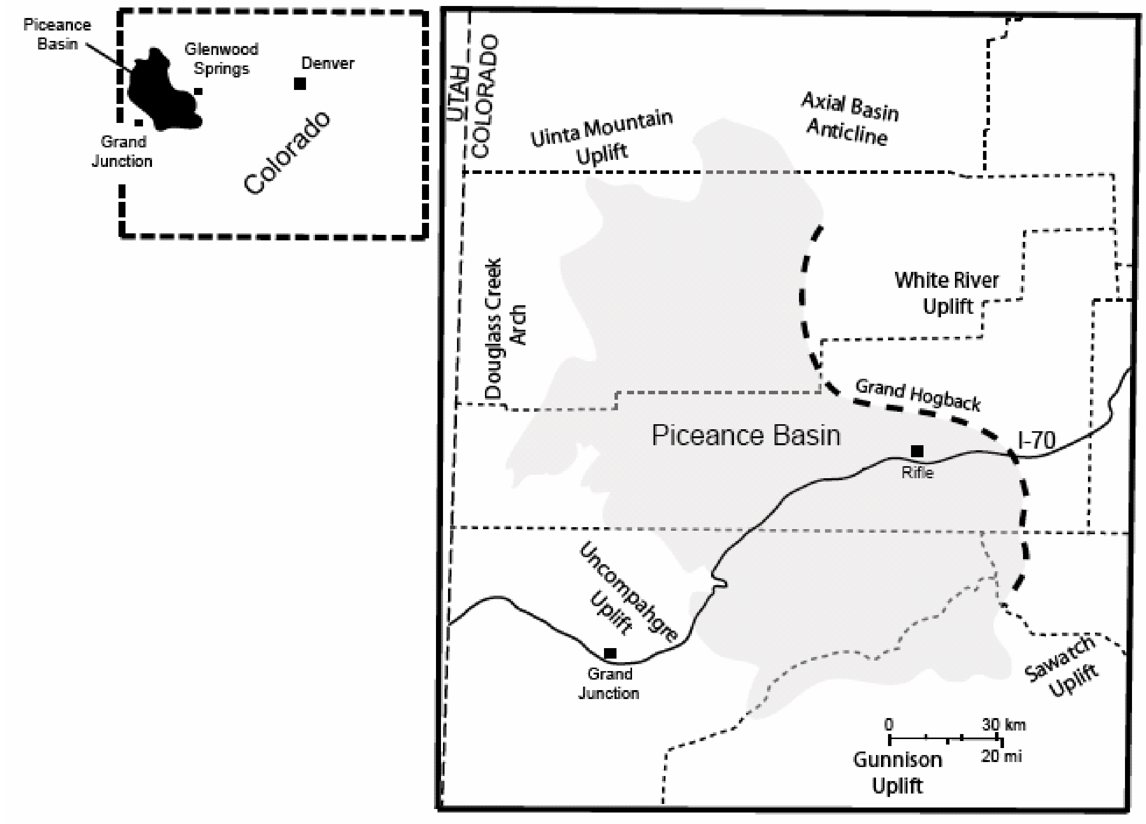

Figure 2.5 – Location of major structural uplifts that bound the Piceance Basin, modified after Jensen (2005).

The structural history of the Piceance Basin is very diverse. Kuuskraa et al (1997) discuss the entire structural history of the Piceance Basin area in detail. However, in relation to the reservoir interval, as well as for this study, the basin's structural history can be broken into two distinct phases. This structural history includes a foreland basin phase followed by an east-west compressional phase. These structural phases have been discussed separately buy several authors (Hoak and Klawitter (1997), Picha (1986), Cumella and Ostby (2003), Currie (2002)). These authors as well as this author believe that the current structural features within the basin have been influenced by deeper preexisting features.

The foreland basin structural phase is important because this controlled most of the reservoir deposition within the intervals. In the early Cretaceous a major thrust belt was located in what are now California, Nevada, and east-central Utah. This structural zone was known as the Cordillera Jurassic-Cretaceous aged compressional tectonic feature. It was bounded on its western margin by a subduction zone and on its eastern margin by the Sevier Thrust Belt. This major zone of crustal thickening created an additional load on the crust. This loading created a flexural foreland basin that covered most of Montana, Wyoming, Colorado, Eastern Utah, and parts of Arizona and New Mexico. Development of this foreland basin has been attributed to thrust load-generated flexural subsidence associated with deformation in the Sevier Thrust Belt region as discussed by Currie (2002). While this foreland basin's foredeep was close to the Sevier Thrust Belt, Currie (2002) suggests that reactivation of preexisting structures was too subtle and did not control the foreland basins structural architecture or the deposition of sediments into the basin at the time. Figure 2.6 shows estimates by Currie (2002) of where the foredeep, forebuldge and back bulge were located. As tectonic activity increased during the Campanian stage, the Sevier Thrust Belt migrated eastward (Johnson, 1989).

The second structural phase occurred in the Late Cretaceous. This phase is the Laramide Uplift or the Laramide Orogeny. The Laramide Uplift dissected the aging foreland basin into many smaller basins. This deformation was dominantly controlled by deeper basement features. The current structural features we see across most of the western United States owe their existence to the Laramide Uplift. This uplift is commonly thought to have occurred during the Late Cretaceous (90-65ma) and was caused by low angle or flat subduction of the Farallon Plate to the west (Johnson et al, 2004). This created east-west compressional forces across most of the western United States.

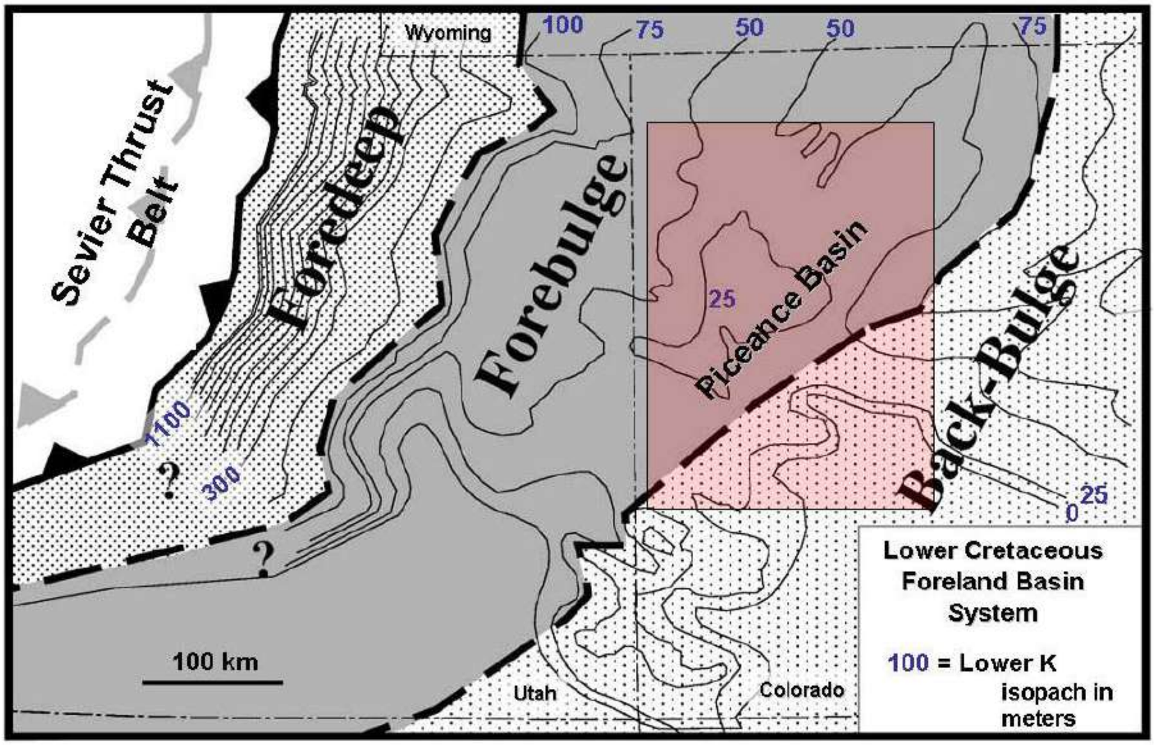

Figure 2.6 – Locations of major foreland basin features of the Cordillera. The Red box roughly indicates the location of the Piceance Basin, modified from Currie (2002).

Today many of the prolific gas basins of the western United States were formed by the east-west compression of the Laramide dissecting the former foreland basin. Locally two of them are the Uinta Basin in eastern Utah and the Piceance Basin of western Colorado. Before Laramide tectonics these basins comprised one larger depocenter.

The Piceance Basin is bounded by Laramide features, as shown in Figure 2.5. Many Laramide features also lie within the basin itself, (Figure 2.7). Many of these features can be directly linked to preexisting deeper level structures in the basin.

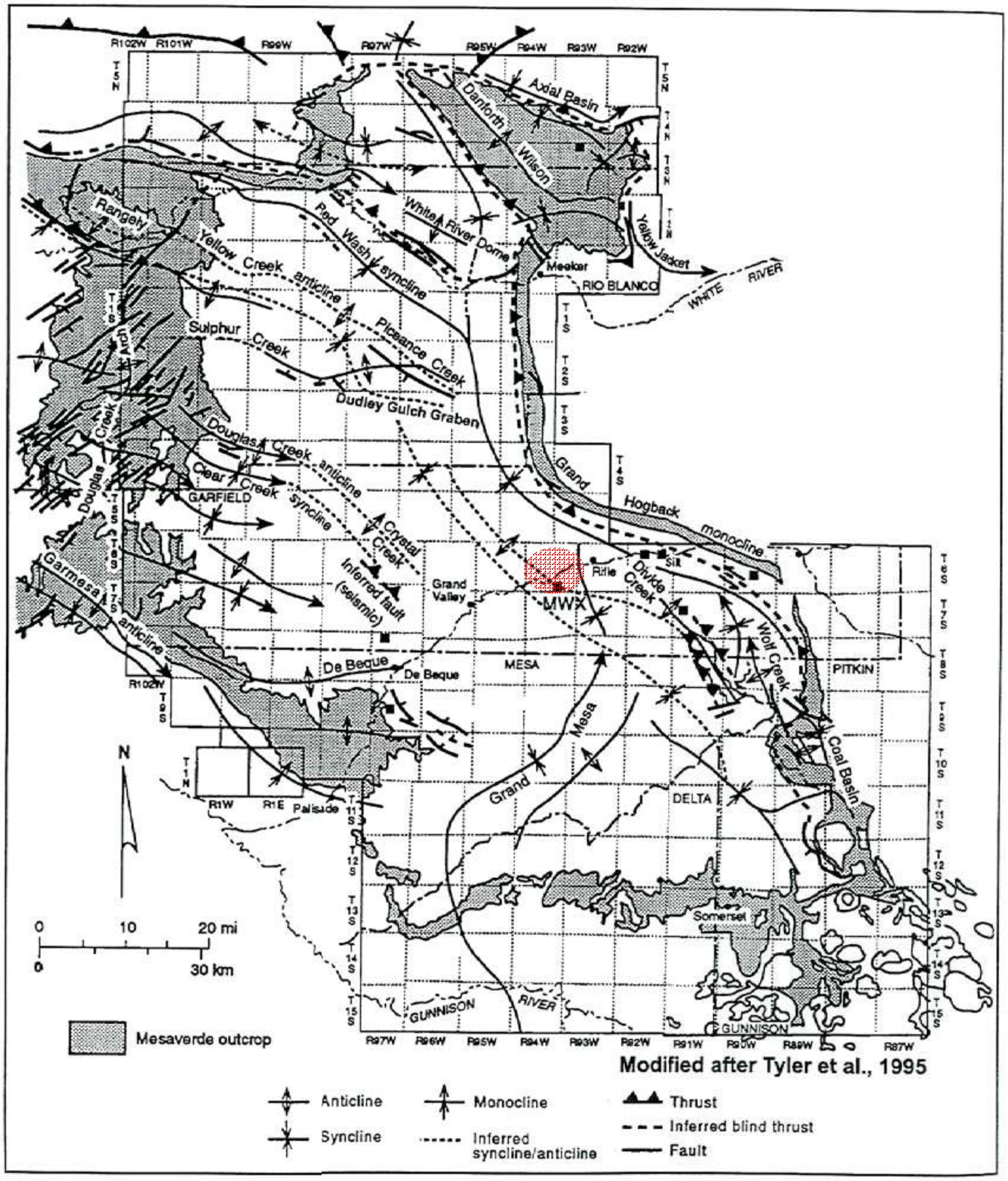

Figure 2.7 – Anticlines, synclines, and other structural features that are present in the Piceance Basin, from Hoak and Klawitter (1997). The red oval is the location of the study area.

Hoak and Klawitter (1997) illustrate a direct relationship between the deep basement structures and fracture and fault distribution within the Mesaverde Group. They accomplished this by looking at parallelism between production contours, shallower subsurface structures, and the basement-fault orientation (Matesic, 2007). Cumella and Ostby (2003) also discuss how production from the low-permeability sands within the Mesaverde Group is enhanced by natural fractures. Matesic (2007) as well as Hoak and Klawitter (1997), have remarked on how their interpreted faults tend to propagate up from the basement and terminate seismically in the lower Williams Fork Formation. Figure 2.8 is the Hoak and Klawitter (1997) interpretation of this phenomenon from 2D seismic lines. These faults have an increasing complexity as they travel up through the section (Matesic, 2007); these complexities include backthrusts, thrusts, and reverse faults. Many of the shallower faults have a northwest trending strike which matches many of the deeper pre-Laramide structural features of the basin.

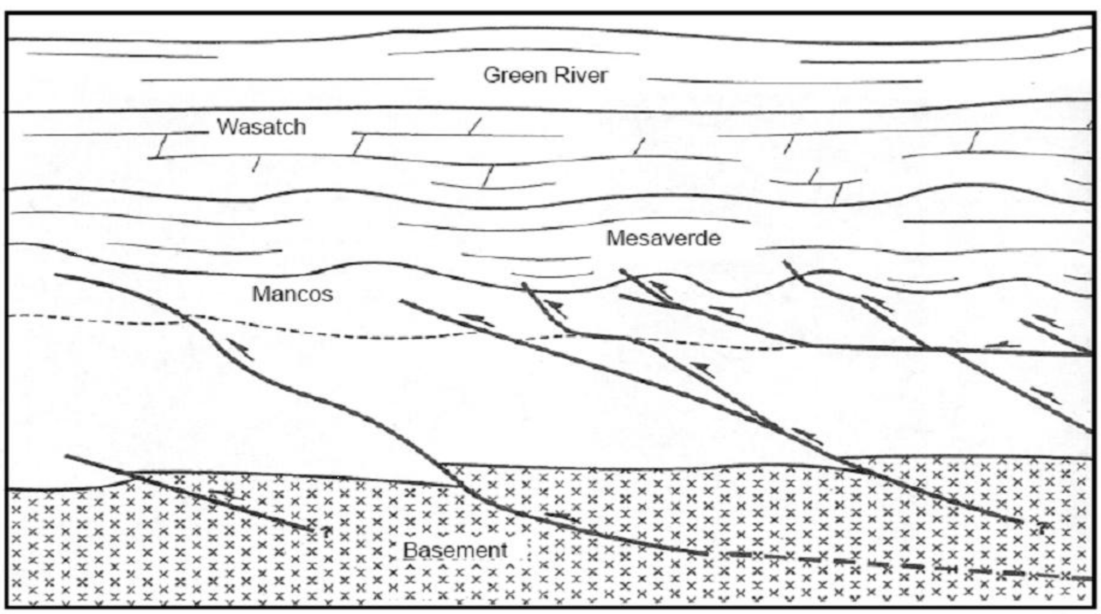

Figure 2.8 – Illustration of interpreted faults from 2D seismic lines that propagate up from the basement in the eastern and central Piceance Basin, from Hoak and Klawitter (1997).

Cumella and Ostby (2003) interpreted these shallow complex zones of faults to have a distinguishable component of left lateral movement on them. They proposed from their interpretation of the Seitel (2003) seismic volume that the east-west compression produced left lateral movement along preexisting northwest trending faults. They also interpreted reverse movement on many of their interpreted faults. These two components would suggest a wrenching faulting style. A study by Matesic (2007) with Formation Micro Image (FMI) logs also suggests that there was left lateral slip along faults.

CHAPTER 3

SEISMIC DATA ANALYSIS

3.1 Methodology

The Seitel (2003) 3D seismic volume has been interpreted for a variety of studies. Most of these analyses have been undertaken in order to better understand the faulting style present in the Rulison area. Cumella and Ostby (2003) used the seismic volume to interpret the geology around the reservoir interval. Jansen (2005) used the volume as a dataset to test the feasibility of using software to interpret the seismic volumes in the Rulison Field and the Piceance Basin. However, it has been noted by these authors, as well as in this study that the Seitel (2003) seismic volume is difficult to interpret, and this is especially true over the reservoir interval. This is one reason why the RCP group proposed using multi-component seismic instead of regular p-wave seismic to better clarify the reservoir interval.

The focus of this study was to interpret the Seitel (2003) 3D volume focusing on the structural geometry and in particular the regional scale geologic features. These features are the underlying control on the reservoir scale variations. The goal for the seismic analysis was to create surfaces that represented the geology of Rulison Field for input into the TrapTester software for analysis of the fault fracture networks.

The first step in the seismic analysis was to map out the horizons across the volume. Four horizons were mapped; the Dakota, Rollins, Cameo, and the UMV Shale. These horizons were chosen based on their lateral continuity as well as their relation to the reservoir interval. The Dakota is considered this structural studies basement as well as the deepest potential sand in this area. The Rollins was picked because it marks the separation between marine and fluvial systems. The Cameo lies within the basal part of the reservoir interval and is considered the source of gas in the reservoir (Cumella and Ostby, 2003). The Cameo is also easily distinguished because of its seismic reflection characteristics. The UMV Shale was picked because it is an easily distinguishable marker bed within the upper Williams Fork and represents the upper extent of the reservoir.

The second step was to interpret regional scale faults. The fault interpretation was difficult within the reservoir interval because of the lack of continuous reflectors. To aid in interpreting the faults a coherency volume was created. During the fault interpretation the various horizon picks were updated based on their fault interactions. My interpretation is completely on the Seitel (2003) volume at a 1:1 scale. I used the RCP data volumes for reference when it came to looking at faults interpreted by other RCP students. Fault picks from other students were also incorporated into my interpretation. (L. LaBarre, 2006, personal communication) showed me where her small scale faults were located at from the RCP surveys. I then tied these faults back to my regional fault interpretation.

After the seismic interpretation step the four horizons and faults were exported. The exported files were in time and needed to be converted to depth for use in TrapTester. The conversion from time to depth is discussed in Chapter 4.2.1. The raw output horizons and surfaces interpreted in Landmark can be found in Appendix B.

3.2 Seismic Data Analysis Results

The Seitel (2003) data volume was scaled close to 1:1 (vertical : horizontal) for the interpretation. The 1:1 ratio was calculated from the vertical thickness of the interval between the UMV Shale and the Cameo in Clough 19 well. When this thickness closely matched the horizontal distance on the seismic the 1:1 ratio was obtained. While the survey is still in time this method allowed me to interpret the seismic at a close to true geologic representation. Figure 3.1 (see also Figure 3.1a in Appendix A) show the difference between interpreting at 1:1 scale and interpreting the seismic at five times vertically exaggerated or a 5:1 scale. While it is easier to see the continuity of the faults from the basement, the faults needed to be double checked on a 1:1 scale.

Figures 3.2 and 3.3 and (see also Figures 3.2a and 3.3a in Appendix A) show a line and a trace through the survey. On each of the seismic lines the four horizons picked are visible as well as the interpreted faults that cross those lines. The data show that there are portions within the seismic that are very difficult to interpret. Figure 3.4, is a time structure map on the Cameo, which shows that the horizon dips gently to the northeast. This gently dipping northeast trend can also be seen in the other horizons.

The interpreted faults have a northwest-southeast strike, (Figure 3.5). The movement on the faults is dominantly in a reverse sense. Lateral movement cannot be determined to a sufficient degree with this data set. The amount of throw on the faults is also difficult to determine. However, it ranges from tens of feet to a few hundred feet for the largest faults. While most of the faults appear to be located within specific intervals two of the larger faults have been interpreted to propagate up from deeper levels.

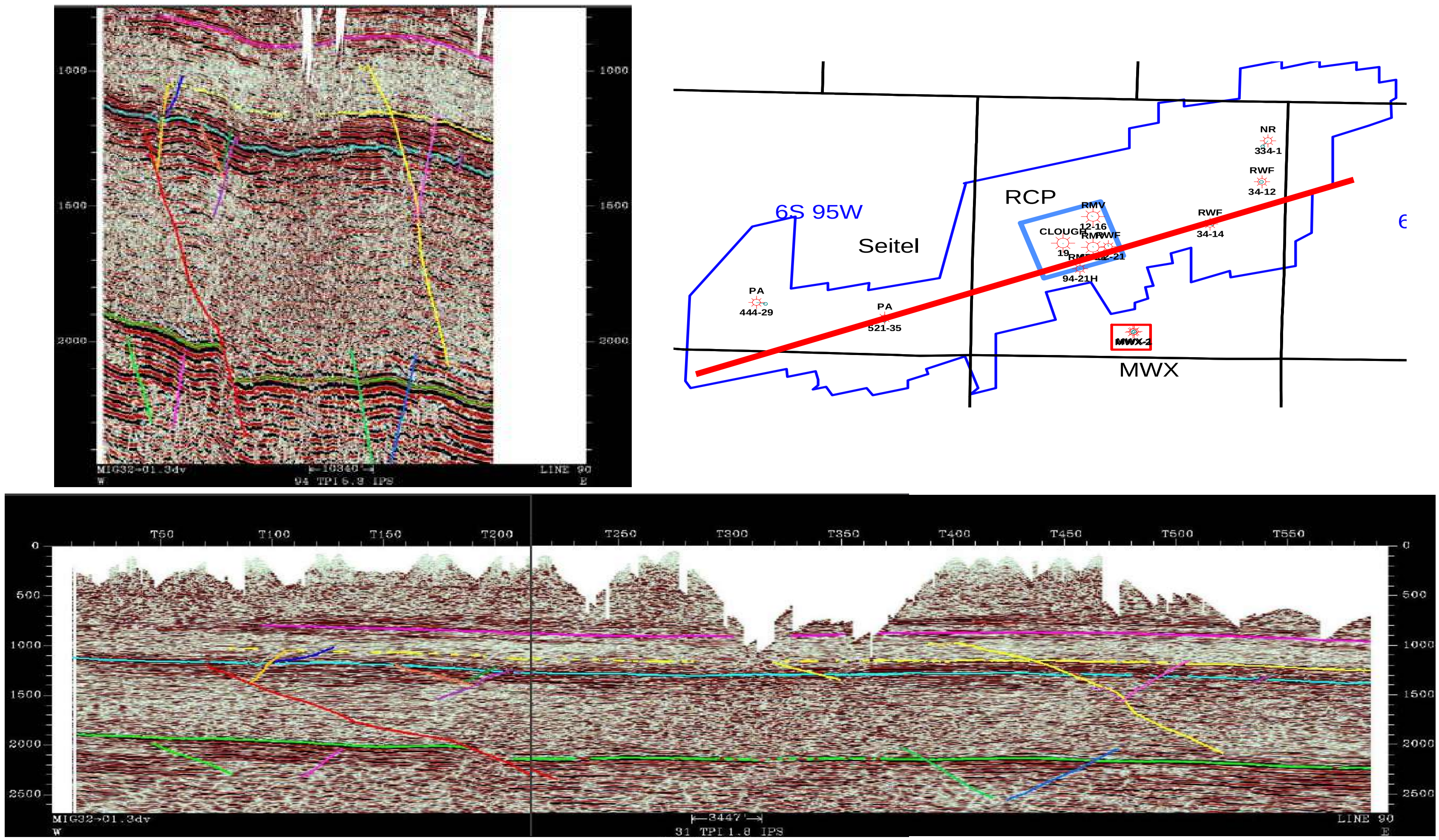

Figure 3.1 – The same seismic line showing the difference between the interpretations viewed at 1:1 and 5:1 scales. The upper left is the 5:1 scale view of line 90 and the bottom is the 1:1 view of line 90. In the 5:1 image the interpreted faults appear to be near vertical while in the 1:1 interpretation the faults have a lower much lower dip angle. However, in the 5:1 the regional structures are easier to see. (see also Figure 3.1a in Appendix A.)

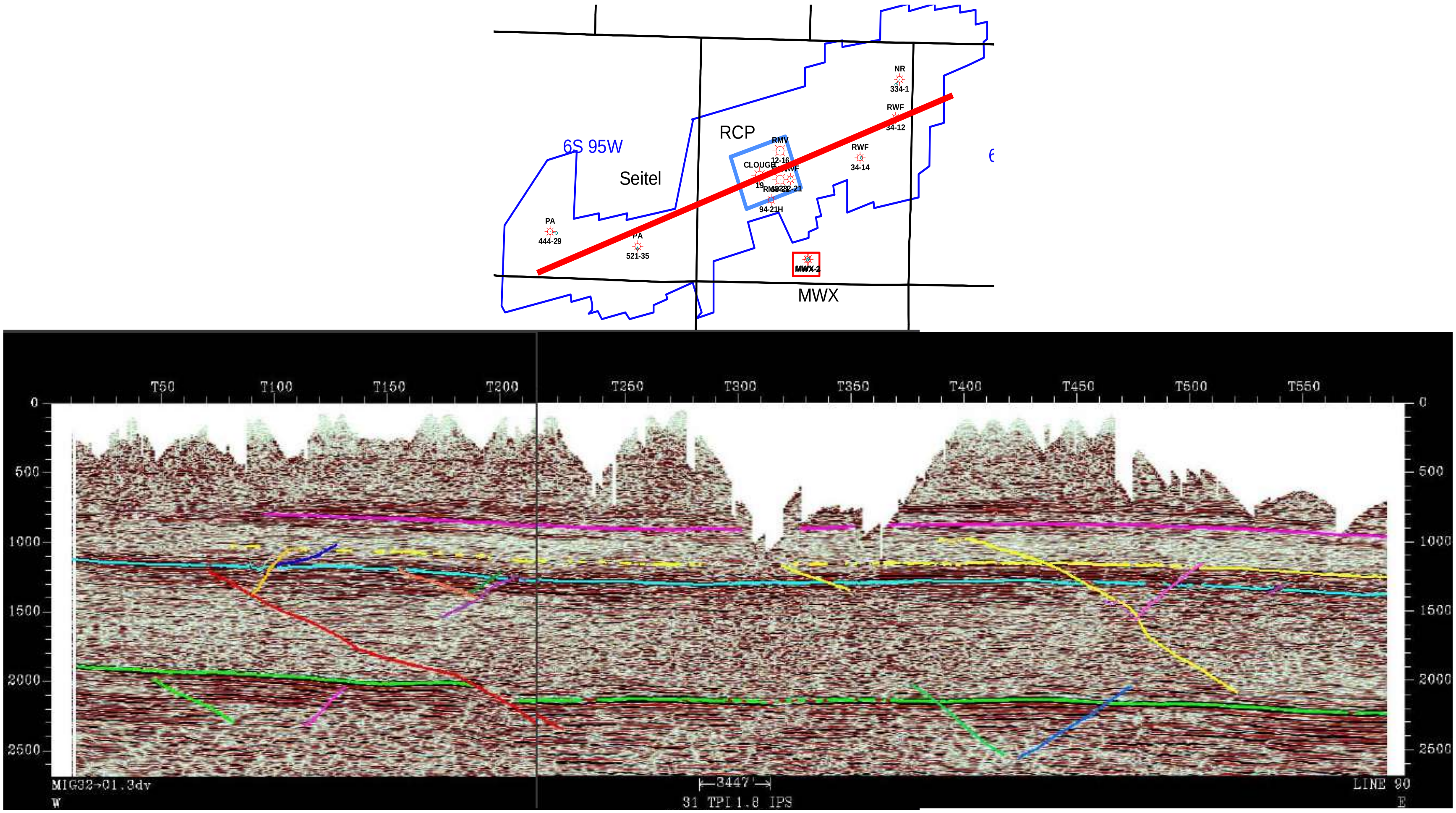

Figure 3.2 – Seismic line 90. This line cuts through the southern end of the survey. Each of the four interpreted horizons is shown as well as the regional fault interpretation. Pink is the UMV Shale, yellow is the Cameo Coal, light blue is the Rollins Sandstone, and light green is the Dakota horizon (see also Figure 3.2a in Appendix A.)

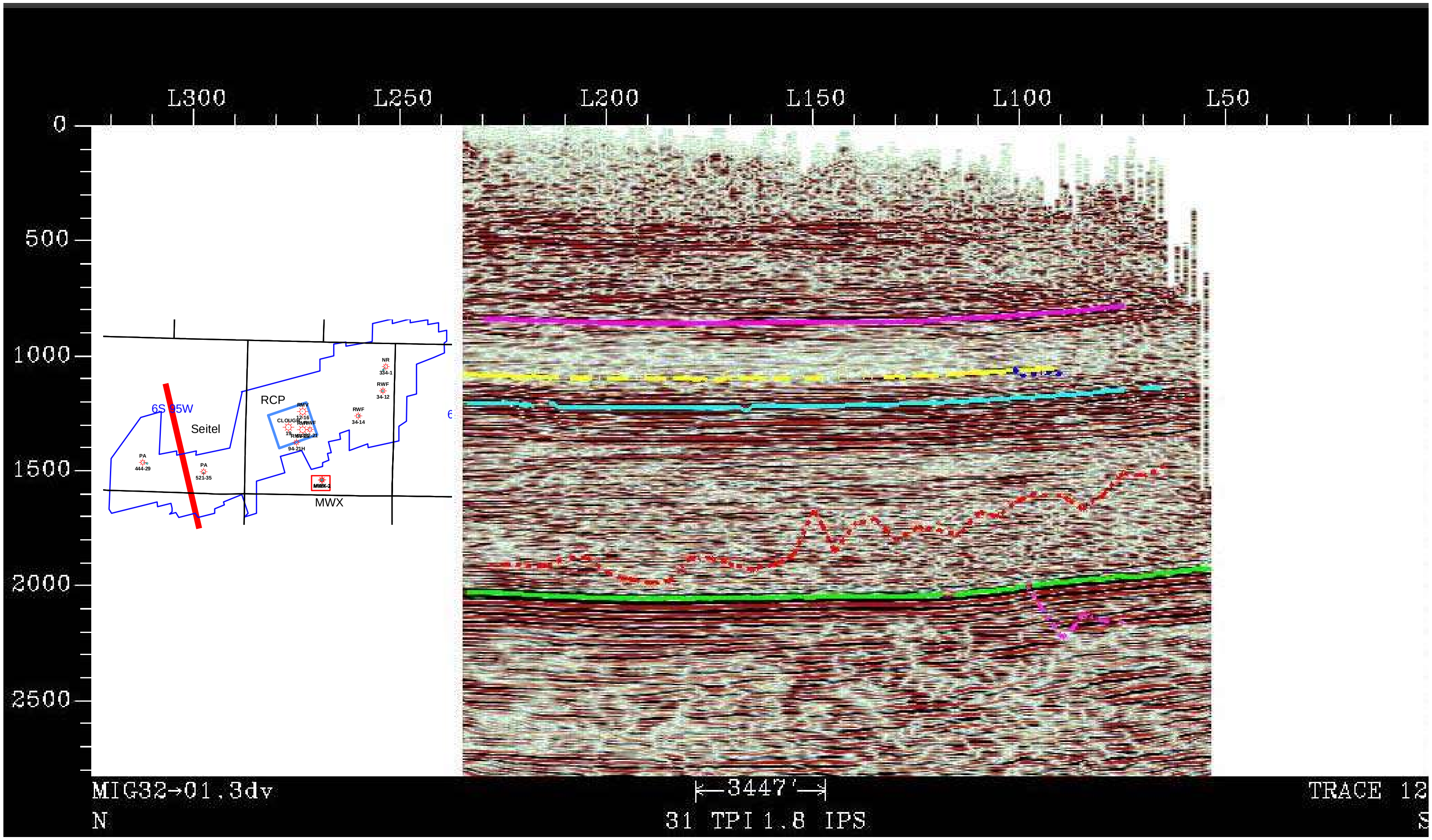

Figure 3.3 – Seismic trace 120. This trace cuts through the western end of the survey. Each of the four interpreted horizons is shown as well as the regional fault interpretation. Pink is the UMV Shale, yellow is the Cameo Coal, light blue is the Rollins Sandstone, and light green is the Dakota horizon. The dashed lines are projections of the various faults cutting across the data in strike view. (see also Figure 3.3a in Appendix A.)

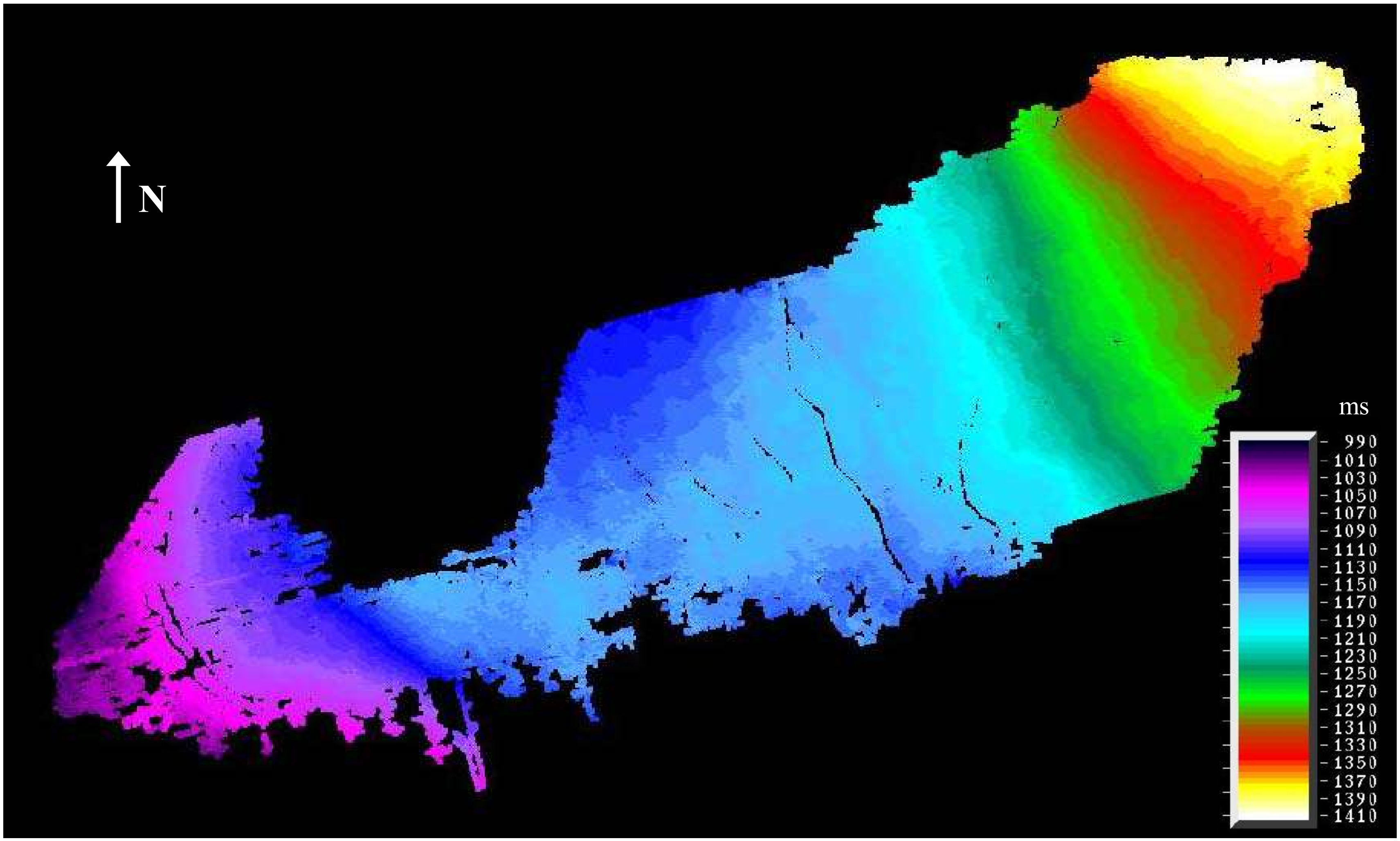

Figure 3.4 – Time structure map of the Cameo Coal horizon pick. The horizon gently dips to the northeast.

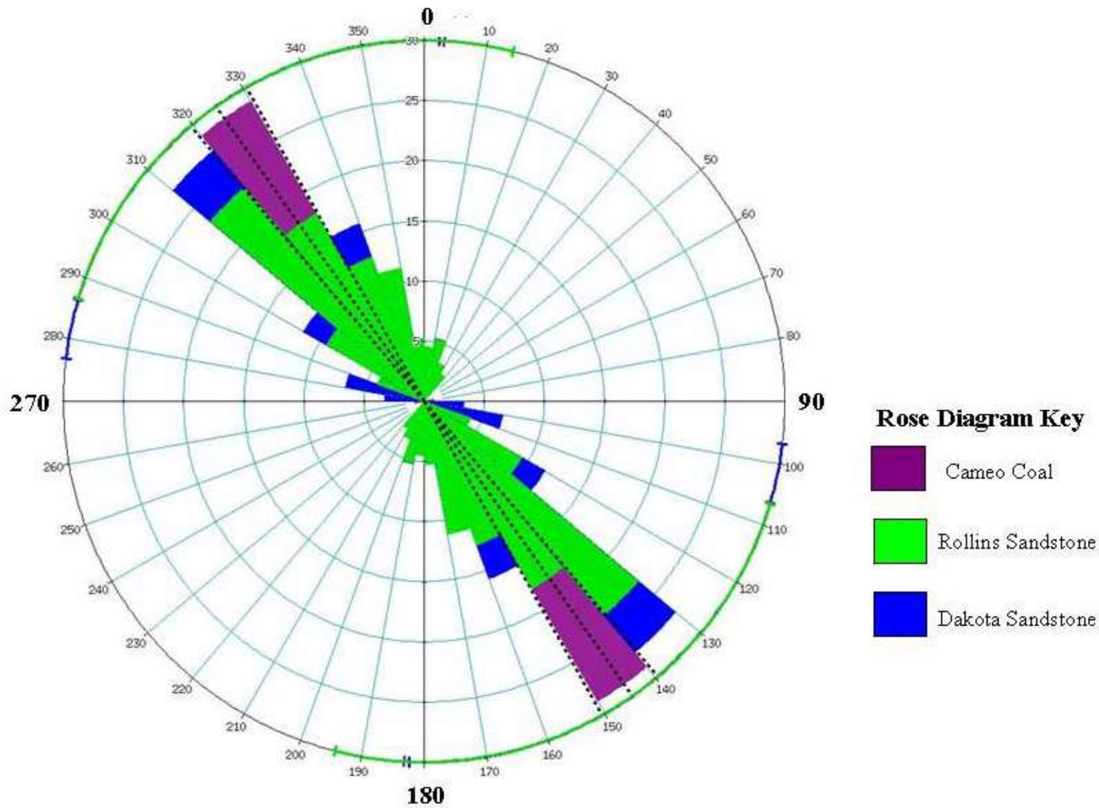

Figure 3.5 – Rose diagram showing the strikes of the regional faults at each horizon.

3.3 Coherency Analysis

To aid in the interpretation of the faults I created a coherency volume using the 3D ESP module in the Landmark interpretation software. A coherency volume looks at the scatter affect that is created by the returning seismic wavelets. The seismic wavelets that are sent into the subsurface are often sent in at an angle. These wavelets will reflect off of various features within the subsurface. These reflected wavelets should return to the surface at a predictable location and at a predictable angle from their reflection point. When they do the wavelet is considered coherent. When they don't return to the surface at their predicted location they are considered to be incoherent. These incoherent wavelets often are caused by the initial wavelet refracting off of something with acoustic properties that is altering the returning wavelet. Fault zones, fracture zones, or unexpected bed contacts are some of the things that can create this effect. Figure 3.6 is an example of how coherent and incoherent wavelets are created.

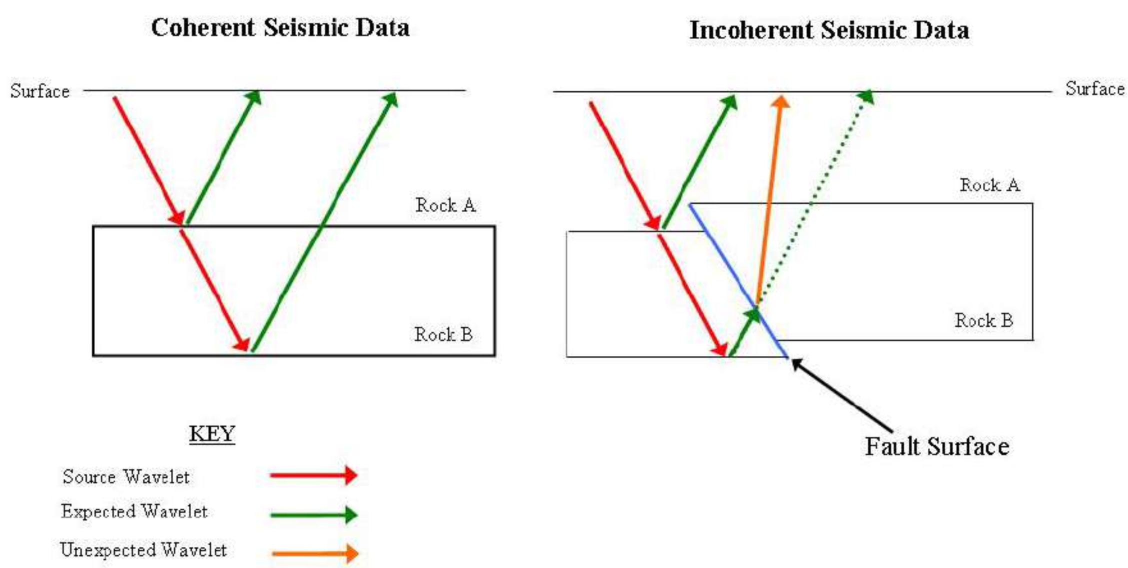

Figure 3.6 – Illustration of the difference between coherent and incoherent seismic wavelets. When the returning expected wavelet is not where it is predicted then the returning wavelets are considered to be incoherent.

The coherency calculation was run across a window of 20 milliseconds from 1,000 milliseconds to 2,500 milliseconds vertically. This method was tested over an area of easily detectable faulting before being used on the entire volume. Figure 3.7, shows the results of the coherency volume at times that are near the Rollins and the Cameo. The faults (lines of incoherent traces) appear as dark lineations within the volume.

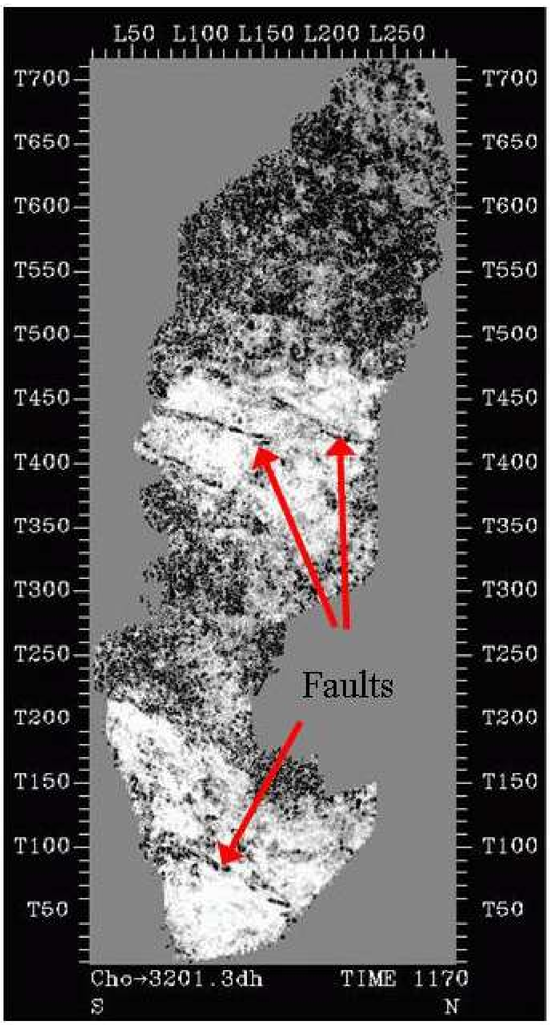

Cameo Interval

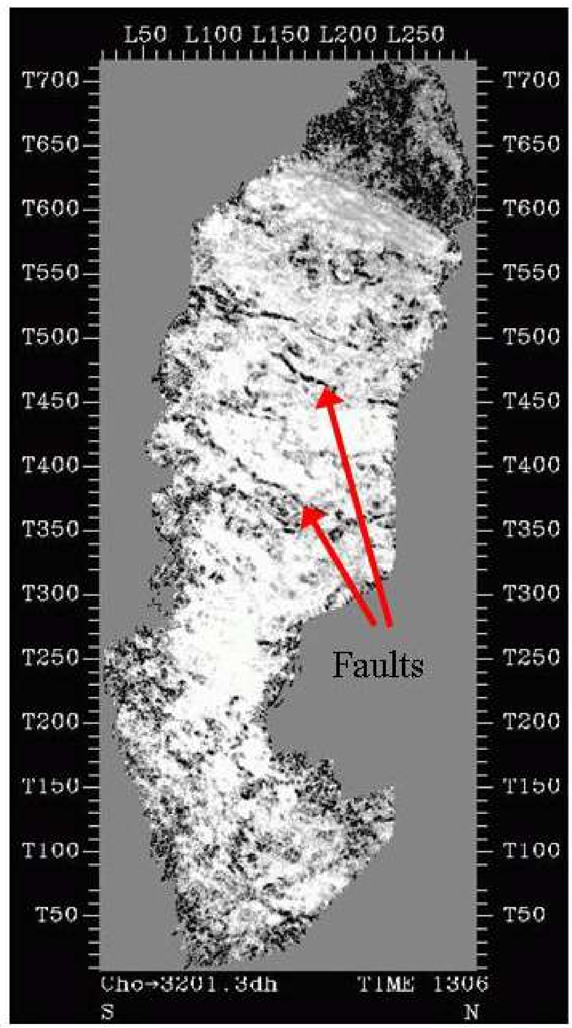

Rollins Interval

Figure 3.7 – Coherency time slices showing where regional faults are located. The black areas are places where the returning traces are incoherent, while the white areas are where the data is coherent. Continuous linear areas of incoherency are interpreted as faults.

CHAPTER 4

STRATIGRAPHIC AND WELL LOG ANALYSIS

4.1 Methodology

To understand the fault network as well as the reservoir interval it resides in we need to know the lithology of rocks that make up the reservoir. For this, several wells that lay within the Seitel (2003) survey, as well as several that are outside of the survey needed analysis. In each of these wells, the stratigraphic tops of each of the corresponding mapped horizons were picked where they were present. Unfortunately, none of the wells drilled to this date within the Seitel (2003) survey have been drilled deep enough to penetrate the Dakota Sandstone. Most wells only penetrate the Cameo Coal interval or the Rollins Sandstone at their deepest. To understand the stratigraphy below the Rollins a well outside of the survey needed to be used as a substitute. There are only two wells within the basin that meet this criterion, the O'Connell F11X-34P and the CB Federal 32-7. The O'Connell F11X-34P, in Township 7S Range 92W Section 34, was selected for this purpose. This well also had the least amount of structural complexity in it (D.S. Anderson, 2006, personal communication) as well as being the closer of the two to the study area.

Modeling in TrapTester requires a number of inputs including the horizons as well as various geologic factors. To input the seismic picks into the TrapTester modeling software, the various horizons and fault picks needed to be converted to depth. However, the Seitel (2003) survey does not have a velocity model. To convert the various seismic picks to depth from time a conversion function was needed that modeled the time versus depth progression of the seismic waves. The last input into TrapTester for modeling was the shale volume logs (Vsh) to predict the Shale Gouge Ratio within fault zones.

The following calculations were compiled and modified in Microsoft EXCEL spreadsheets. The raw spreadsheets and raw .LAS files as well as the modified spreadsheets and .LAS files used for the depth conversion and Vsh calculations can be found in Appendix B. The final spreadsheets were then input into TrapTester as ASCII files.

4.2 Depth Conversion

The outcome for this analysis was a function that could be applied to the seismically picked surfaces (Chapter 3) and convert them from time to depth. The first step in the depth conversion analysis was to pick the four main horizons in the wells. These picks were correlated across eight wells from within the study area and two wells that are outside of the study area. The well locations are visible in Figure 4.1. The wells were initially chosen for specific reasons. They had either the appropriate electronic logs, they reached the required depths for the study, or because of their location. In the end not all of the wells were used. I will discuss the reasons why specific wells were removed from the analysis later. Ultimately, six of the ten wells were used for a later stratigraphic study as well as six for the depth conversion process.

The well picks used in the wells are the picks that can be found in the State of Colorado's public records. These records can be found at the Colorado Oil and Gas Commission's website (COGCC, 2006). This removes any doubt of miss picking the tops in the logs. After the tops had been determined the electronic logs were used to establish the seismic conversion equation. This process involved calculating the average velocity (Vav) at each depth within each well. Then, by plotting the Vav versus the depth of each horizon pick the erroneous data could be removed. After the erroneous data were removed a time versus depth (TvD) plot could then be created. With this plot the seismic conversion equation could be determined then applied to the seismic picks.

The average velocity is calculated on each of the wells with the following Equations 4.1 and 4.2:

$$CumulativeVelocity = \sum_{n} \{(1/DT) * 1{,}000{,}000\} \tag{4.1}$$

$$VelocityAverage = \frac{CumulativeVelocity}{n} \tag{4.2}$$

Six of the wells lie within the RCP study area and are in a completely digital .LAS format, while four of the wells are outside of the RCP study area but still lie within the Seitel (2003) survey. These four wells are raster images. The .LAS format logs were sampled at every half foot. The raster images were sampled every one hundred feet. After the Vav was calculated the corresponding value was pulled in relation to the depth of each horizon and plotted on a Vav versus depth plot, (Figure 4.2). Looking at Figure 4.2 there is a lot of scatter of Vav's for each of the different horizons. We can also see that the limited number of points for some of the horizons makes them invalid for further analysis this mostly applies to the Dakota Sandstone values. The Cozzette, Corcoran, and Mancos values from the CB Federal 32-7 well are plotting at depths shallower then the Cameo Coal. Since this does not match with what is known about the stratigraphy of the area this well was also removed from further analysis. The last of the raster image values seem to plot velocities of different horizons very close to that of the UMV Shale from other wells. This is attributed to the limited sampling rate and therefore makes the raster values invalid.

After removing all of the erroneous data I was left with Vav values only from wells within the RCP study area. This means that the model will be conditioned more specifically to that region of the study area then any where else. This will impart varying degrees of error on the seismic picks outside of the study area when the function is used to convert the seismic picks to depth.

The scattering of the different Vav's from wells that are relatively close and with depths that don't vary that much is and interesting problem. To deal with it the different Vav's from the wells as well as the different depths for each horizon were averaged to get a single Vav and depth for each horizon. The Vav values were then converted from velocities to times using the corresponding depths. Then the times versus the depths were plotted together in a TvD plot, and a best fit line was fit through the data, (Figure 4.3). A surface time and depth of zero was assumed. Equation 4.3 is the best fit line through the data points:

$$Depth = 6.7431 \times Time - 0.7252 \tag{4.3}$$

The above equation along with the four seismically picked horizons and the numerous faults were put in to *Midland Valley's* 3D Move software package (see Appendix B for input and export files). The horizons and faults were then converted from time to depth and output for use in the TrapTester modeling. The converted time horizons near the RCP study area are in error from eight to ten percent. This makes the newly converted seismic horizons within the RCP area off anywhere from 820 to 1,100 feet (249.93 to 335.28 m) deeper then their actual depths. This offset varied across the surface. The main source of error here is most likely trying to use a limited number of data points to depth convert the entire survey.

4.3 Shale Volume Determination and Pseudo-Intervals

Fault zone properties can be used to determine not only the composition of the fault zone but the potential for fluid flow along or across that zone. For TrapTester to calculate properties along the fault plane the stratigraphy of the reservoir interval or the interval of interest must be input along the well bore. For this study I was interested in the potential of the fault to allow fluids to flow along the fault zone. Knowing what percentage of the fault zone is shale gouge will help determine the potential for fluid flow. To move forward with this analysis of the fault zones I needed to know what the volume of shale (Vsh) within the reservoir was at any point. I then needed to input that into TrapTester along the well bores and use it then to determine the potential for fluid flow.

Shale Volume Calculation

The process of calculating Vsh is relatively straight forward. The Vsh is calculated by analyzing the gamma ray log and calculating the percentage of shale at any depth. This percentage of shale is the volume of shale for that point. The volume of shale is determined by taking the maximum and minimum gamma ray counts over the interval of interest and then calculating any point's gamma ray count in relation to that maximum and minimum.

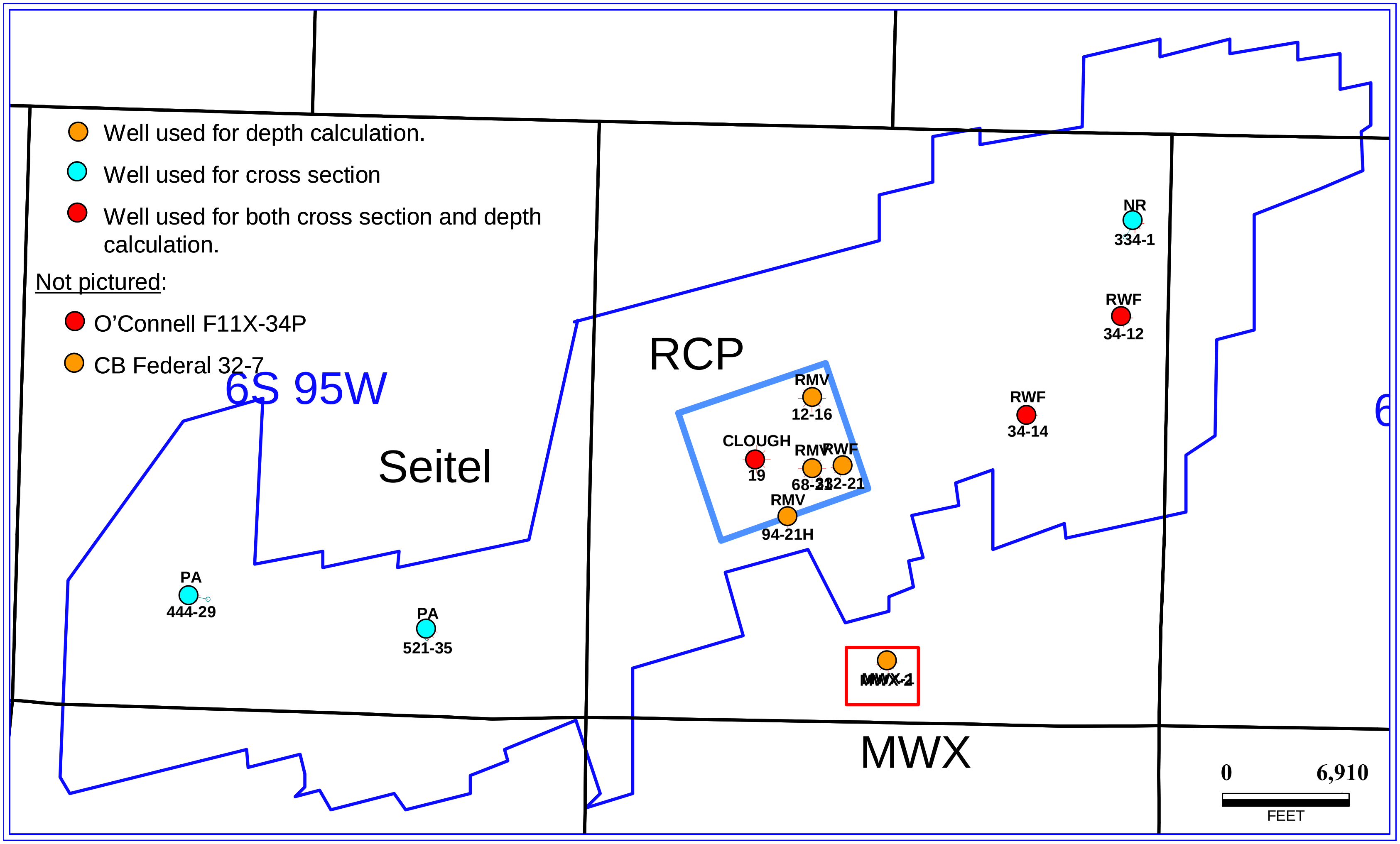

Figure 4.1 – Map showing what wells were used for determining the depth function used to convert the seismic picks, as well as the wells used in the cross section. Two wells were used in the MWX study area but are so close to each other that they overlap on this map at this scale. Two wells are also not shown on this map because they are several miles outside of the study area.

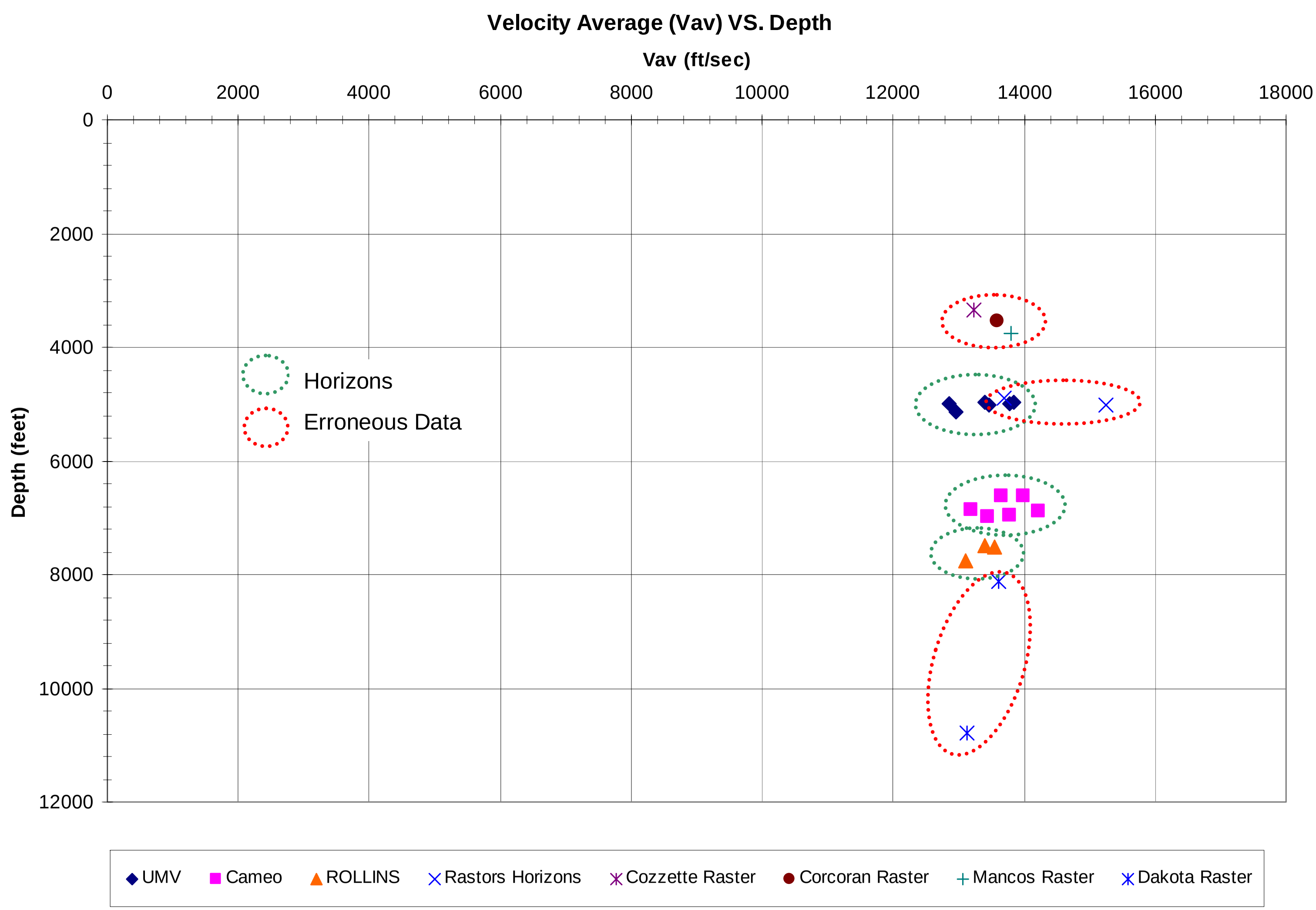

Figure 4.2 – Plot of Velocity Average versus depth. Erroneous data were removed and not included in determining the depth conversion function.

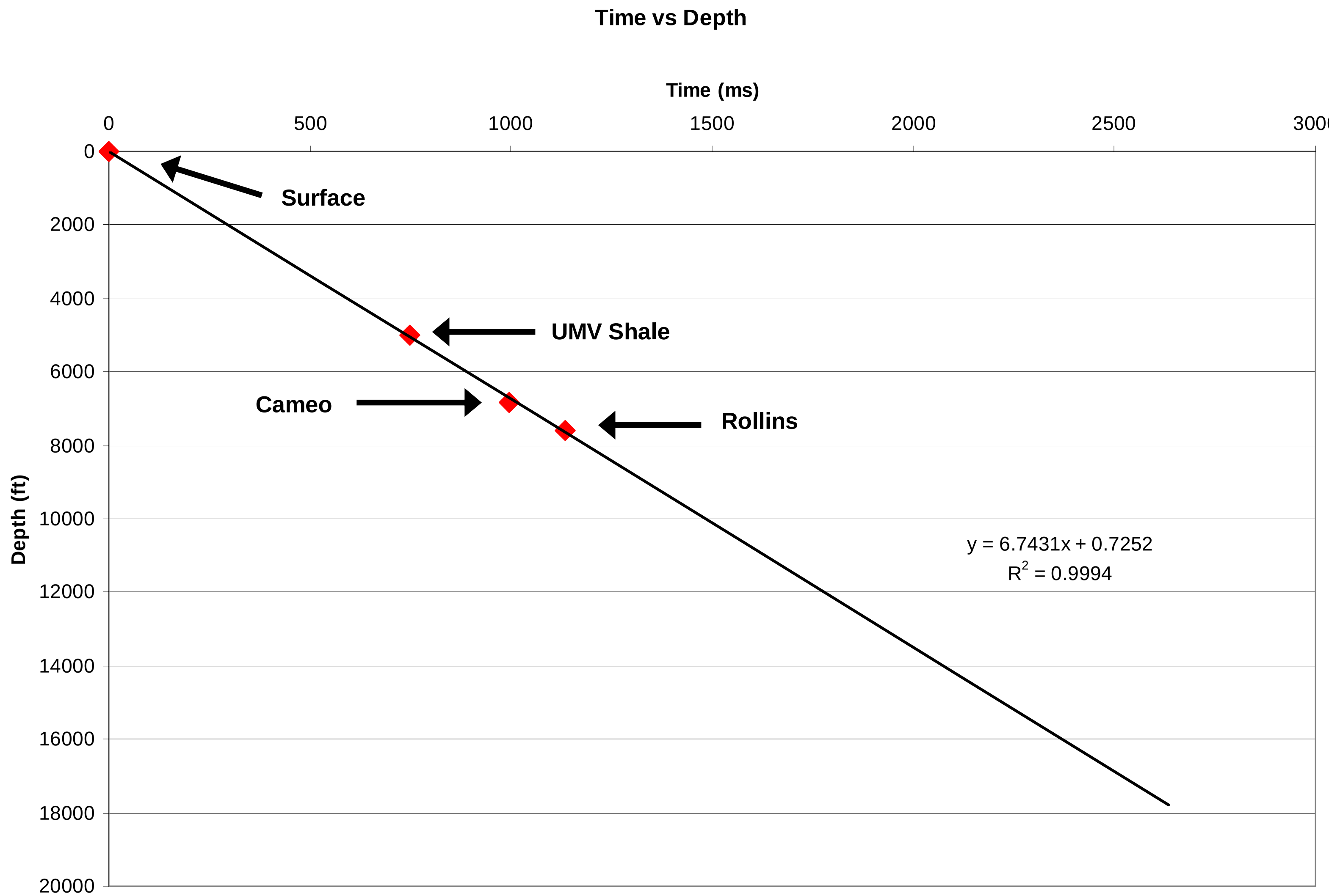

Figure 4.3 – Plot of Time versus Depth. These values came from averaging the different Vav's and Depths for each horizon. Then the averaged Vav for each horizon was converted to time using the average depth for that horizon.

The maximum gamma ray count over the interval is considered to be one hundred percent shale, while the minimum gamma ray count over the interval is considered to be one hundred percent sand and no shale.

Six wells were used for determining the Vsh over the interval of interest, the interval of interest being between the UMV Shale and the Dakota Sandstone. These six wells were spaced out over the study area to give a representative sampling of each area, cross section wells in Figure 4.1. The Vsh was calculated with Equation (4.4) in PETRA's log calculation module for each of the six wells:

$$Vsh = \frac{GammaRayCount - SandValue}{ShaleValue - SandValue} \tag{4.4}$$

The maximum and minimum counts used were those of the entire gamma ray log. This normalizes the log over its entire depth. While normalizing the log does remove some detail it was deemed necessary because of the regional nature of the study. Each well had different max and min values used in an attempt not to normalize them to much and keep some of the wells stratigraphic character. This process unfortunately removes some lithological aspects that could be important. For example the coals that we know are present are removed with this process. They must be added in later modeling steps because of their significance.

Pseudo Interval Determination

However, none of these wells were drilled past the Rollins Sandstone. This proved to be an issue since the interval of interest included the stratigraphy below the Rollins. To make up for this problem the interval below the Rollins pick of each well was removed and the interval between the Rollins and Dakota Vsh log of the well O'Connell F11X-34P was inserted. This new log portion was added to the .LAS files in Microsoft EXCEL spreadsheets. This pseudo interval allowed the depths of the wells to be extended down to the Dakota Sandstone for calculation purposes in TrapTester. A diagram explaining this process is shown on Figure 4.4. Where the Rollins pick did not exist in a well the end of the log was assumed to be the top of the Rollins Sandstone.

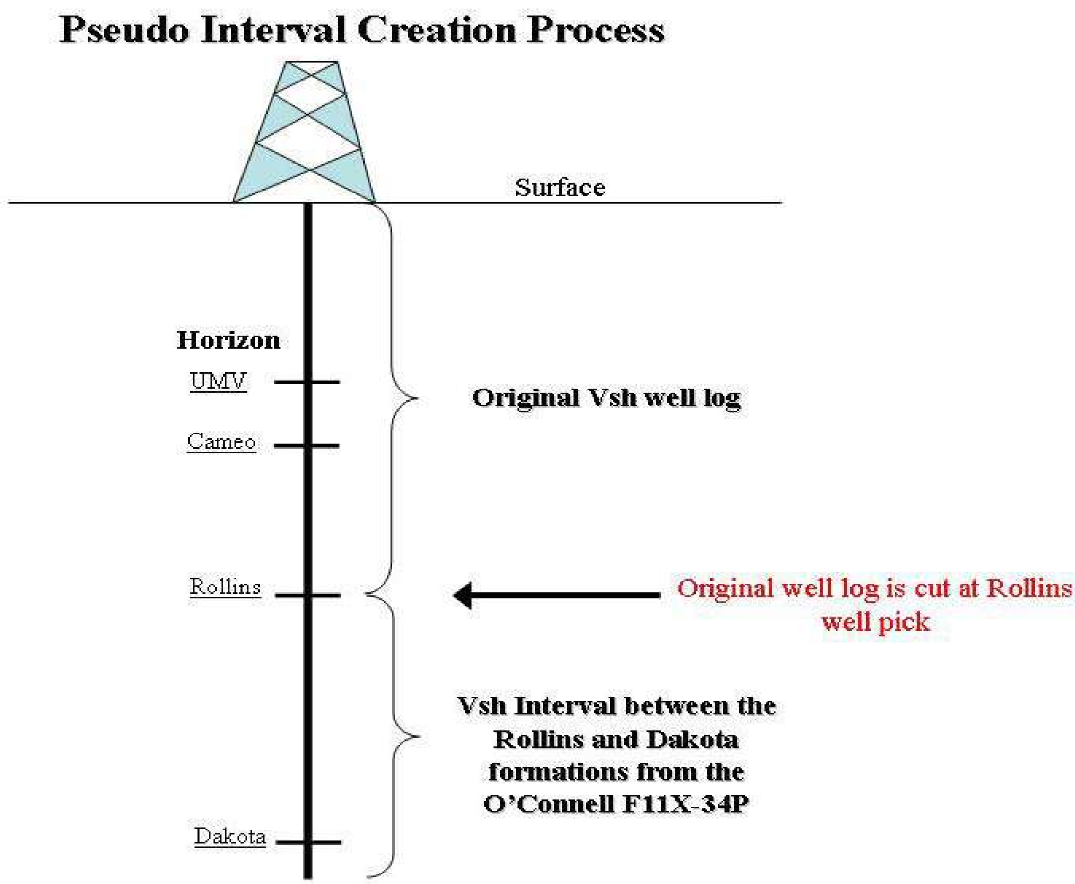

Figure 4.4 – Pseudo interval creation process was applied to each of the six wells and was used to infer a stratigraphy below the Rollins Sandstone in Rulison.

4.4 Shale Gouge Ratio

This part of the analysis is focused on the process used to calculate Shale Gouge Ratios (SGR). The SGR is a fault zone property that can be used to determine the potential for a fault zone to allow fluid movement. While SGR is relatively easy to determine the process used to condition the data for import in to TrapTester is somewhat complicated. The next few paragraphs will discuss the process used on the data.

After the Vsh logs were created they needed to be analyzed and correlated. One of the essential inputs into TrapTester for an SGR analysis is a representative stratigraphic column for the reservoir interval. This is difficult because the reservoir interval we are interested in is composed of fluvial sediments and a detailed stratigraphic correlation of those sediments is beyond the scope of this project. The large well spacing of the six wells as well as the nature of fluvial deposits however presents a problem in creating a representative stratigraphic column needed for modeling. This problem can be overcome by simplifying the electronic log characteristics and loosely correlating the sand packages in the wells.

To simplify the log characteristics of the Vsh logs a smoothing process was applied to them. This enabled the logs to be broken into generalized intervals of sand, shale, and shaley sand. These intervals could then be correlated between the wells. This process undoubtedly removes a lot of detail from the logs. However, this process does preserve the nature of intervals that are of a dominate lithology. Unfortunately, rapidly changing lithologies over short intervals are underestimated or removed. The Vsh log was smoothed by using a window of 301 points, 150 points on either side of the point of analysis. A new log is created by averaging the point of analysis over this window and assigning a new Vsh value at that depth. Figure 4.5 shows the generalized steps of how this method is applied to the six study wells.

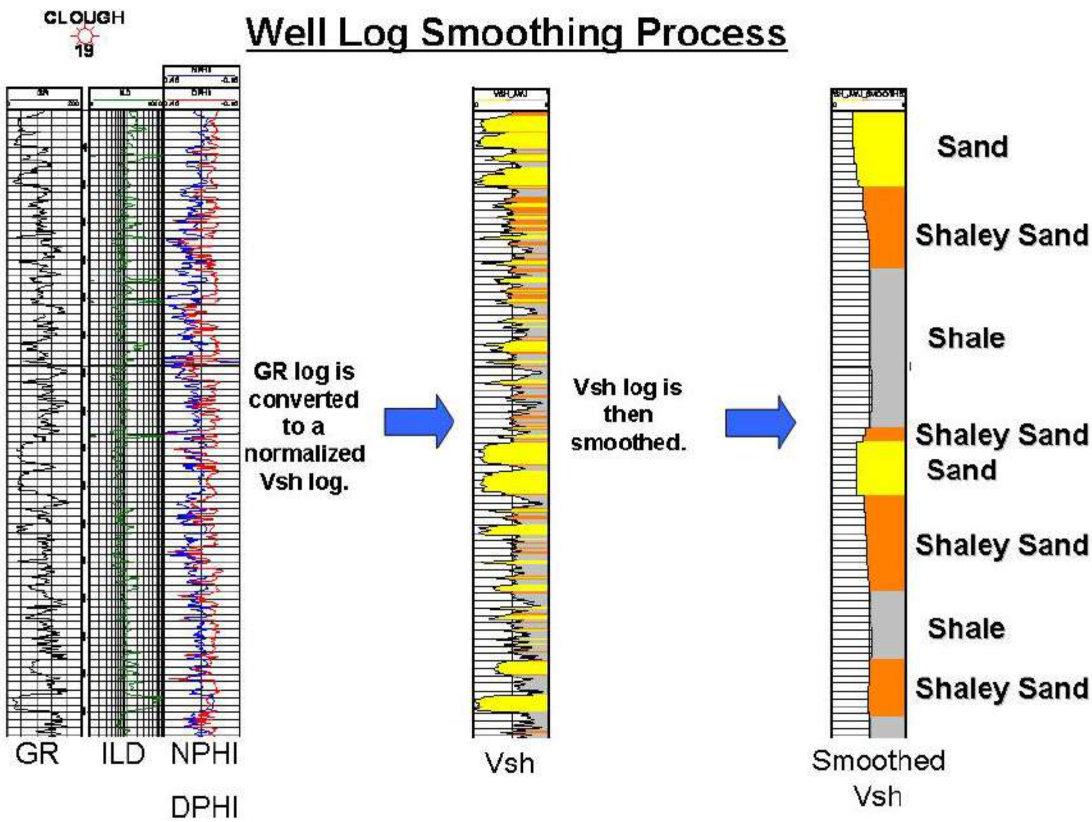

Figure 4.5 – Smoothing process applied to the shale volume logs (Vsh) of the six wells. This process preserves intervals of the logs that are dominantly one lithology while it underestimates intervals of rapidly changing lithology. The cutoffs used in assigning lithology type can be seen in Table 4.1. Yellow = sand, orange = shaley sand, and gray = shale.

The cutoffs used in determining what is shale and what is sand in all of the wells can be seen in Table 4.1. These cutoffs were chosen based on the assumption that there are a lot of authogenic clays present in the reservoir interval (Cumella and Ostby, 2003, Pitman et al., 1989) suggesting that the sands present would have higher gamma ray signatures. This makes border line pure shales or sands appear to be shaley sands. This process was applied to each of the six wells before the pseudo interval was added. I applied the smoothing separately too the pseudo interval well before the pseudo interval was added below the Rollins pick. This removed any smoothing affects that would have been created by the Corcoran and Cozzette members to the original logs if they had been added before smoothing. The final logs that I created in this process and then loaded into TrapTester can be found in Appendix B.

Lithology Type	**Vsh Cutoff Interval**
Sand	≤35% - 0%
Shaley Sand	≤45% - >35%
Shale	100% - >45%

Table 4.1 – Shale volume (Vsh) cutoffs used for each lithology type.

After the Vsh logs were smoothed a correlation was needed between the wells to create a representative stratigraphic column for the study area. To do this marker tops needed to be defined and picked in each well. The definition of each marker top depended on its contact between different lithologies. The pick was defined by what lithology appeared below that contact either sand, shaley sand, or shale. The picks were then assigned across the six wells in attempt to follow as many contacts across the study area. Picks that could not be followed across all the wells were ended in pinch outs. This method substitutes some of the lateral discontinuity of the fluvial system for a more continuous system. This method is also in no way following sequence stratigraphic principles. It does however simplify the reservoir interval for modeling purposes. A completed cross section, hung on the UMV Shale, between the six wells can be seen in Figure 4.6 (see also Figure 4.6a, in Appendix A). This cross section shows the gamma ray, Vsh, and Smoothed Vsh logs for each well. This cross section only represents the interval between the UMV Shale and the Rollins Sandstone Member.

The pseudo interval was treated in a similar way. The gamma ray log of well O'Connell F11X-34P was converted to a Vsh log. The Vsh log was then smoothed and the lithology contacts were then determined. Since this pseudo interval will be the same for all six wells there was no correlation needed. Figure 4.7 (see also Figure 4.7a, in Appendix A), is the pseudo interval with its various contacts marked. Figure 4.8 is the complete stratigraphic column that was input into TrapTester.

After the horizons were converted and the electronic logs were prepared they were input into the TrapTester software package. The module for this calculation in TrapTester is called the CurveMapper. The CurveMapper module takes any number of user defined well parameters and either projects them onto the fault surfaces or it takes them and puts them in to various equations and then projects the outputs onto the fault surfaces. Equation 4.5 is used to determine SGR is based on the work of Yielding (2000). Equation 4.5 is shown below and can also be seen in Figure 4.9:

$$SGR = \sum \frac{(Vsh, \Delta z)}{t \times 100\%} \tag{4.5}$$

This equation looks at the amount of juxtaposition between the hangingwall and footwall of a specific bed, the beds thickness, and it's composition in relation to the beds above and below it. Figure 4.9 is a diagram from Yielding, (2000) that shows how this equation is derived from the stratigraphy. The inputs that the module uses and how it uses them are described briefly below.

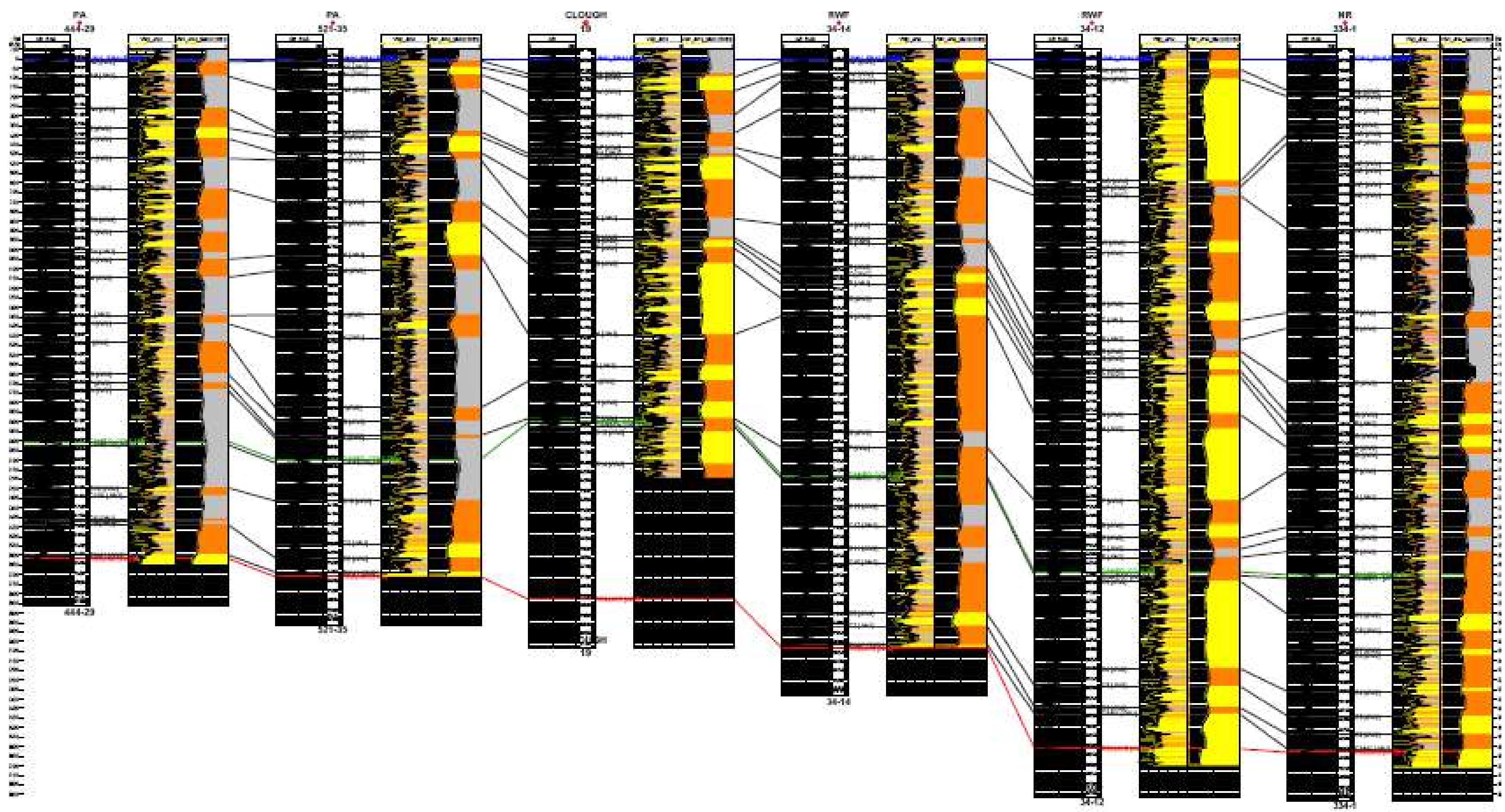

Figure 4.6 – A cross section through the study area. Logs shown are the Gamma Ray (GR) the Shale Volume (VSH_JWJ) and the Smoothed Shale Volume (VSH__JWJ_SMOOTHED). Picked tops are shown as well. Colored tops are also mapped in the Seitel (2003) survey. Blue is the UMV Shale Green is the Cameo Coal and Red is the Rollins. Black picks are various stratigraphic markers used for the TrapTester modeling. (see also Figure 4.6a in Appendix A.)

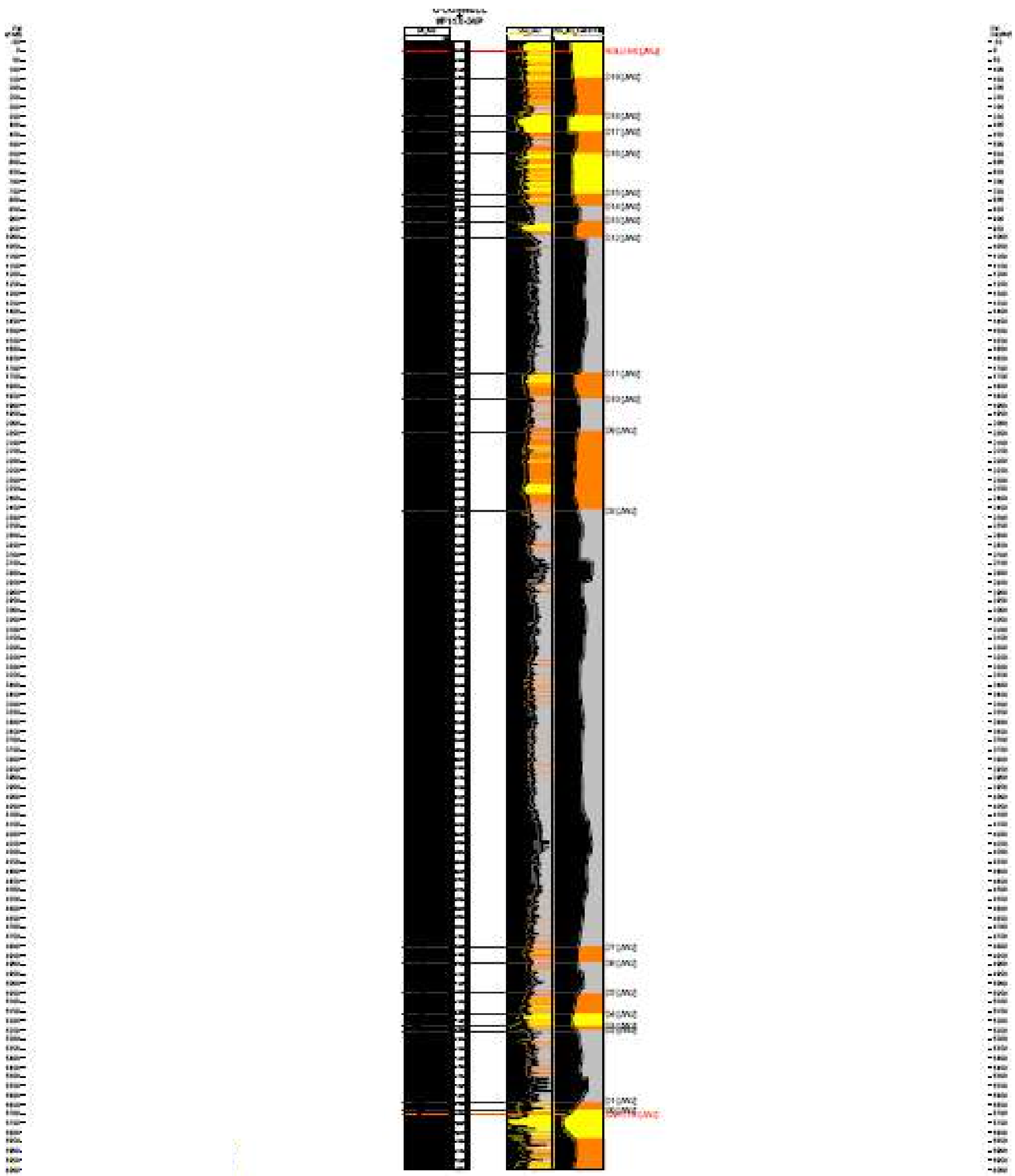

Figure 4.7 – Interval from O'Connell F11X-34P well. This interval was attached to each of the six wells in the cross section of Figure 4.6 and 4.6a in Microsoft Excel. (see also Figure 4.7a in Appendix A.)

First the program defines the resolution of the output attribute to be mapped on the fault surface based on user defined inputs. These inputs define a box based on the vertical and lateral distance input. When attribute calculations are completed these blocks represent the output onto the surface, the smaller the blocks the finer the resolution. This process is used to map any well attribute properties onto the fault surfaces. For this a study a high resolution was desired so a vertical distance of 13.12 ft (3.99 m) and a horizontal distance of 26.25 ft (8.00 m) were used for the blocks.

For the SGR calculations to be computed the horizons and various bed contacts, or marker tops, must be defined on the fault surfaces. Therefore, the horizons and bed contacts defined in the wells are projected onto the fault surfaces. In the case of more then one well being projected on to the fault surface the program uses the natural neighbor method of combining each of the attributes from each well to provide the final estimate of the property. The natural neighbor method weighs the contributions of each well based off of the wells distance from the projection surface. This method creates a hangingwall and footwall projections of the attribute of interest on to each desired fault surface. With this information the SGR calculation can now be performed using the equation defined by Yielding (2000).

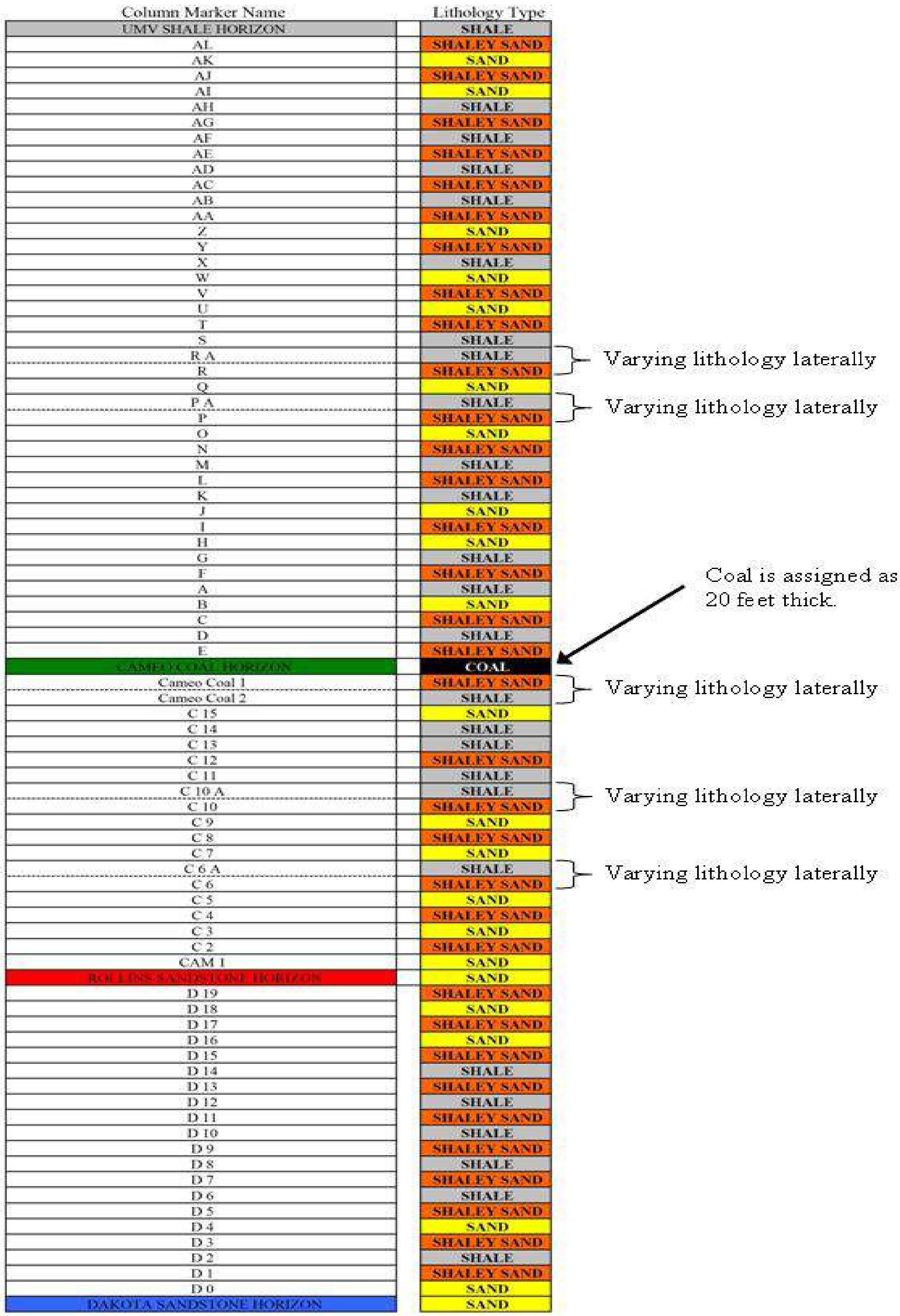

Figure 4.8 – Stratigraphic column that was used for input into TrapTester. See Figure 4.6 and 4.7 for reference to locations of picks in well logs.

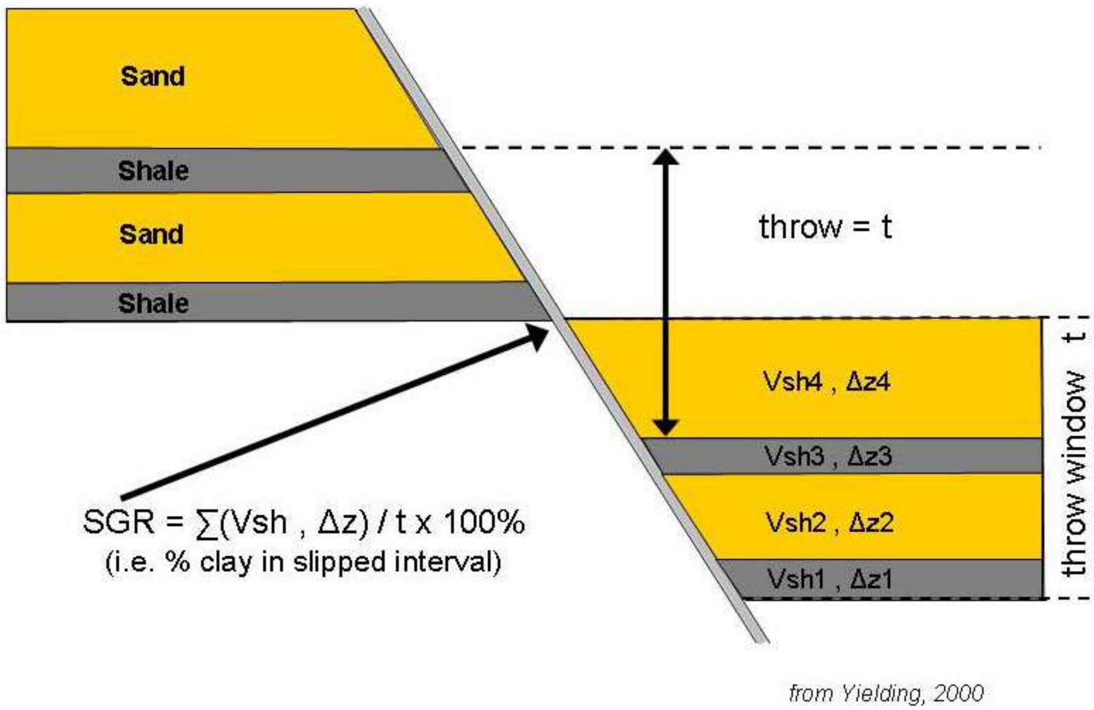

Figure 4.9 – Shale Gouge Ratio (SGR) is a representation of the percent of clay that is in a slipped interval of a fault plane. It is a measure of the thickness of a series of beds and their composition divided by the amount of throw that they have undergone.

The amount of SGR along a fault surface can be used to qualitatively determine the sealing ability of a fault and SGR values higher then 23 percent are considered to be sealing (Yielding, 2000). Figure 4.10 represents an example of this relationship on a fault surface. A portion of fault C in the image has a low SGR value, while the rest of the fault has moderate to high SGR values along with faults A and B. Figure 4.11 is a south looking view of the regional faults interpreted from the seismic. Mapped out on the faults is the SGR calculated along each fault. The wells can also be seen in this image. It should be noted that some of the faults have high SGR values covering them while some of the faults have patches of low SGR values. Figure 4.12 is a close up of the RCP study area looking to the southeast. The RCP study area is bounded by two large faults (fault A and fault C) with a small splay (fault B) branching off one of them.

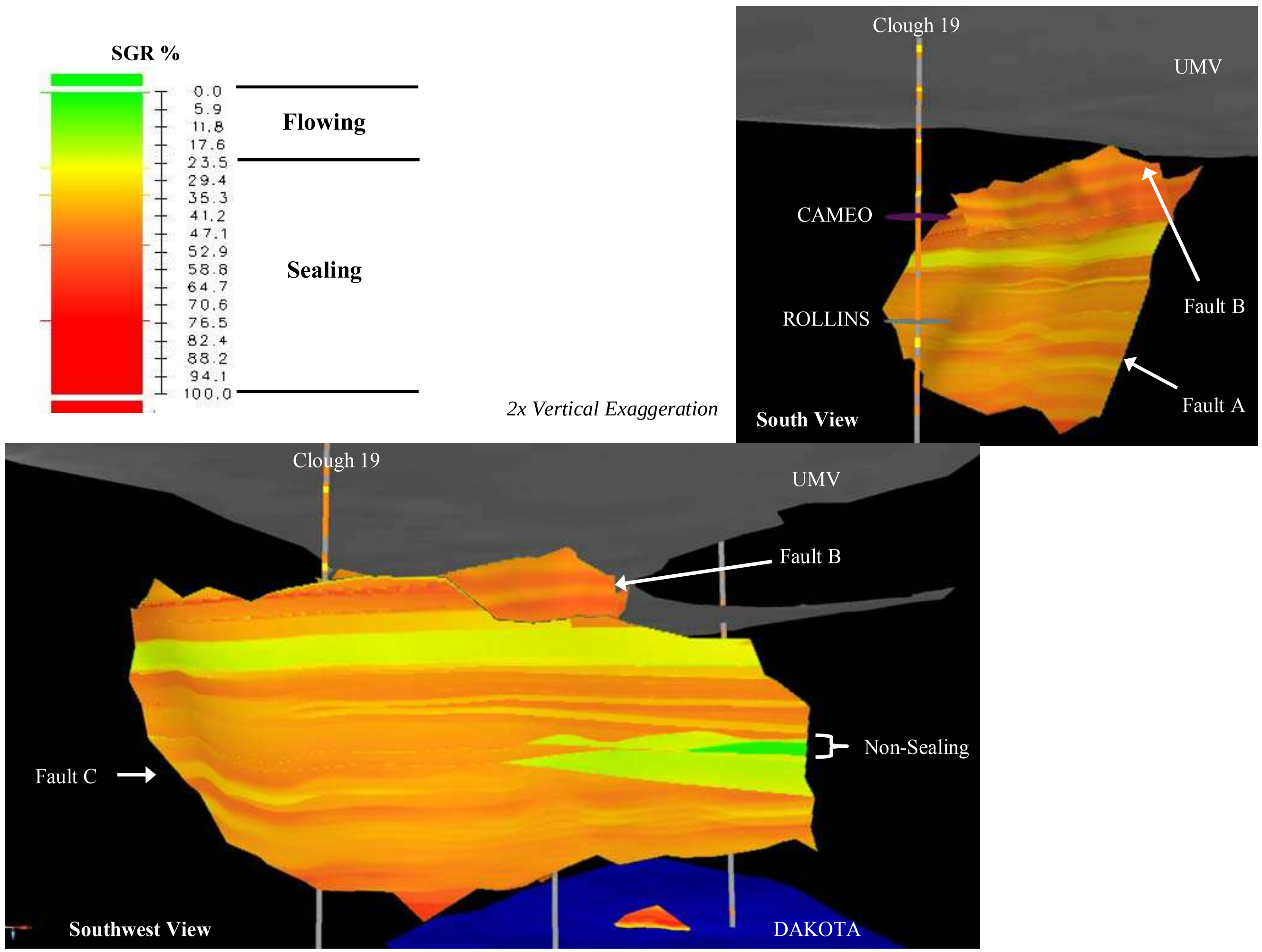

Figure 4.10 – Shale Gouge Ratio (SGR) along three faults. There are portions of fault C that show the potential to be non sealing faults. These faults also bound the RCP study area. The wells the vertical banded lines with the shale volume log (Vsh) values represented as the bands. The gray surface is the UMV Shale and the blue surface is the Dakota Sandstone.

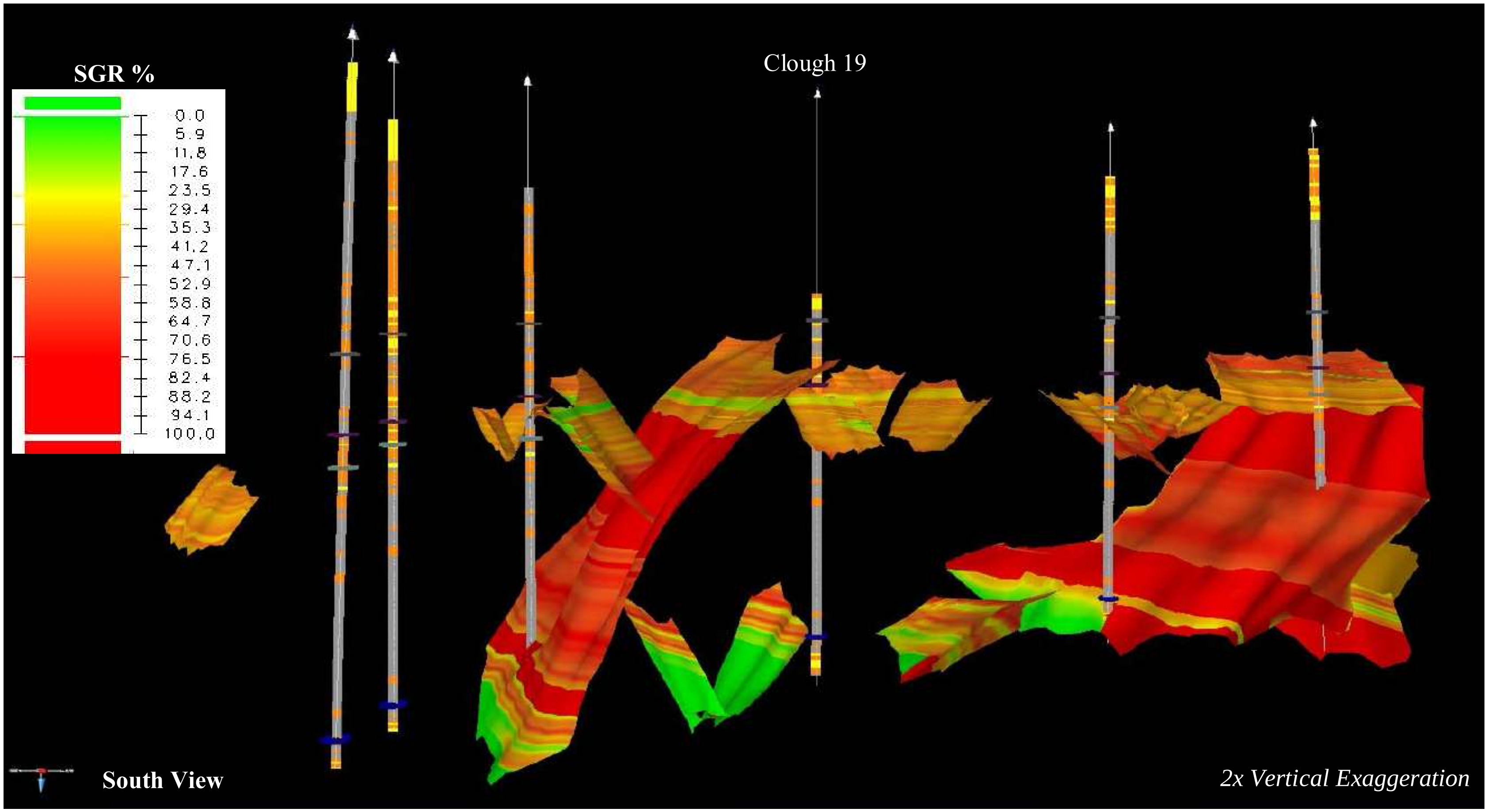

Figure 4.11 – Shale Gouge Ratio (SGR) mapped out on all of the fault surfaces. There are areas of low SGR along some fault surfaces, while most of them tend to have higher SGR values. The vertical banded lines are the wells with the shale volume logs (Vsh) values represented as the bands.

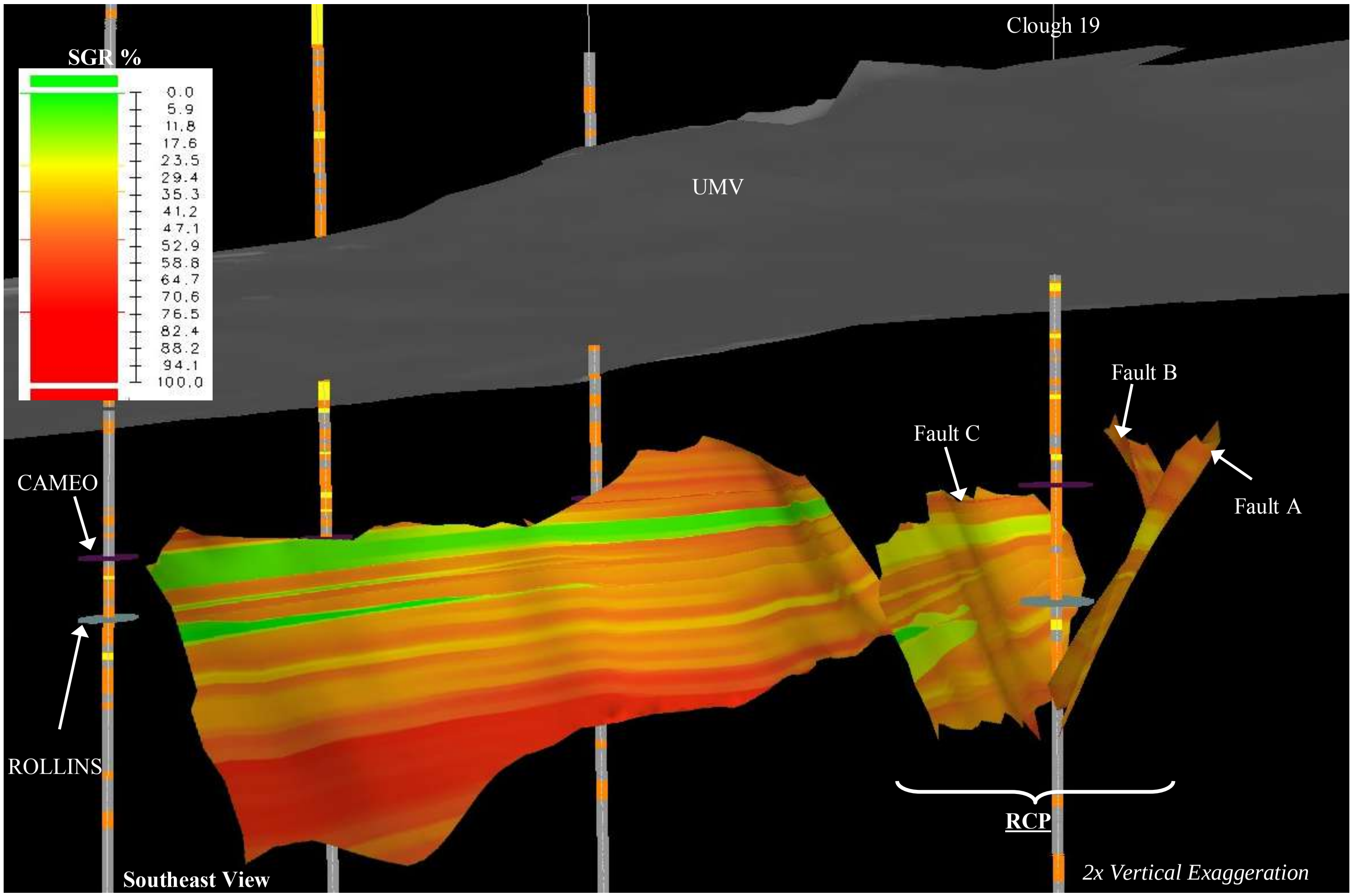

Figure 4.12 – A close up of the RCP study area representing the Shale Gouge Ratio (SGR) along the faults. Also, in the background is a fault that lies to the east of the RCP study area showing the potential to be non-sealing (green areas). The gray surface is the UMV Shale and the vertical banded lines are the wells with the shale volume logs (Vsh) values represented as the bands.

CHAPTER 5

FIELD STRESS ANALYSIS

5.1 Methodology

Presented in this chapter is an analysis of the stresses present in the basin. This analysis also looks at how these stresses have affected the regional fault system. The in-situ stresses that are present in the basin control many of the present day properties of the faults. The various properties of the faults are of great interest to us because of their control on fluid flow within the fault zone. These properties also tell us about how fractures have formed and their characteristics. The property that I focused on during this part of the analysis is the dilation tendency and its relation to the in-situ stress regime.

The dilation tendency provides information about physical properties of the fractures present in the reservoir; e.g., the orientations at which a set of fractures and faults will be dilated and allow fluids to flow is useful information. If fractures are open they can then transmit fluids.

This analysis was performed using TrapTester. The inputs came primarily from Shannon Higgins 2006 masters thesis work. Higgins (2006) worked on ways of using geomechanical modeling as a tool for reservoir modeling. Her modeling results for wells within the RCP study area were used as the realistic magnitudes and orientations of the in-situ stresses.

5.2 Stress Field Analysis

TrapTester requires specific data inputs before it can determine the various fault and fracture properties. Most of this information came from Higgins (2006) and her work with geomechanical modeling. This section is going to be a brief summary of some of her work and how it was applied to this study. A copy of her work should be consulted for a complete understanding of how she derived her data as well as her conclusions.

The inputs for the TrapTester Stress Editor module are relatively simple; A vertical or overburden stress (σ 3, or σV), the maximum horizontal stress (σ 1, or σH), the minimum horizontal stress (σ 2, or σh), the pore pressure of the reservoir, and some basic rock properties. These inputs define a stress regime for the modeled surfaces. These values are used to model below the UMV Shale all the way down to the Dakota Sandstone. Unfortunately, many of these inputs must be derived from other sources of available data.

Stress Orientation and Magnitude Inputs

Higgins (2006) determined the magnitude and orientation of σh in several wells within the RCP study area using mini fracture tests in combination with leak off tests and well bore images. In each of the mini fracture tests data sets she assigned gradients to the general trends within the data. Higgins (2006) found that the gradients changed with depth. There is a greater increase in pressure at depths below 7,000 ft (2,133.60 m). This is attributed to an increase in pore pressure with depth. The pore pressure is controlled by the expulsion of source gasses from within the coals interacting with permeability barriers such as clays (Higgins, 2006). Figure 5.1 represents the results of the mini fracture tests performed in the Rulison field area. For the modeling in TrapTester the gradient derived from the UMV Shale to a depth of 7,000 ft (m) was used. This gradient is about 0.85 psi/ft. This gradient value is assumed to be a good representation of the reservoir interval.

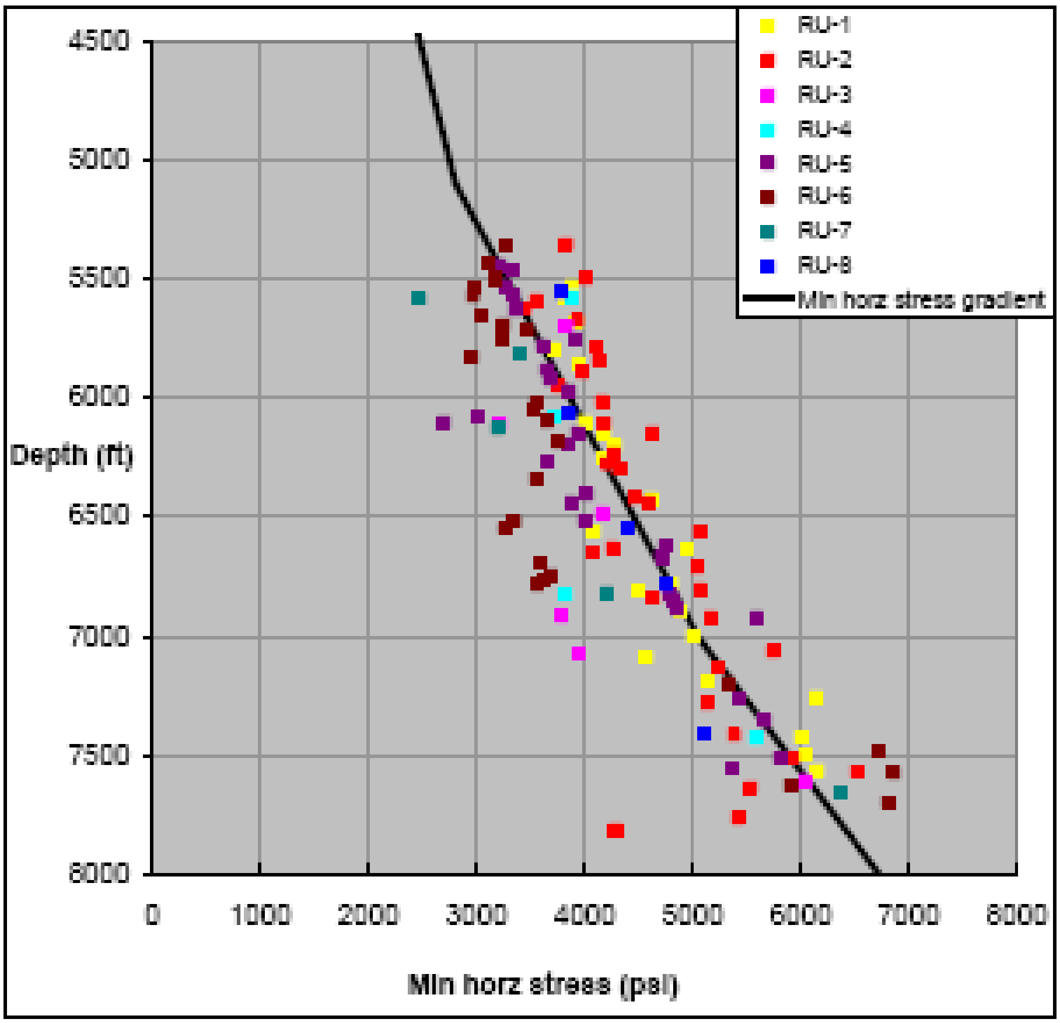

Figure 5.1 – Minimum horizontal stress magnitudes (σh) from mini fracture tests done at Rulison. The gradient of the best fit line between 5,200 ft to 7,000 ft was used for modeling, image from Higgins (2006).

The orientation of σh in the Rulison field was determined from well bore images. Higgins (2006) discusses how the breakouts from the well bore can be interpreted as being in the direction of the minimum horizontal stress. The interpreted direction of the minimum horizontal stress from the wells in Rulison is roughly 12 degrees east of north (N12E). However, this value does vary from well to well and with depth (Higgins, 2006). For modeling in TrapTester though this value was assumed to be representative for the reservoir interval.

The magnitude and orientation of σH cannot be directly determined from test data. Higgins (2006) used geomechanical modeling to derive it. However, a few assumptions were made for this. The gradient for σH was assumed to be the same as the gradient used for σh. Estimation for the magnitude of σH was achieved by assuming that by taking a constant and adding it to the magnitude of σh a reasonable magnitude that matched observations could be determined for σH (Higgins, 2006). The constant value used for modeling in TrapTester was determined by Higgins (2006) from well RWF 542-20. This well lies close to the Clough 19 well. The σH used is assumed to be 2,000 psi greater then the σh used. The orientation of σH is also considered to be perpendicular to the orientation of σh.

Higgins (2006) derived the σV by integrating the density logs. Four modeled wells were created after modifying their true density logs. The missing upper portions were extrapolated to the surface then any washouts or breakouts were reconstructed using the neutron density cross plot method. The method can also be used for determining lithology properties of the logs. However, the lithology determinations were not used in my modeling. The magnitude gradient used for σV was taken from analysis of Higgins

(2006) modeled results of RWF 542-20. Figure 5.2 shows the results of Higgins (2006) geomechanical modeling of that well. The assumed gradient is 0.85 psi/ft.

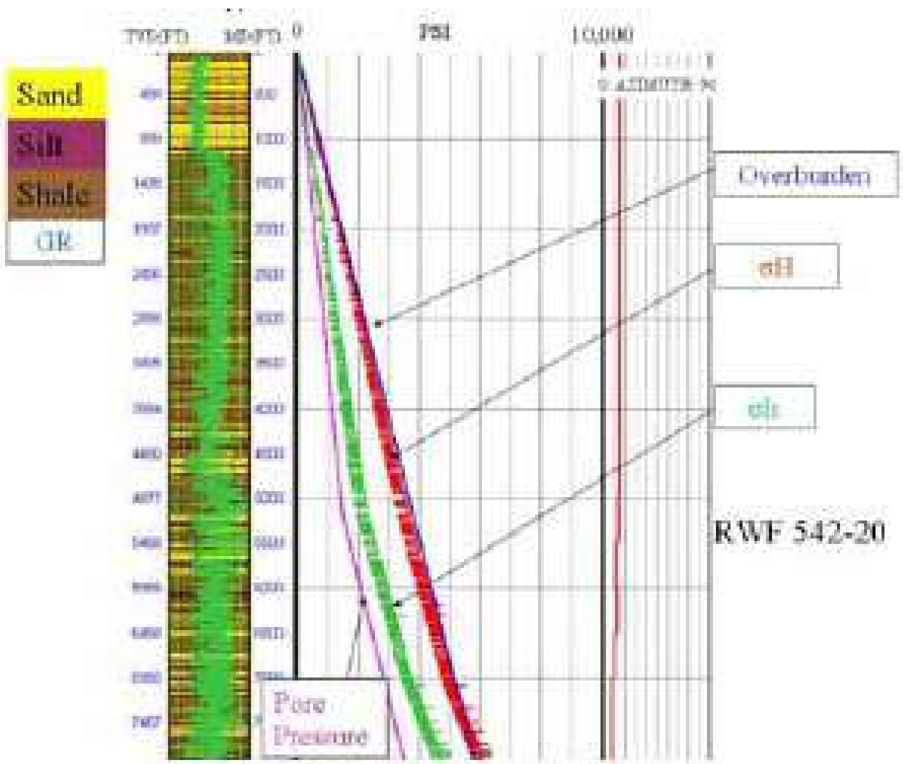

Figure 5.2 – Higgins (2006) modeling results of well RWF 542-20. The gradient used for σV (Overburden) was calculated from the slope of the Overburden line above.

Pore Pressure Input

The pore pressures were derived from mini fracture tests analyzed by Higgins (2006). A gradient line was fit through the data again. Here as well as in the σh magnitude calculations there is a change in the gradients above and below the UMV Shale. Here the pore pressure gradients come from the RWF 523-20 which is assumed to be analogous for the rest of the wells in the area. For my modeling I used the gradient below the UMV because that is the reservoir interval of interest. Higgins (2006) comments on how these pressures are not virgin pressures but are used at estimates of the pore pressures for other wells in geomechanical modeling. Figure 5.3 is a plot of the various pore pressures with depth from Higgins (2006). The gradient used for modeling in TrapTester is 1.11 psi/ft.

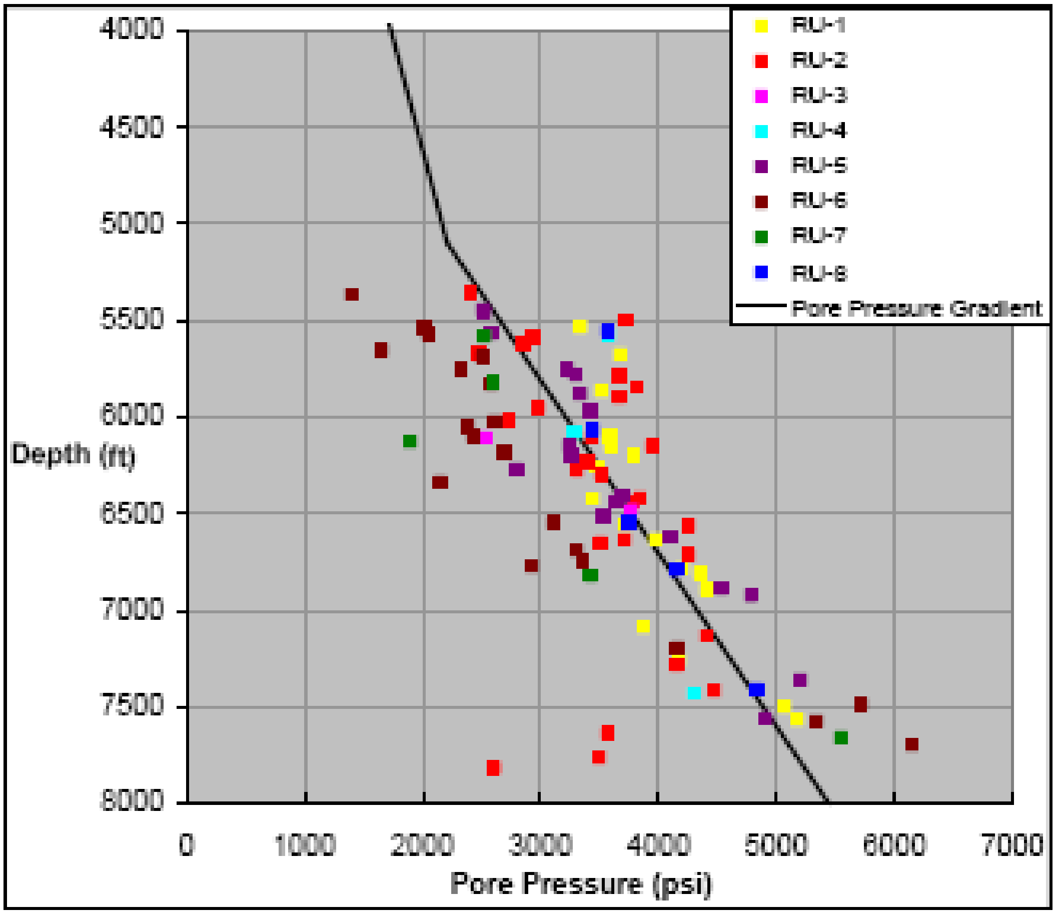

Figure 5.3 – Pore pressure estimates from mini fracture tests in Rulison. The pore pressure gradient comes from RWF 523-20 which is assumed to be representative for the rest of the wells in the area, from Higgins (2006).

Rock Property Inputs

The last inputs needed for the modeling process are related to the actual rock properties of the reservoir. The first is the intrinsic material strength or the cohesive strength of the rock. The second is the coefficient of internal friction. These properties come from stress tests on rocks from the reservoir. Higgins (2006) measured 17 samples from the MWX -1 well using the Mohr-Coulomb failure criterion. The cohesive strength of sandstone at 6,462 ft (1,969.62 m) resulted in shear failure occurring at 3,767 psi. This cohesive strength value was assumed to represent the strength of the rock for all depths below the UMV Shale for modeling purposes. Unfortunately, the coefficient of internal friction was either never determined by Higgins (2006), or it was not reported. This value was determined using a default value for cataclastic sediments from within the TrapTester software. That default value is 0.75.

Table 5.1 represents the stress field inputs used for modeling the stress field within the reservoir interval at Rulison. These inputs were used for the entire rock body from 5,000 ft (1,524.0 m) to the Dakota Sandstone. Table 5.2 shows the rock properties used for modeling the same interval.

Parameter	**Gradient** (psi/ft)	**Stress** (psi)	**Depth** (ft)	**Orientation** (degrees)
σh	0.85	3,800	6,000	192.00
σH	0.85	5,800	6,000	102.00
σV	0.85	4,500	6,000	N/A
Parameter	**Gradient** (psi/ft)	**Pressure** (psi)	**Depth** (ft)	**Orientation** (degrees)
Pore Pressure	1.11	4,000	6,675	N/A

Table 5.1 – Stress Field Editor inputs used in modeling the stresses between the UMV Shale and the Dakota Sandstone, values were derived from Higgins (2006).

Cohesive Strength	**Coefficient of Internal Friction**
3767 psi	0.75

Table 5.2 – Rock properties used for modeling between the UMV Shale and the Dakota Sandstone.

5.3 Dilation Tendency

This section focuses on the process of calculating the Dilation Tendency (DT) of the regional faults. The DT provides a criterion to highlight which fracture orientations are more likely to be open (Badley, 2007). The higher the value of DT the more likely that the fault will be dilated and transmit fluids. To calculate the DT of a fault surface a stress field must be known. For the Rulison area an in-situ stress field was determined by Higgins (2006). Determining the DT of the regional faults will present insight into the likely hood of the regional faults to be dilated under the current in-situ stress regime. Higgins (2006) comments on how this stress field is similar to that of the Laramide stress field, however, the magnitudes are probably not the same.

Equation (5.1) is used to calculate the DT:

$$DT = \frac{(\sigma 1 - \sigma n)}{(\sigma 1 - \sigma 3)} \tag{5.1}$$

Figure 5.4 shows how these various values in the above equation are determined from the Mohr Stress diagram. These values are plotted on the fault surface in the same way that the Shale Gouge Ratio attributes. The block sizes used to map the DT are the same that were used to map the Shale Gouge Ratio. This keeps the same resolution along the fault planes.

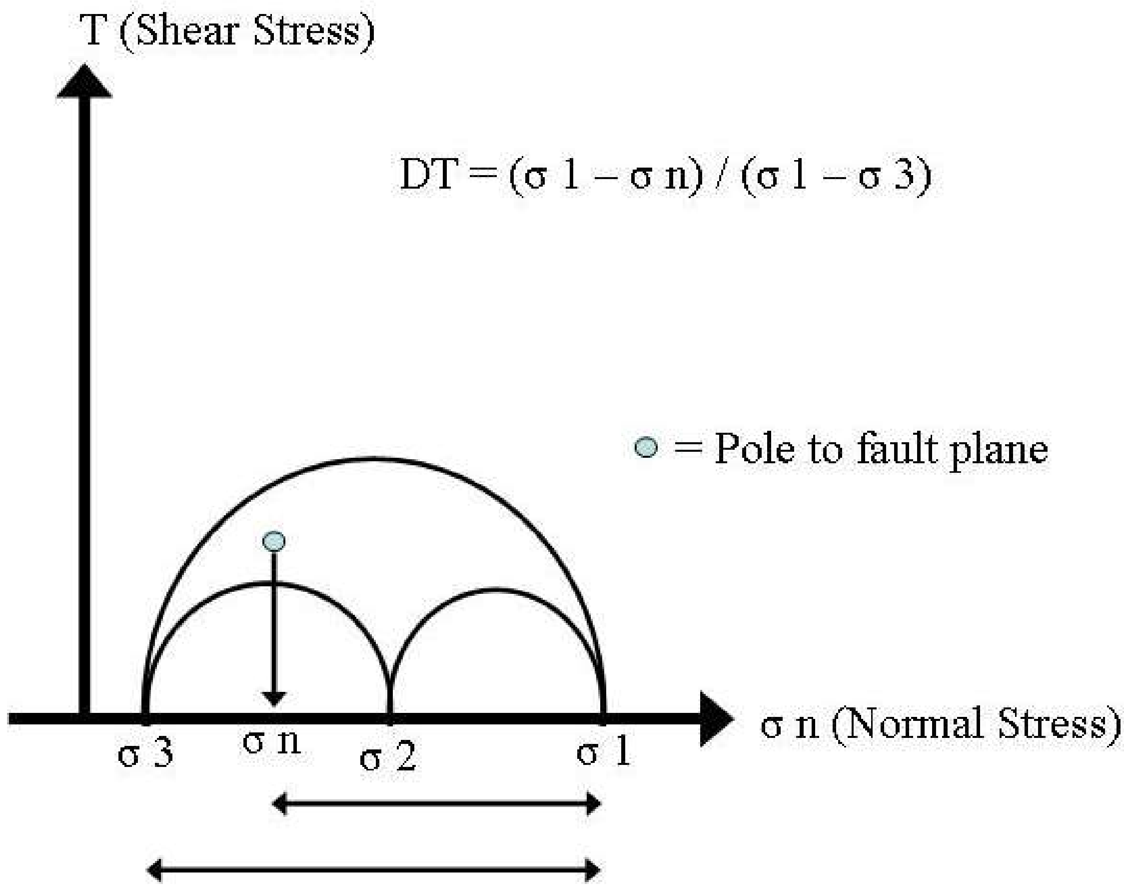

Figure 5.4 – This figure shows how the Dilation Tendency (DT) at any point along a fault is calculated from the Mohr diagram, from Badley (2007).

The DT along a fault surface can be used to qualitatively determine if in-situ stresses acting on the fault has caused dilation of the fault. Figure 5.5 represents an example of the DT values mapped on a fault surface. There are areas along the fault surfaces that have low DT values and areas that have higher DT values. Figure 5.6 is a south looking view of the regional faults interpreted from the seismic. Mapped out on the faults is the DT calculated along each fault. Figure 5.7 is a close up of the RCP study area looking to the southeast. The RCP study area is bounded by two large faults (fault A and fault C) with a small splay (fault B) branching off one of them.

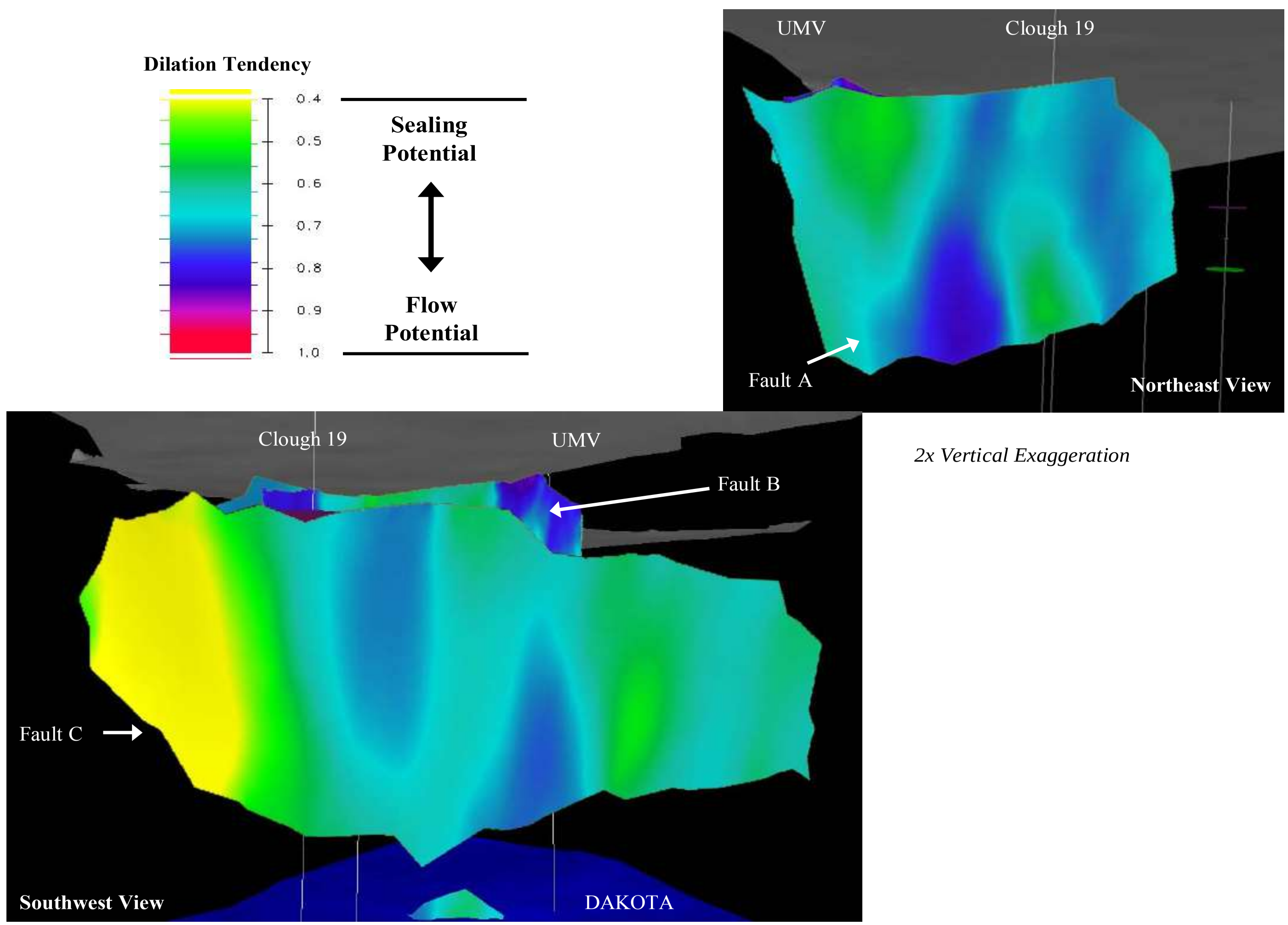

Figure 5.5 – Strike view of faults with Dilation Tendency (DT) mapped out on them. There are portions along the faults that show the potential to be dilated. The greater the DT the more likely the fault will allow fluids to flow. These faults also bound the RCP study area. The gray surface is the UMV Shale and the blue surface is the Dakota Sandstone.

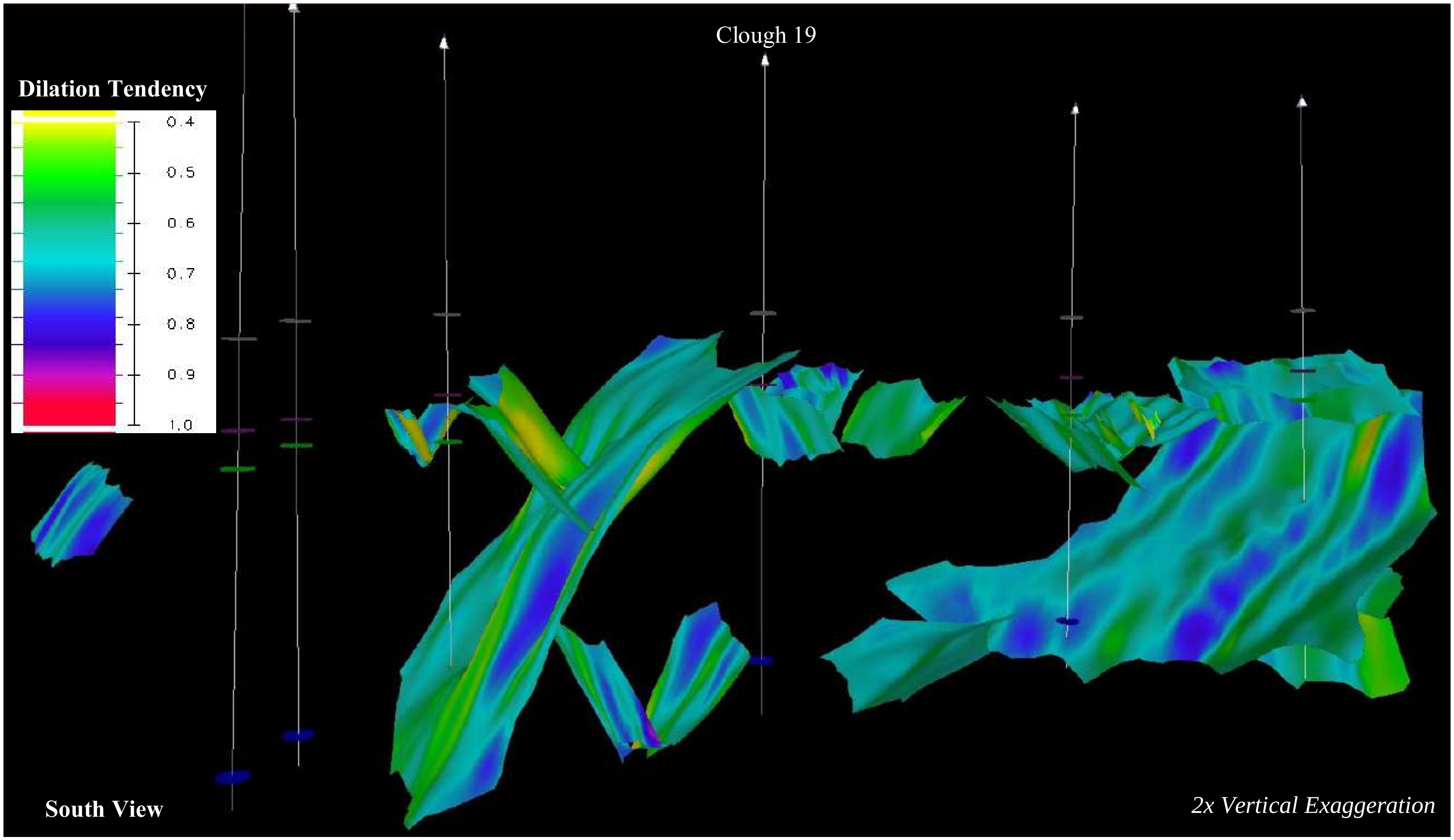

Figure 5.6 – Dilation Tendency (DT) mapped out on all of the fault surfaces. There are areas of high DT along some fault surfaces, while other has low DT values.

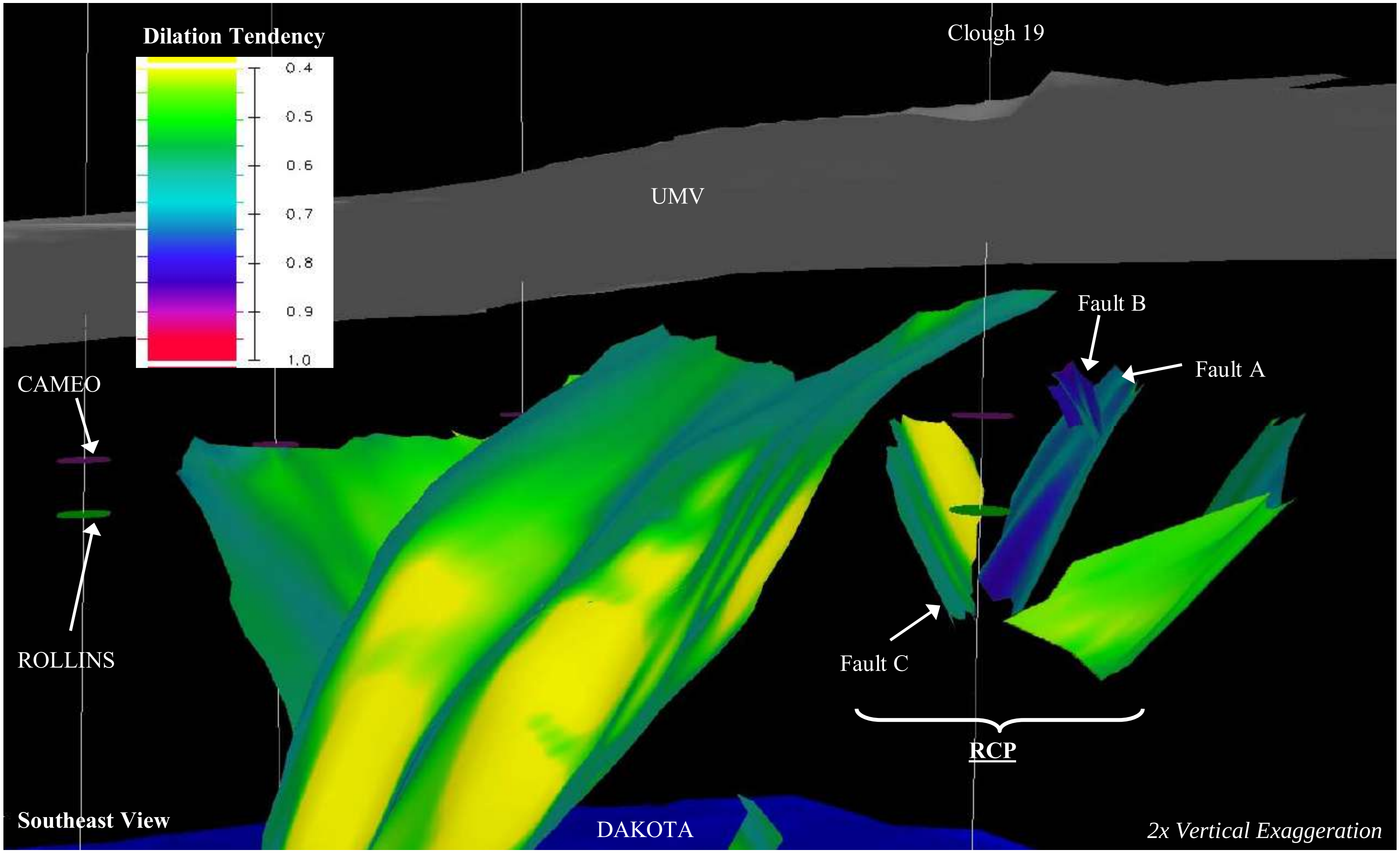

Figure 5.7 – A close up of the RCP study area representing the Dilation Tendency (DT) along the faults. Also, in the background are faults that lie to the east of the RCP study area. The gray surface is the UMV Shale the blue surface is the Dakota Sandstone.

CHAPTER 6

ELASTIC DISCLOCATION MODELING

6.1 Methodology

In this chapter I will discuss the elastic dislocation modeling that I performed on my regional fault interpretation. Elastic dislocation modeling will allow us to analyze how the faults have affected the total rock volume. The affects on the rock that we are interested in are the sub-seismic fractures associated with the larger the faults. We would ideally like to predict their orientation and the density of them within the reservoir. My analysis produced two outcomes. The first is the Maximum Coulomb Shear Stress (MCSS) measurement. The second is a mapped attribute that represents predicted fracture types and orientations. Unfortunately, the outcomes from this modeling are strictly related to the faults and do not take into account any of the regional affects (e.g. background strain).

The maximum coulomb shear stress is a measurement of stress in a body of rock caused by the movement of faults. The greater the stress that has acted on the rock body, the more strain the rock will have undergone. The more strain the rock has undergone the higher the density of fractures we should expect. Having this information will help us understand the distribution of the natural fractures within the rock volume.

This modeling was achieved using the FaultED module in the TrapTester software. With FaultED we can create a surface that we want to deform. This surface could be a horizon or any arbitrary plane of interest. The module then uses various fault property inputs to deform that surface. The deformation on the surface can then be analyzed with respect to its structural significance.

6.2 Results

To understand the elastic dislocation modeling process it is important to understand how the software models the stresses created by the faults. This process is completed through forward modeling of the fault surfaces affects on the deformation plane in combination with any regional, or background, stresses. The software breaks the faults into a series of user defined panels that are used for dip-slip calculations. The amount of movement on each panel is then translated in to a strain tensor at each node or point of a defined observation grid. The resulting strain tensors are then converted to stress tensors using elastic rheology. These stresses are pseudo stresses because they do not represent any relaxation as fault slip was accumulated. The vector attributes (displacement, stress/strain orientations, and stress type) of the nodes can then be visualized at each node point as vectors (Badley 2006). This modeling is performed in the FaultED module of TrapTester.

6.2.1 Elastic Dislocation Inputs

This section will discuss the inputs that the FaultED module uses. FaultED calculates the affects of a series of fault panels on a defined plane within the model. The inputs used focus on the faults and the deformation plane. Some of the fault property inputs are the throw and strike of each fault. The inputs of the deformation surface include various rock properties, such as Poisson Ratio, Young's Modulus, and cohesive strength. This information is run through a series of equations by Okada (1992) that model the elastic properties of rock. Okada (1992) should be consulted for more information on the exact equations.

The fault inputs are rather limited. They are basically the position of the fault and the dip-slip calculations that have been performed on the fault panels. The position of the fault was defined by mapping it in the seismic volume, see Chapter 3. The amount of movement or slip that has occurred on the fault is determined by intersecting the raw horizon data with the fault surface. When the faults and horizons were input into TrapTester they needed to be modeled in a way that they intersect each other. To do this Allen lines are created. Allen lines represent the intersection of a mapped horizon onto a fault surface. The hangingwall and the footwall are both mapped out as lines onto the surface of the fault by projecting the horizon to the fault surface. These lines allow for calculating the displacement or throw that a horizon has undergone because of movement along the fault. Figure 6.1 is a depiction of what the Allen lines look like in TrapTester.

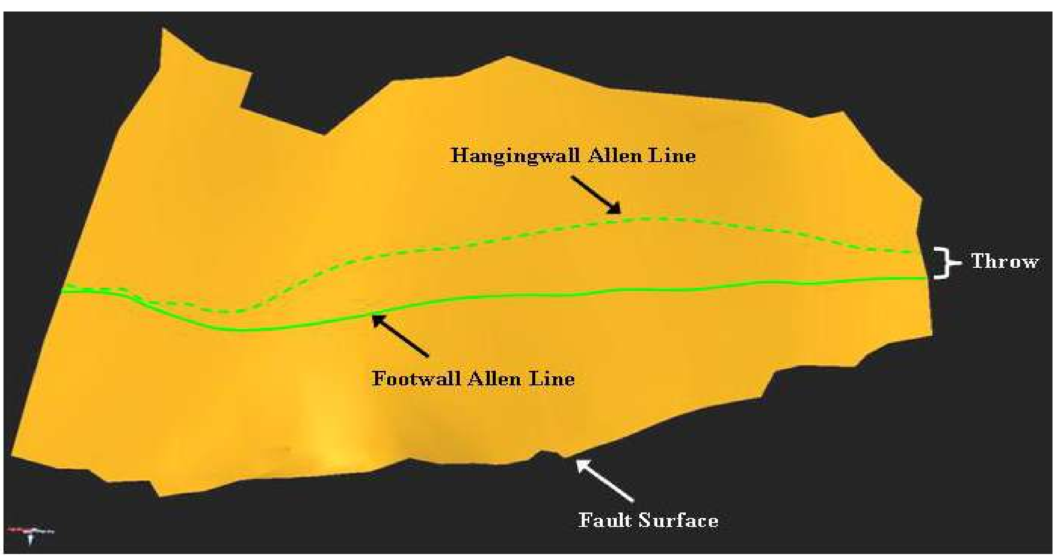

Figure 6.1 – Illustration of Allen lines that have been projected from the Rollins Sandstone on to this fault surface. The amount of throw is determined by calculating the vertical separation between the hangingwall and footwall Allen lines.

The observation grid / deformation surface is where the fault panel calculations are applied and visualized. Here all the rock properties of a surface are input by the user. I decided to use various inputs from the geomechanical modeling work by Higgins (2006). These included Poisson's Ratio, Young's Modulus, and cohesive strength. The values are presented in Table 6.1. The remaining inputs were derived from logs and tables within the software; they include the total density and the coefficient of internal friction.

Five deformation surfaces were created in the software. These surfaces were given definite values for their rock properties and lack any lateral variability. The surfaces represent how a sand body with these properties would deform at any point within the reservoir. Tables 6.1 and 6.2 show each of the inputs used for each deformation surface. The only input that was varied was the total density. Changes were made in the total density to try and reflect the rock densities at that depth or location. However, much of the data is from the RCP study area and is likely to represent the rocks there more than anywhere else on the deformation surface.

	Poisson's Ratio	**Young's Modulus**	**Cohesive Strength**	**Coefficient of Internal Friction**
Input Parameter	0.25	6,000,000 psi	3,767 psi	0.75

Table 6.1 – The inputs used for each deformation surface. The values came from geomechanical modeling done by Higgins (2006).

	UMV Shale	**Cameo Coal**	**Rollins Sandstone**	**Dakota Sandstone**	**Vertical Plane**
Total Density	2.56 gm/cm^3	2.56 gm/cm^3	2.58 gm/cm^3	2.60 gm/cm^3	2.56 gm/cm^3

Table 6.2 – The different total densities used for each deformation surface. The values came from well logs within the RCP study area.

The total density for the vertical plane is the same as the Cameo Coal's total density. This allows us to see how the surface was deformed vertically near the reservoir interval. These surfaces create a three dimensional view of the region surrounding the Cameo Coal.

Four of the five deformation surfaces used were altered so that they would best match the horizon that they represented. The deformation surfaces were designed to cover as much of the horizon as possible. They were also assigned a dip which closely matched the dip of the actual horizon. These dips varied from 1.6 to 2.0 degrees to the northeast. However, each of the deformation surfaces was created on a similar grid. The grid used is a grid that is 500 feet by 500 feet (152.4 m by 152.4 m). This grid gave the greatest amount of resolution with out over stressing the computer. An example of the grid used for the Cameo Coal can be seen in Figure 6.2. The grid used for the vertical plane is the only grid that varied. It had a spacing of 1,000 ft by 250 ft (304.8m by 76.2 m). This plane was also given a dip of 90 degrees relative to horizontal.

The UMV Shale deformation surface was created using the same values defined for the Cameo Coal. This surface doesn't have any mapped seismic faults crossing it. The reason for looking at the deformation surface at this level is to try and understand how the faults deeper in the strata are affecting this level.

6.2.2 Maximum Coulomb Shear Stress

Calculating the Maximum Coulomb Shear Stress (MCSS) is a relative way of measuring the potential shear failure that a rock body has undergone. Shear failure can be directly related to fractures.

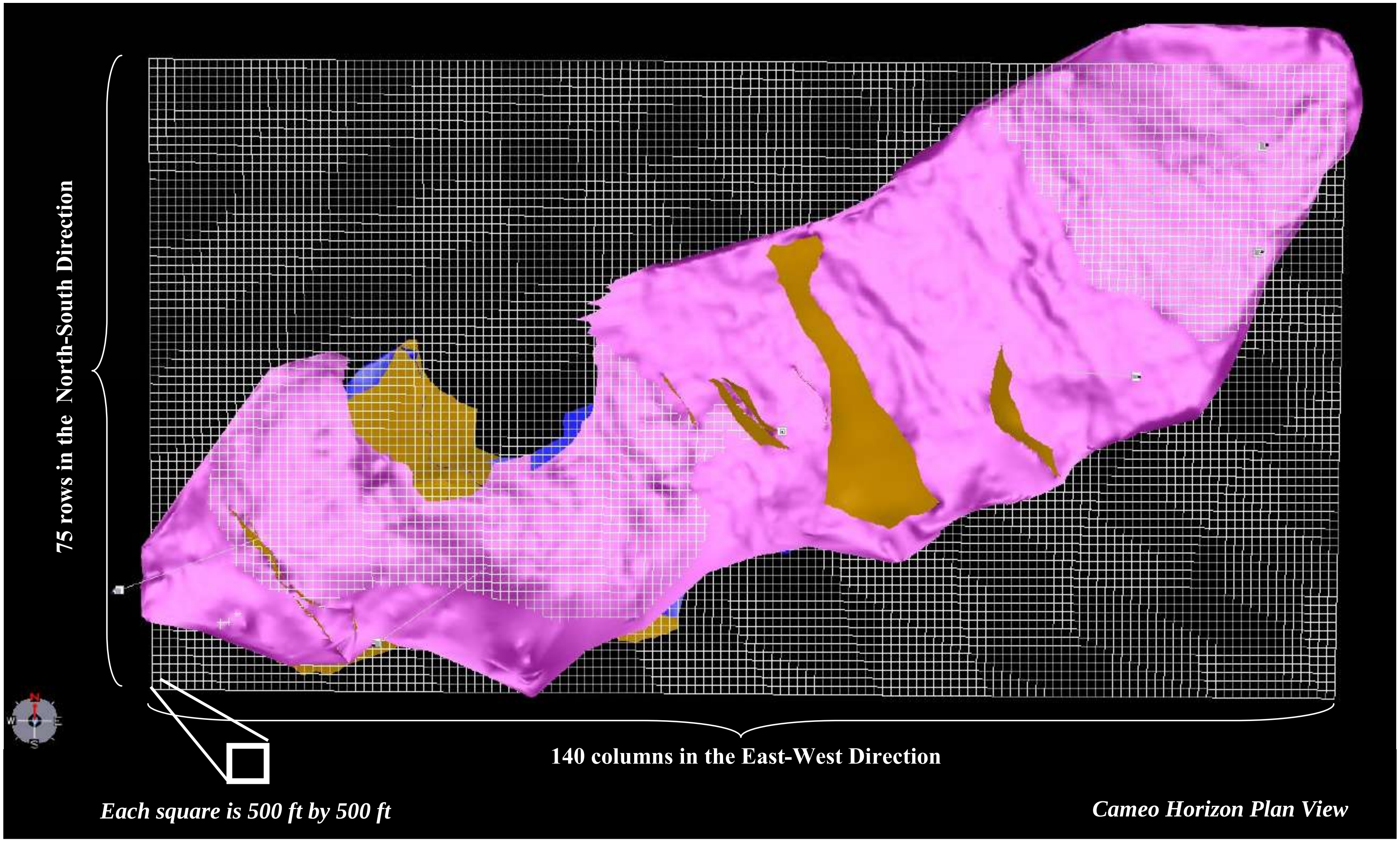

Figure 6.2 – Plan view of the Cameo Coal horizon (pink). The grid shown is the grid used for the elastic dislocation modeling. The brown planes intersecting the pink Cameo are faults. Each square in the grid is 500 ft by 500 ft. This same grid was used for all of the deformation surfaces.

The more shear failure a rock has undergone the higher the fracture density we should expect (Badley, 2006). While being able to predict where, when, and how many fractures is a distant goal, we can use the Maximum Coulomb Shear Stress (MCSS) calculations to help predict fracture density. MCSS is the intercept, on the shear stress axis, of a tangent to the Mohr circle having the same slope as the Coulomb failure envelope, (Figure 6.3). Shear failure of the rock is expected when the MCSS exceeds the cohesive strength of the rock. Larger values of MCSS are expected to correlate with higher fracture densities, (Badley, 2006). Figure 6.3, shows that when the intercept of the tangent to the Mohr circle is below the cohesive strength (C) of the rock there is no shear failure of the rock. When the intercept of the tangent is higher then the cohesive strength of the rock shear failure occurs. The greater the difference between the cohesive strength of the rock and the MCSS value the greater the deformation of the rock body. The more deformation the more sub-seismic fractures we would expect within the rock volume.

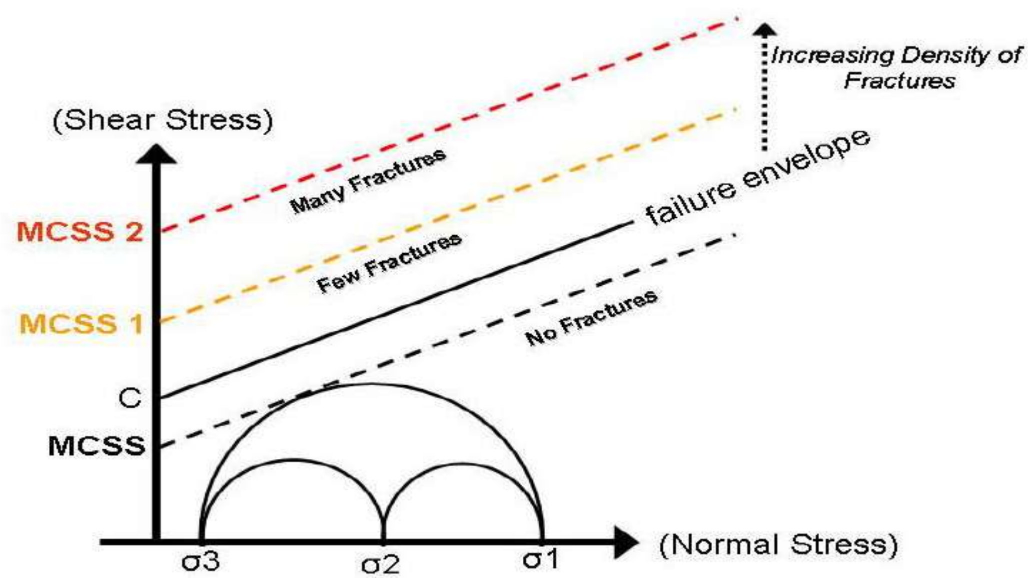

Figure 6.3 – Diagram representing how Maximum Coulomb Shear Stress (MCSS) is determined. This diagram also shows the relationship between MCSS, cohesive strength (C), and fracture density. Image modified from Badley, (2006).

Figures 6.4, 6.5, 6.6, and 6.7 show the results of the modeling the MCSS on the Cameo Coal, Rollins Sandstone, Dakota Sandstone, and an arbitrary vertical plane through the survey. The MCSS results are strictly related to the affects of the faults movement on the deformation planes. There is no larger regional deformation being considered within these models. From the models it is evident that not all faults are the same. The MCSS changes along strike on several of the fault planes.

Figure 6.8 shows the result of modeling the MCSS on the UMV Shale interval. This interval has no seismically mapped faults penetrating it. However, we can see that the faults deeper in the reservoir are having an affect on the UMV Shale. This affect can also be seen in Figure 6.7 to a limited extent.

6.2.3 3-D Subseismic Fracture Model and Fault Stress Analysis

The fracture model is a prediction that is based on the various stress tensors that have been created in the elastic dislocation model. The elastic dislocation model generates fault panels that create a stress field independently for each panel. When two panels interact with each other their stresses generate compression or tension depending on the kind of interrelationship (Gutierrez, 2007). The predicted fracture planes are orthogonal planes that represent the orientations of the stresses. Figure 6.9 represents a generalized two dimensional example of how the panels determine compression and tension in the software.

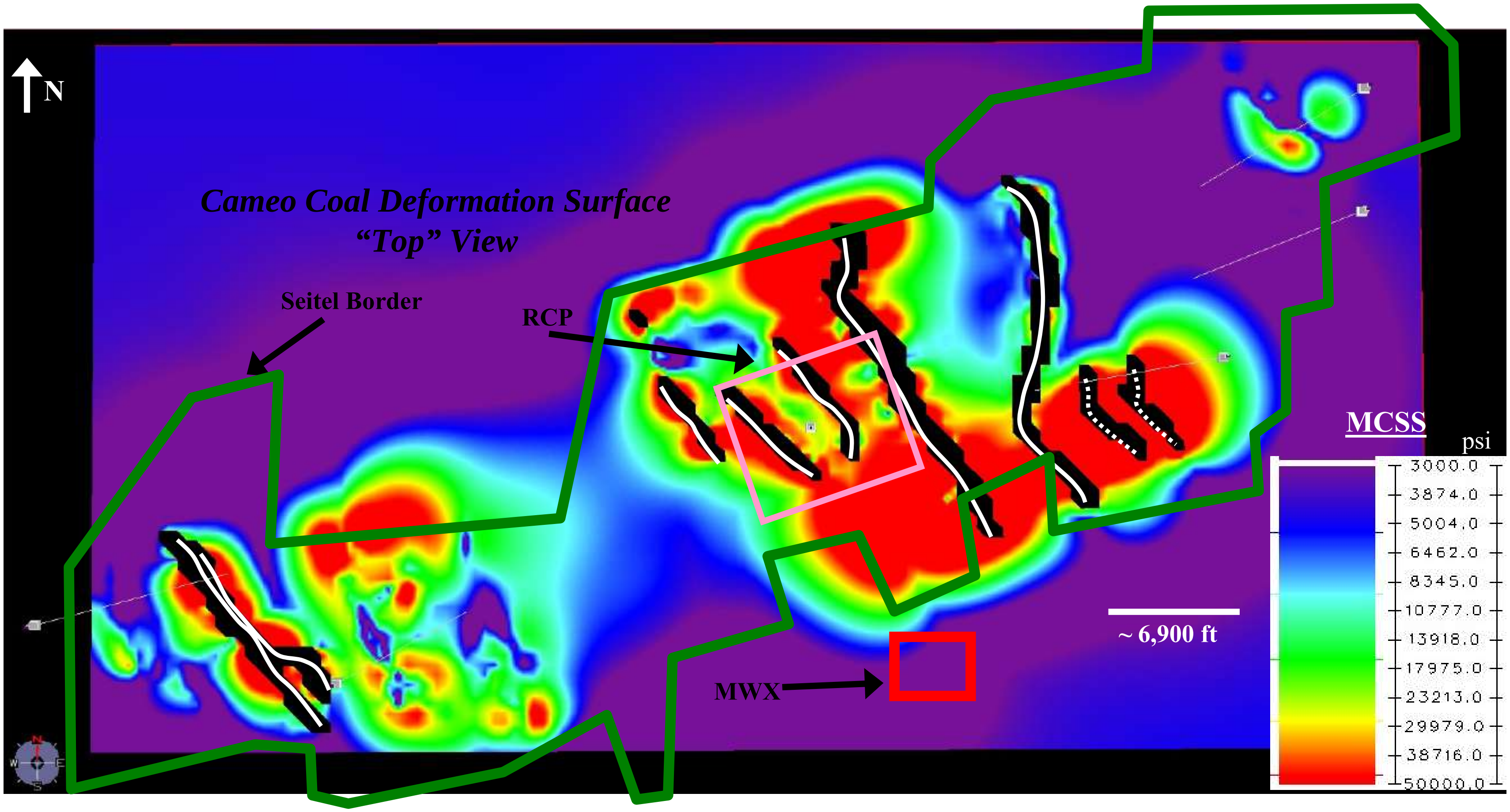

Figure 6.4 – Top view of the modeled deformation surface at the Cameo Coal depth. The colors mapped out represent the amount of MCSS at that point on the surface. Solid white lines are where the faults cut the surface, dashed white lines are where a fault above or below is deforming the surface with out contacting the surface.

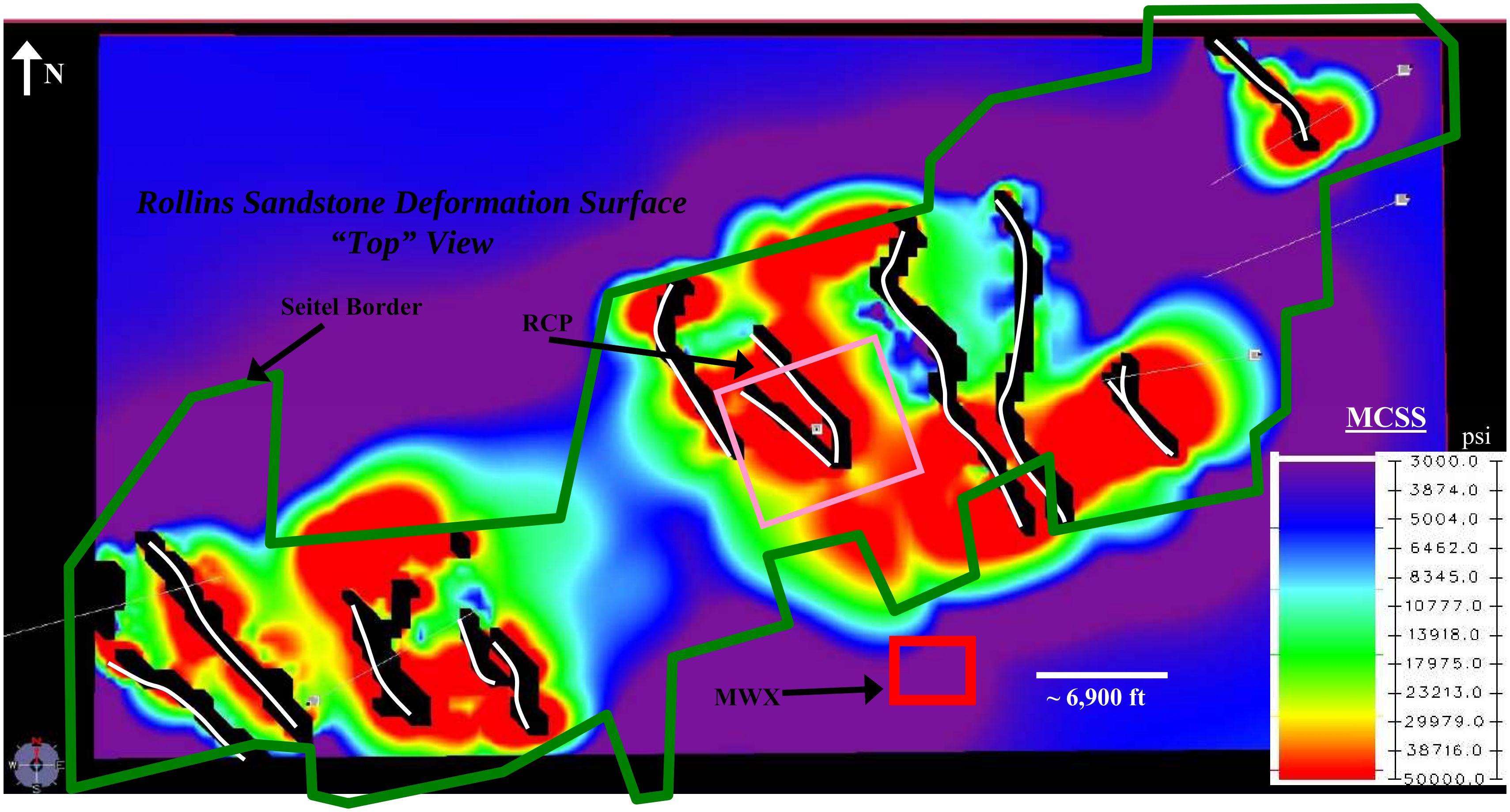

Figure 6.5 – Top view of the modeled deformation surface at the Rollins Sandstone depth. The colors mapped out represent the amount of MCSS at that point on the surface. Solid white lines are where the faults cut the surface, dashed white lines are where a fault above or below is deforming the surface with out contacting the surface.

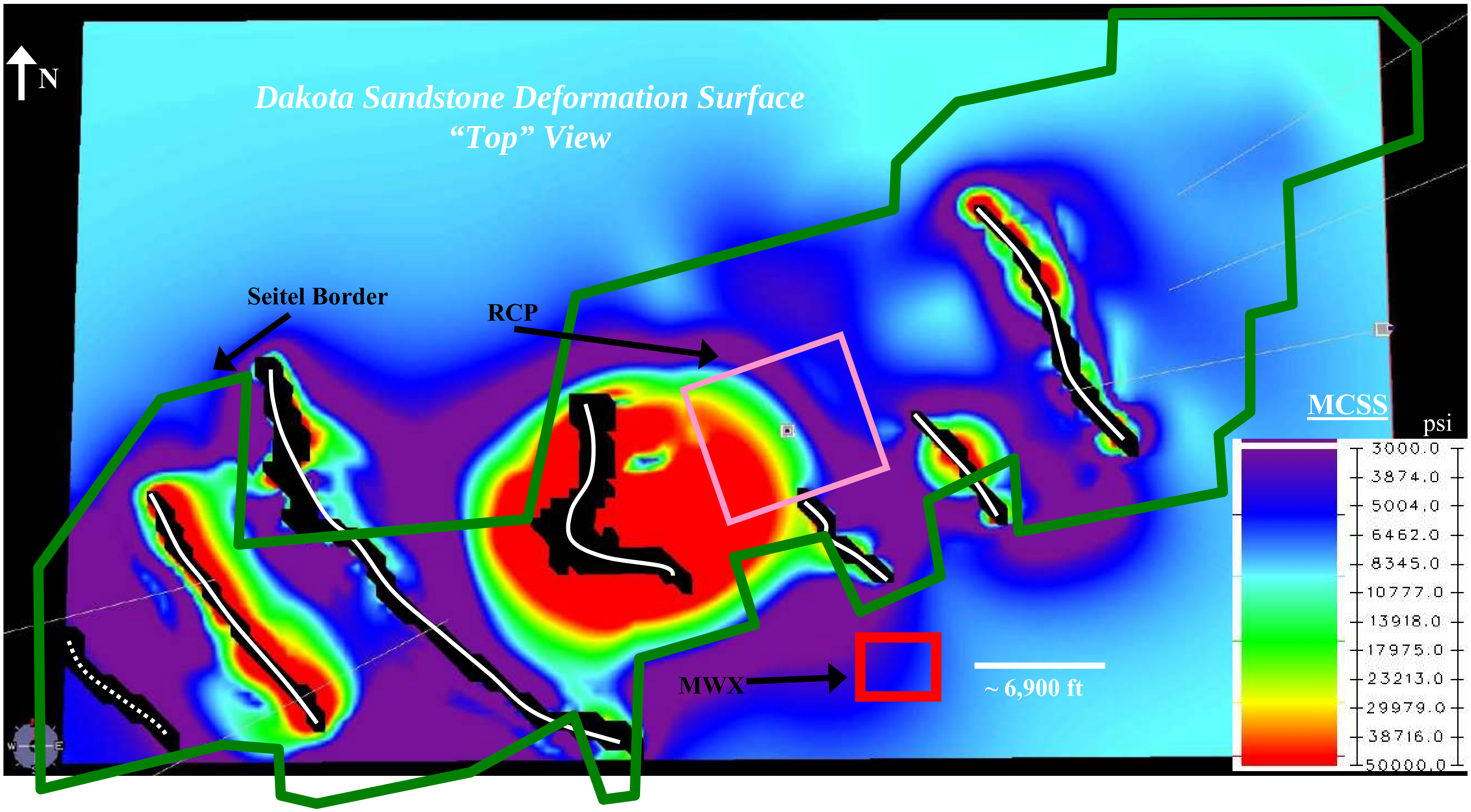

Figure 6.6 – Top view of the modeled deformation surface at the Dakota Sandstone depth. The colors mapped out represent the amount of MCSS at that point on the surface. Solid white lines are where the faults cut the surface, dashed white lines are where a fault above or below is deforming the surface with out contacting the surface.

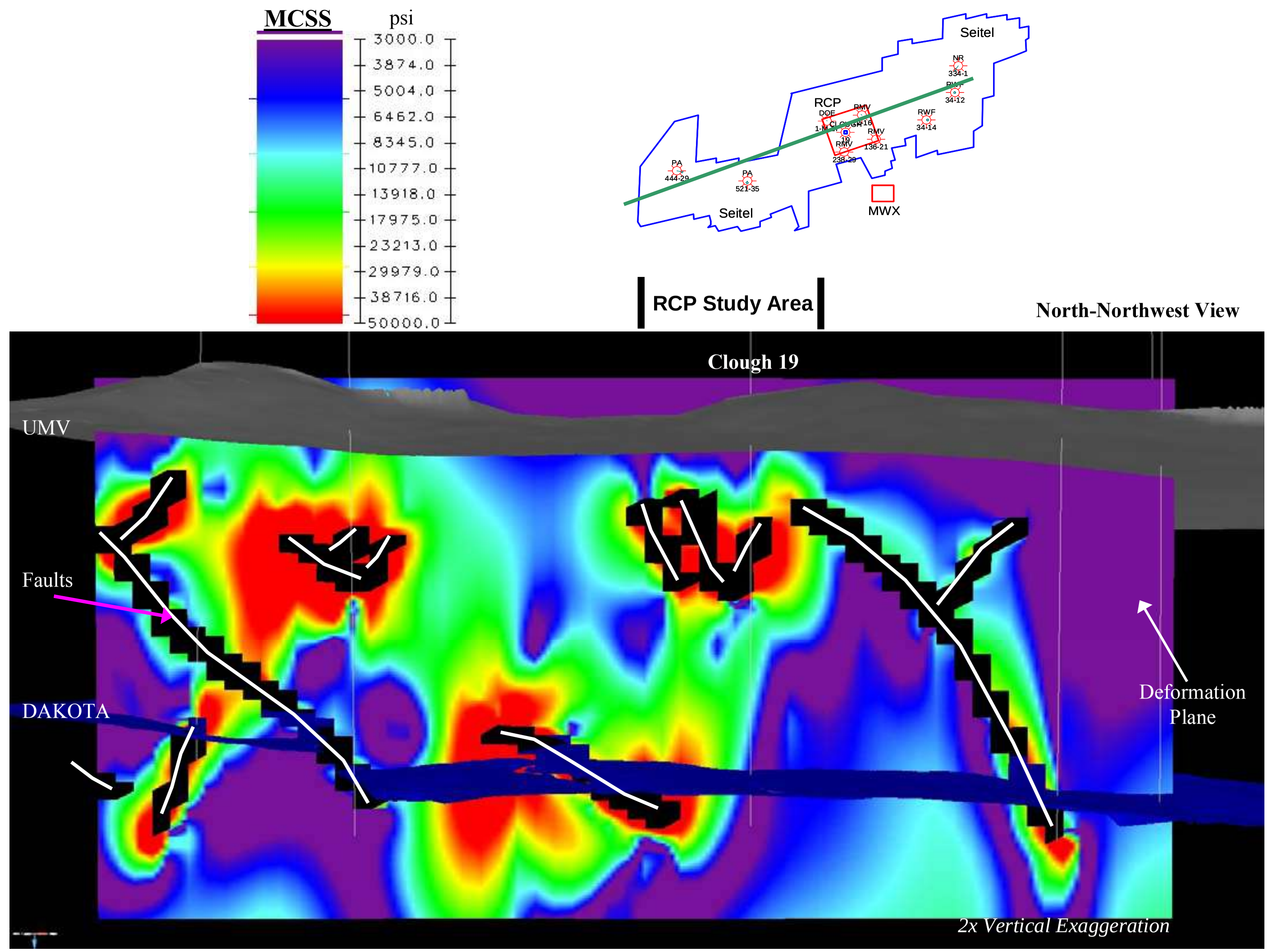

Figure 6.7 – A Side view of an arbitrary deformation plane cut through the survey. This view shows the vertical planes deformation caused by the faults. The white lines are where the fault intersects the plane.

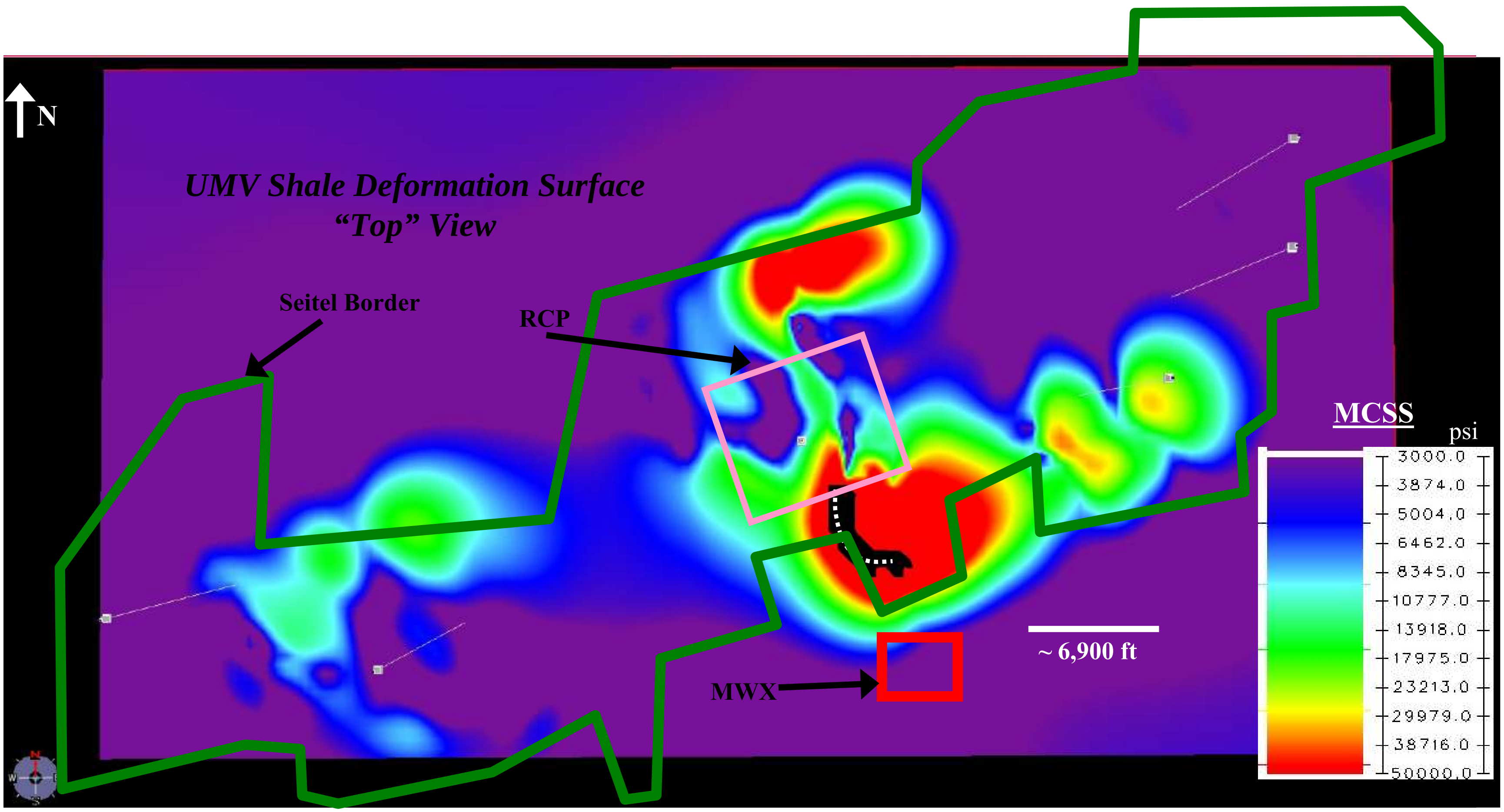

Figure 6.8 – Top view of the modeled deformation surface at the UMV Shale depth. The colors mapped out represent the amount of MCSS at that point on the surface. Solid white lines are where the faults cut the surface, dashed white lines are where a fault above or below is deforming the surface with out contacting the surface.

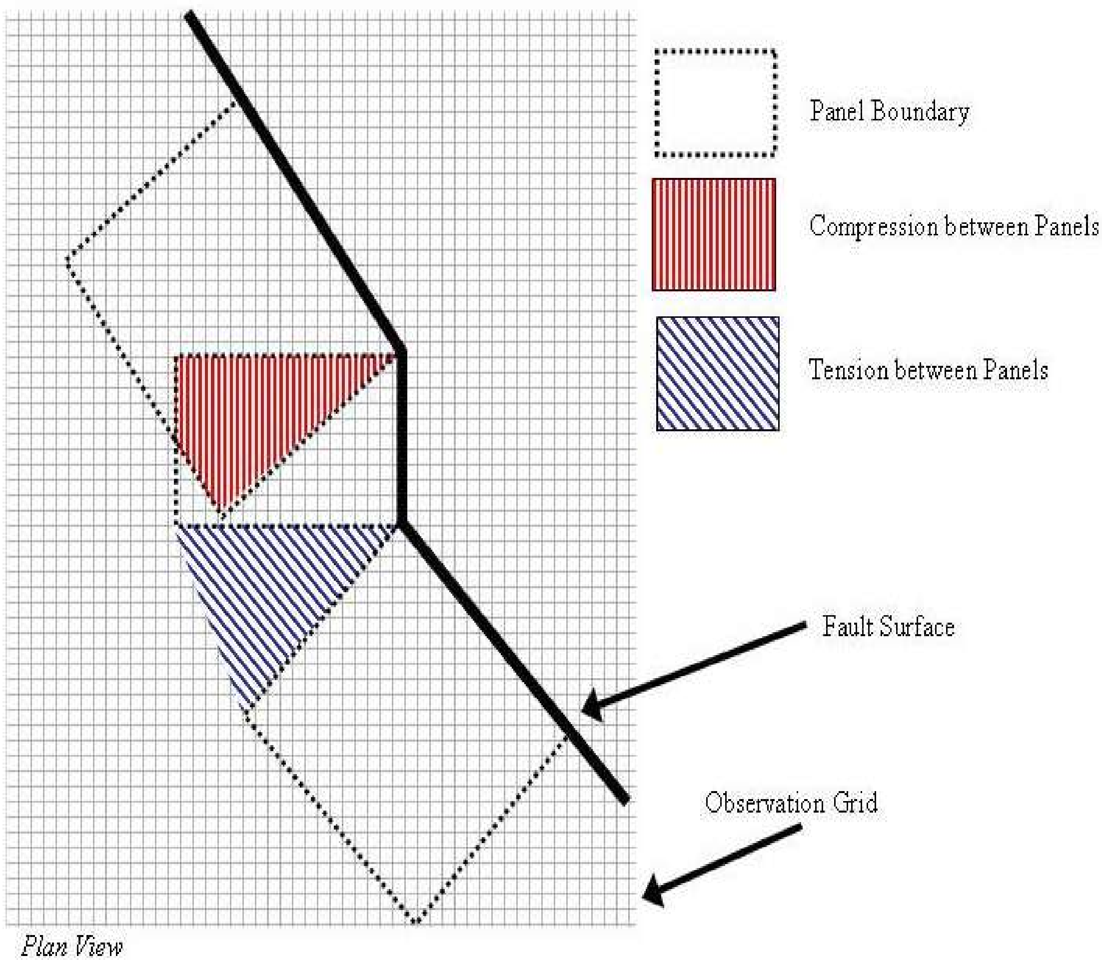

Figure 6.9 – Generalized example of how the FaultED module determines compressional and tension orientations from the fault panels.

Figure 6.10 shows what the different stress arrows / vectors look like in the software. The green arrows represent a net compressional pseudo stress in the direction indicated by the arrow, while the red arrows represent the net tensional pseudo stress. Some of the nodes have either both tensional stress arrow, both compressional, or one of each. The arrow also represents the orientation of either the maximum stress or the minimum stress. The color does not tell which is which. The planes present indicate which set of arrows represents the maximum stress (light green plane) or the minimum stress (light pink plane). The set of arrows that is perpendicular to the plane are representing that planes stress designation. The stress arrow attributes below have all been produced from the interaction of the fault panels described above.

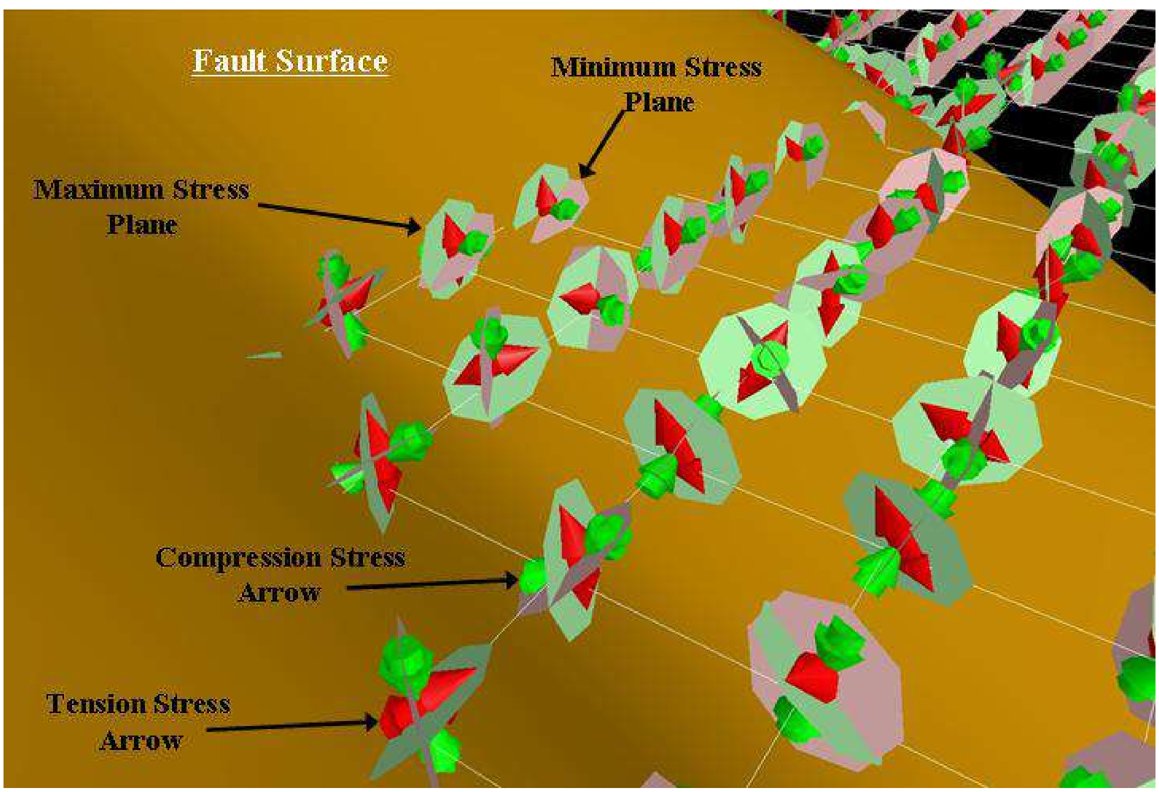

Figure 6.10 –Pseudo stress directions and vector attribute explanation. Green arrows are compressional stresses, red arrows are tensional stresses, light green plane is perpendicular to maximum stress direction, and light pink plane is perpendicular to minimum stress direction.

From the vector attributes determined at each node we can predict the failure planes. The failure planes predict what fracture orientation would be present at that node. The software will predict five different failure planes based off of the calculated vector attributes:

- Normal Shear Planes - conjugate normal faults.
- Reverse Shear Planes - conjugate reverse faults.
- Dextral Strike-slip planes - dextral plane in strike-slip conjugate pair.
- Sinistral Strike-slip planes - sinistral plane in strike-slip conjugate pair.
- Tensile Failure planes - tensile fracture plane.

When the failure criterion is met in the software failure planes are generated at the various nodes. Each type of failure plane gives valuable information on how the stresses at that node are deforming the rock body. When we analyze all of the failure planes generated on the deformation surface we can understand how the faults are deforming that surface.

Fracture Generation

The surfaces/grids used for the Maximum Coulomb Shear Stress calculation in section 6.2.2 are the same surfaces/grids used for the fracture generation. Using the same surfaces gives us a link allowing us to analyze the orientation and type of failure planes in relation to the Maximum Coulomb Shear Stress. The analysis of each of the horizons as well as the vertical plane in relation to the MCSS is discussed in Chapter 7.

Fracture Types and Orientations

The grids for the UMV Shale, Cameo Coal, Rollins Sandstone, and the Dakota Sandstone can be seen in the following Figures (6.11, 6.12, 6.13, and 6.14). Each grid shows the failure planes color coded by type:

Failure Plane Color Code

Dark Blue – Normal Shear

Red – Reverse Shear

Purple – Sinistral Strike-slip

Light Blue – Dextral Strike-slip

Green – Tensile Shear

The strike of each fracture set tends to vary based on their proximity to a fault zone and the complexity of that fault zone. This is because of the various components that have been derived from the faults that have been used to determine the vector attributes at each node. The deformation surface is just that, a deformation surface. Stresses active at one point on the surfaces affect those around that point. What is visible here is the net affect of all the stresses created by the faults.

Fracture sets that are far away from the Seitel (2003) boundary should be treated with caution, since the calculations in these areas are unconstrained, as there are no mapped faults out side of the Seitel (2003) survey. However, from these four images we are able to see the relationship between the fault locations and the deformation the faults have created on the various surfaces. Areas in the figures that do not have colors are areas of the grid that have not been deformed enough to create failure of the rock. Figure 6.15 is a view of the vertical deformation plane.

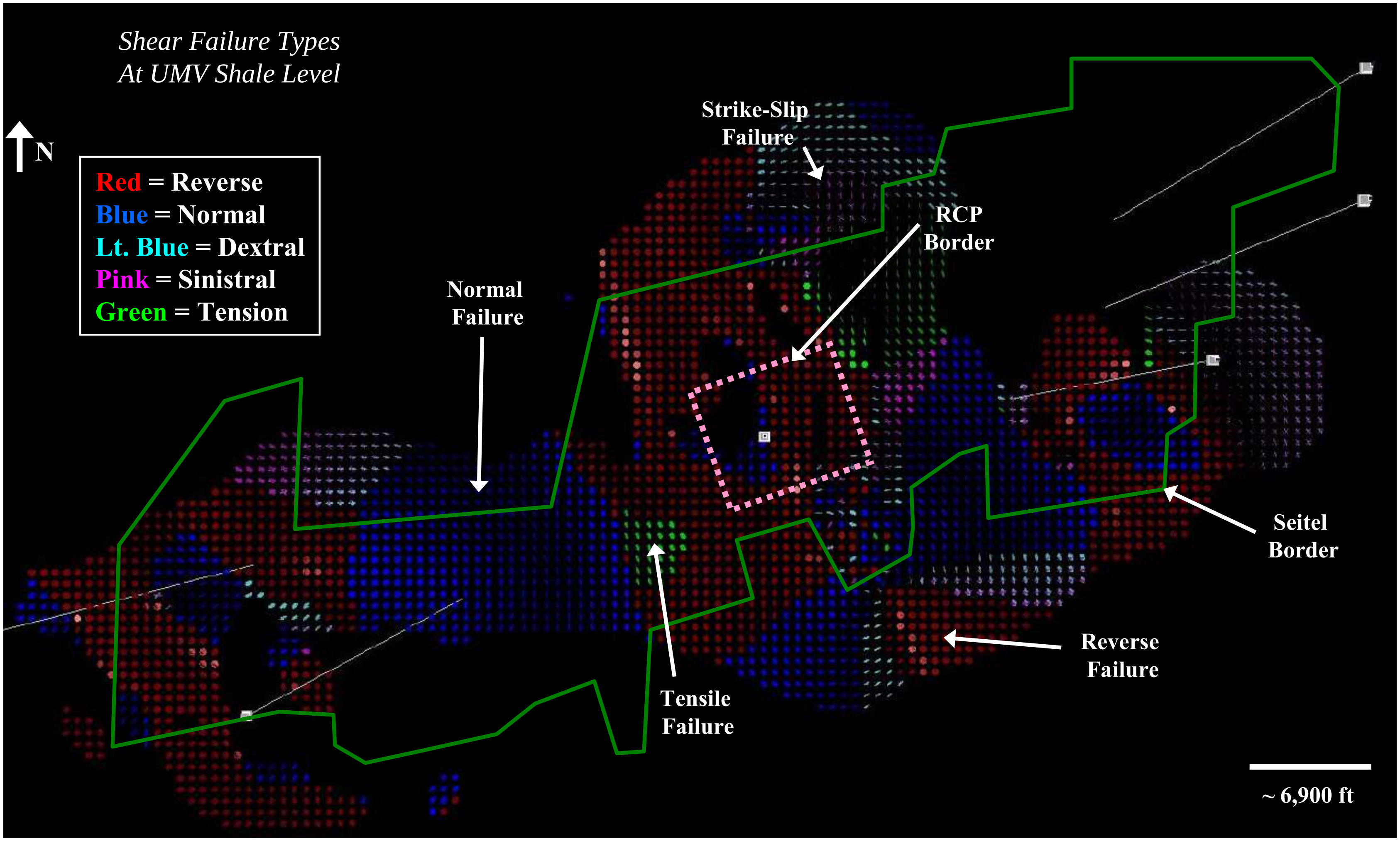

Figure 6.11 – Top view of the various fracture types generated on the UMV Shale deformation surface. Areas of no color represent areas on the deformation surface where the stresses did not exceed the threshold limit.

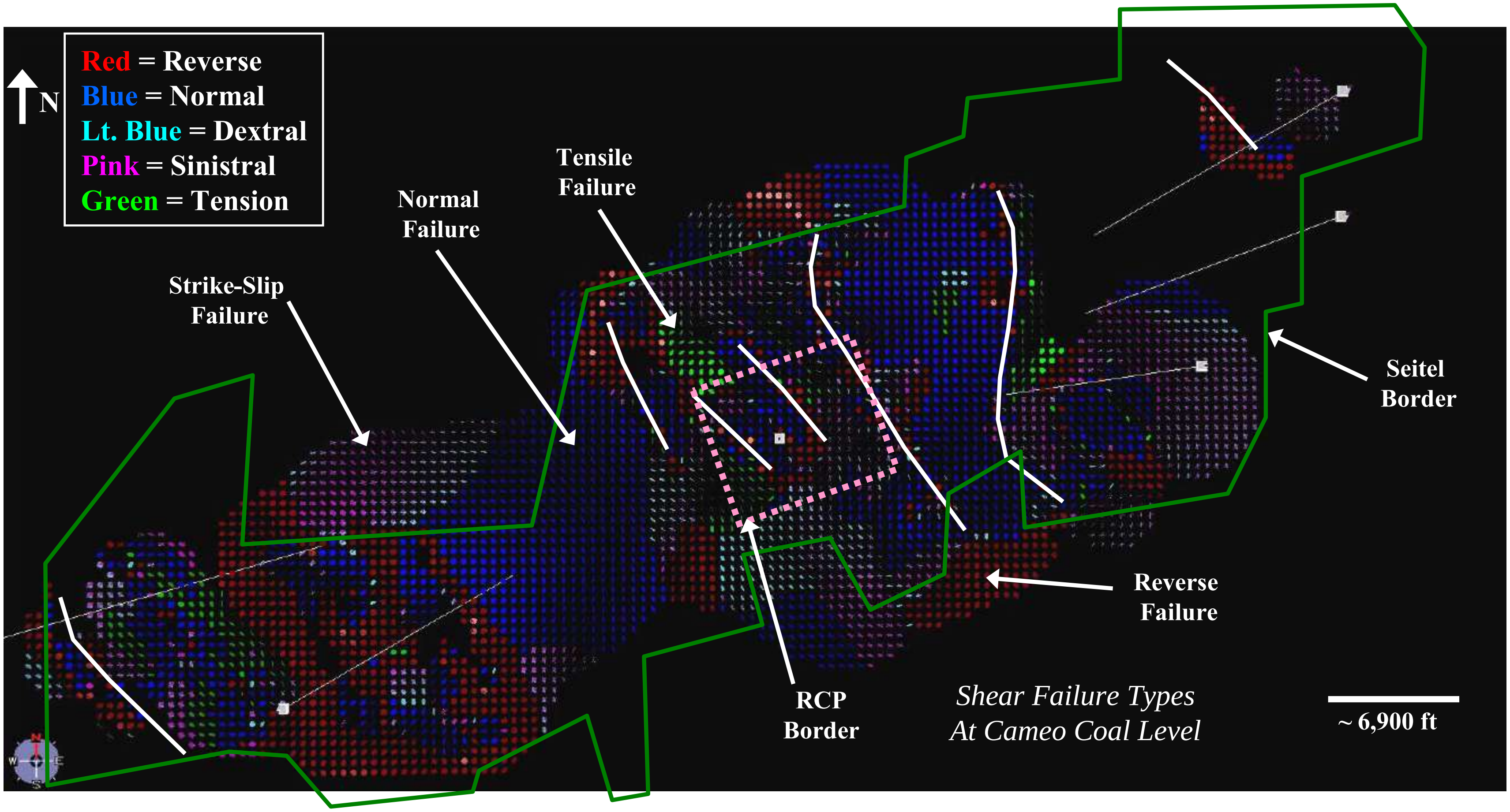

Figure 6.12 – Top view of the various fracture types generated on the Cameo Coal deformation surface. Areas of no color represent areas on the deformation surface where the stresses did not exceed the threshold limit. The white lines are faults.

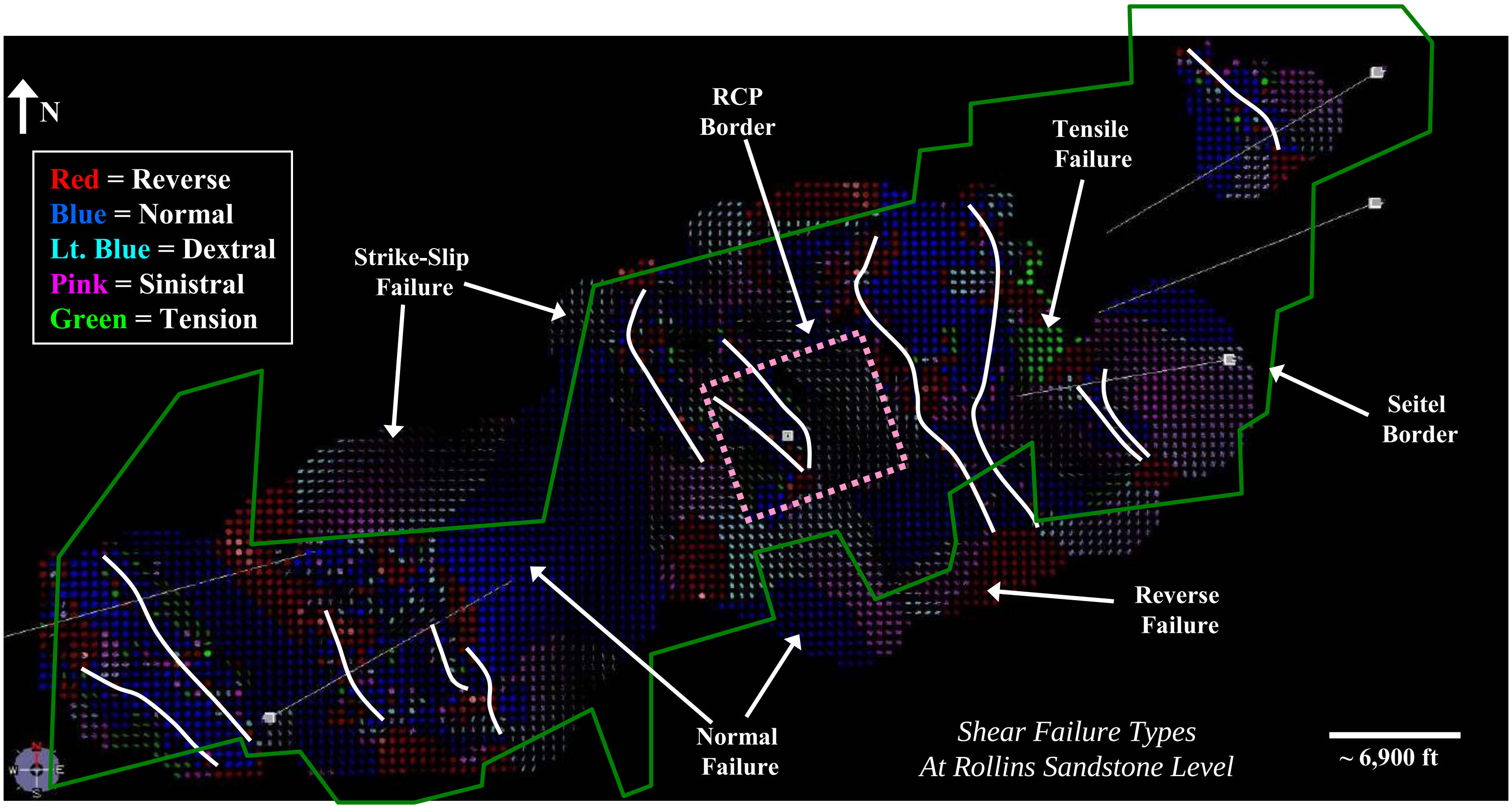

Figure 6.13 – Top view of the various fracture types generated on the Rollins Sandstone deformation surface. Areas of no color represent areas on the deformation surface where the stresses did not exceed the threshold limit. The white lines are faults.

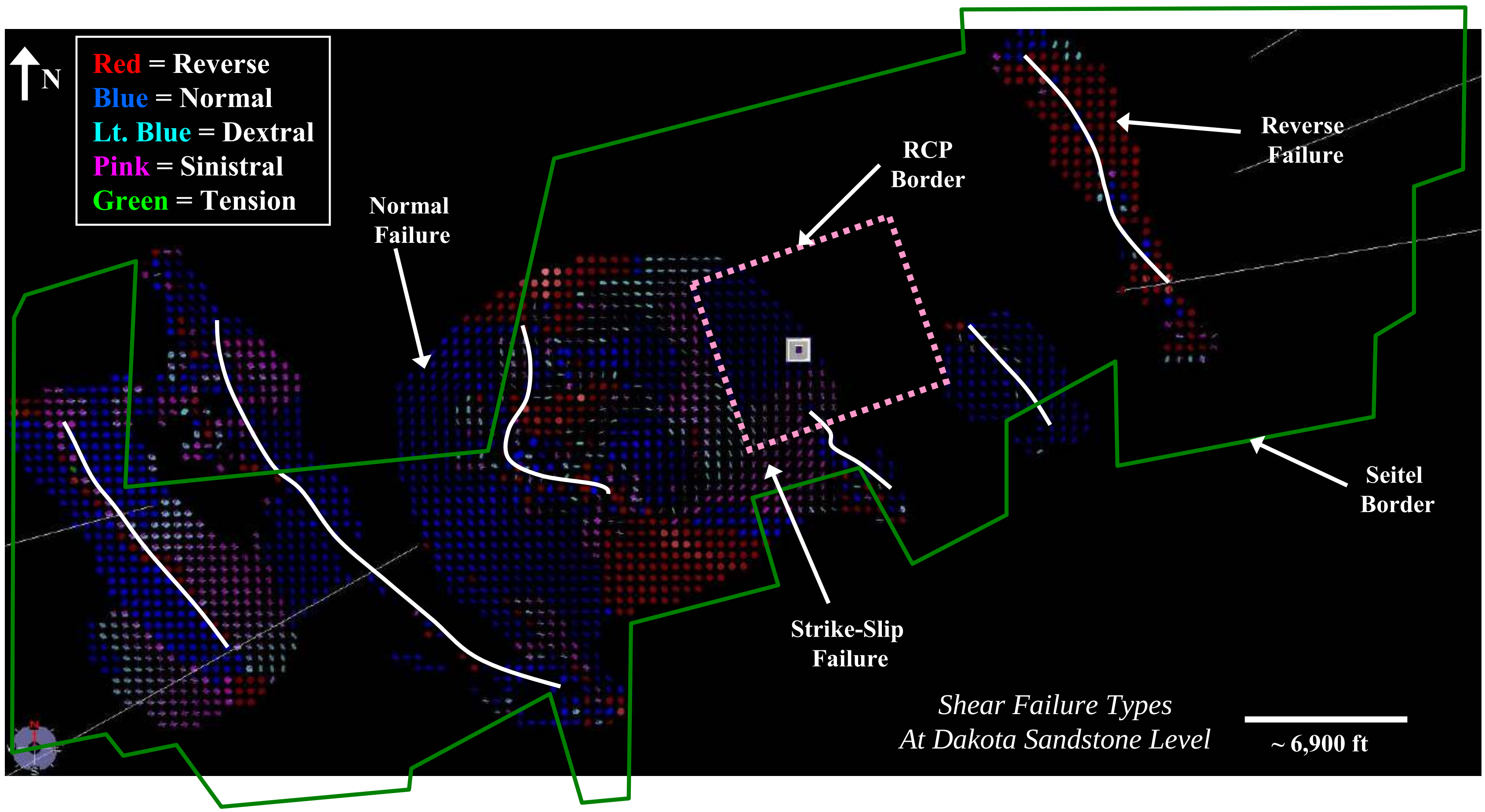

Figure 6.14 – Top view of the various fracture types generated on the Dakota Sandstone deformation surface. Areas of no color represent areas on the deformation surface where the stresses did not exceed the threshold limit. The white lines are faults.

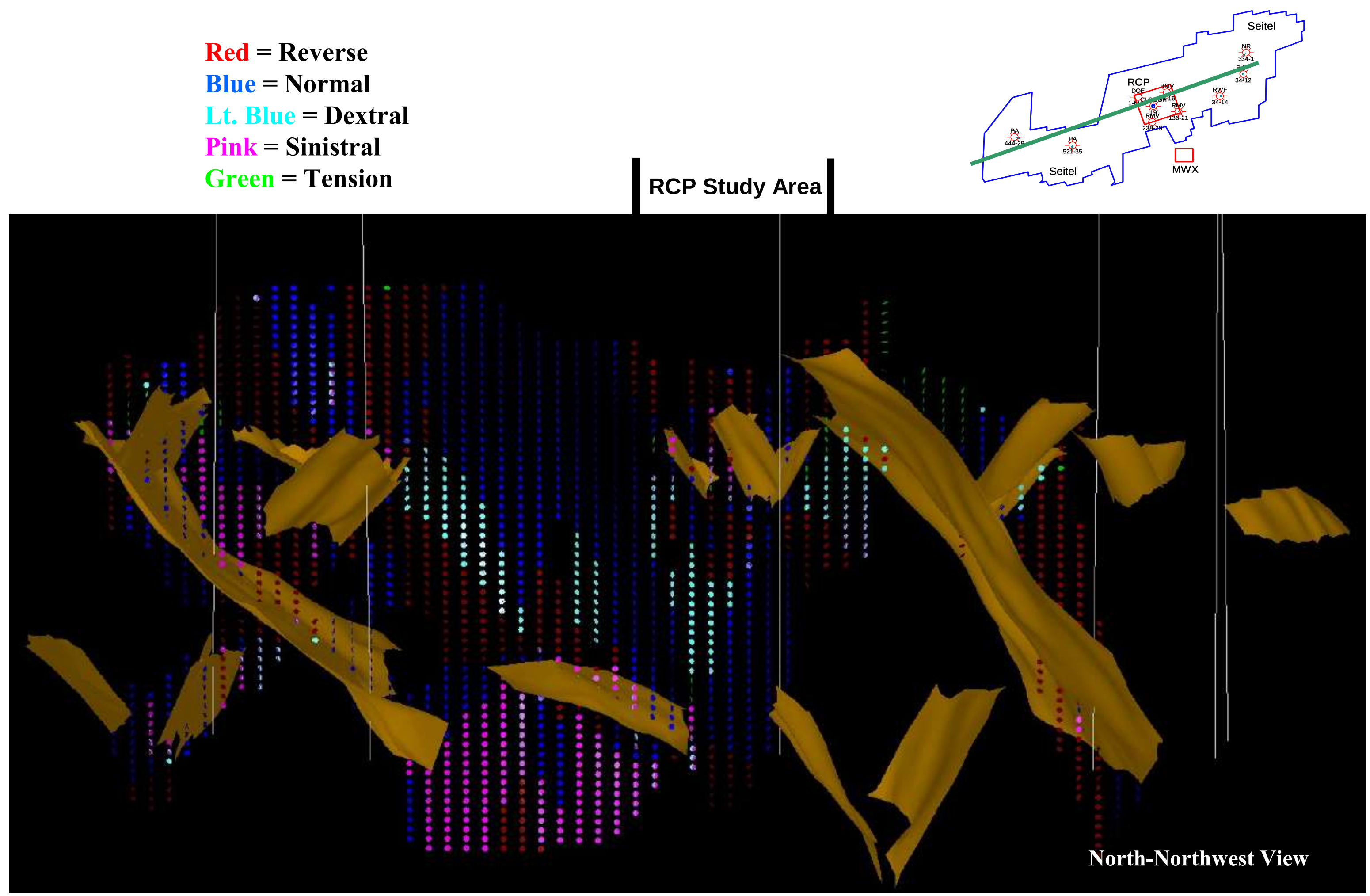

Figure 6.15 –Side view of the arbitrary plane through the model. Areas of no color represent areas on the deformation surface where the stresses did not exceed the threshold limit. The tan surfaces are faults.

CHAPTER 7

DISCUSSION

7.1 Structural Evolution of the Rulison Field Study Area

From the interpretation described in Chapter 3, there is direct subsurface seismic evidence for at least two structural styles to have been active during structural evolution of the Rulison area; initially an extensional phase, followed by a compressional phase. These phases were separated by the partial deposition of the Mesaverde Formation. During the compressional phase several of the older extension faults were reactivated with a reverse sense creating inversion geometry. These inverted faults propagate up from deeper in the stratigraphic section. Figure 7.1, represents a simplified version of this concept.

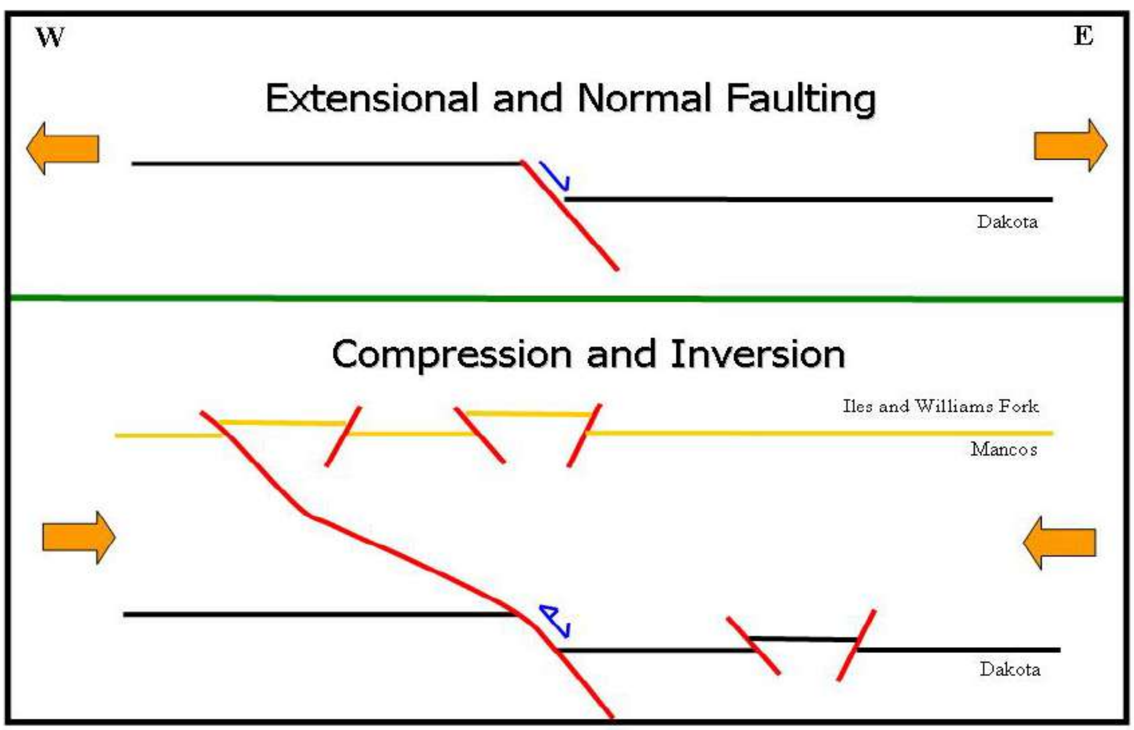

Figure 7.1 – A simplified representation of the two structural styles that are present in the Seitel (2003) survey.

During the compressional phase, not only were several of the older faults reactivated by inversion, but small thrust "pop-up" blocks developed within the reservoir interval, as well as at the Dakota Sandstone level. These small pop-up blocks can be seen in line 90 (Figure 3.2 and 3.2a, see Appendix A). Many of these thrust blocks are bounded by reverse faults, internal splays, and back thrusts, as represented in Figure 7.2. While some of these pop-up blocks are connected to the deeper inverted faults, others are confined to the brittle intervals through out the stratigraphic section.

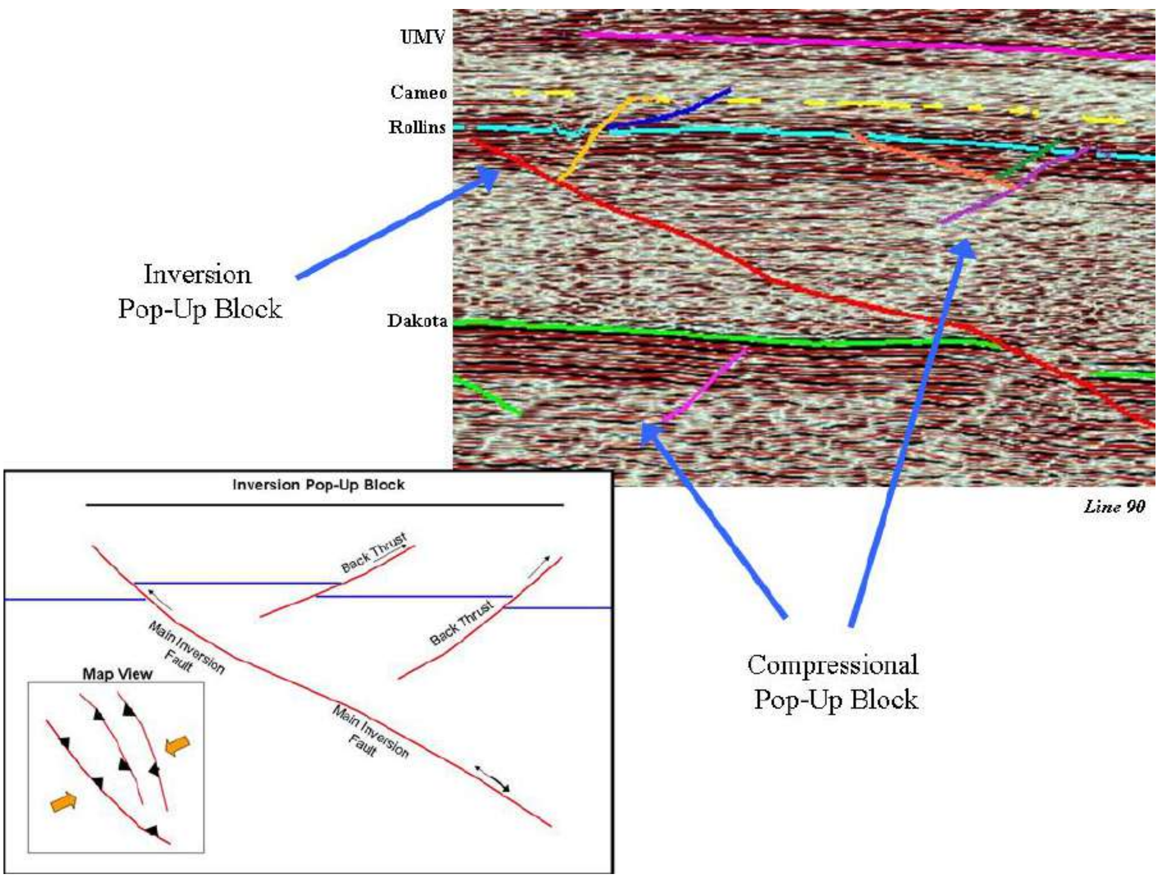

Figure 7.2 – Seismic line 90 showing the difference between inversion pop-up blocks as well as normal compressional pop-up blocks.

The regional stress field that would have caused the final structural style that is present in this area of the Piceance Basin must have been compressional in nature and with sigma 1 ($\sigma 1$), or the maximum horizontal stress, in an east-west direction. This coincides with the $\sigma 1$ orientation of Laramide stresses during the late Cretaceous.

When we look at the locations of the brittle deformation zones within the Dakota and the Rollins/Cameo we can see there is a lateral offset. The stresses during the Laramide, that reactivated the deeper previous faults systems, seems to have propagated further to the west about a mile and half through the more ductile Mancos interval than through the more rigid Rollins/Cameo interval. This effect can be seen in the previously shown seismic lines of Chapter 3 (Figures 3.1 and 3.2, (Figures 3.1a and 3.2a, see Appendix A)).

Timing of Faulting

From the interpretation we can also derive some basic ideas about the timing of the faulting with in the reservoir as well as some indication as to how the various formations were deposited in this area. Figure 7.3 is an interpretation of line 90 from the Seitel (2003) survey. Figure 7.4 is the stepped evolution of line 90 and is described below. Line 90 can also be seen in Figure 3.2 (Figure 3.2a, see Appendix A) un-interpreted.

It is apparent from the figure that right after the deposition of the Dakota Sandstone the extension occurred. Evidence for this is that the interval of reflectors including the Dakota is the only interval that has a normal component of movement to it. There is also evidence from the seismic line for a hiatus of deposition at this time after the extension occurred. There is a small wedge of sediment deposited adjacent to the major normal fault of line 90. After this wedge formed the deposition of the marine Mancos Shale began. The Mancos Shale comprises the middle portion of the seismic line, and is composed of highly discontinuous reflectors. Deposition then continued through the Rollins, Cozzette, and Corcoran Members of the Iles Formation and into the Cameo Coal interval of the Williams Fork Formation.

During the deposition of the fluvial Williams Fork the compressional faulting of the Laramide began. Many of the Laramide aged faults are confined to the middle Williams Fork and formations stratagraphically lower than the Williams Fork. Cumella and Ostby (2003) also noted that the thickness of the Cameo drastically increases near the faults suggesting structural growth of the faults during deposition. These lines of evidence suggest that Laramide faulting was still occurring through the deposition of the Cameo Coal.

Within the Williams Fork is the UMV Shale marker. This shale marker clearly drapes across the entire survey and has no seismically visible faults crossing it. This draping suggests the UMV Shale marks the end of Laramide related faulting within the survey.

With this information we interpret that the major faulting within the Rulison area began with extension during the late Albian or early Cenomanian, and ended in the middle to late Cenomanian. The next major faulting episode within the Rulison area began and ended in the Campanian as compressional faulting. This faulting included the reactivation of deeper pre-existing structures.

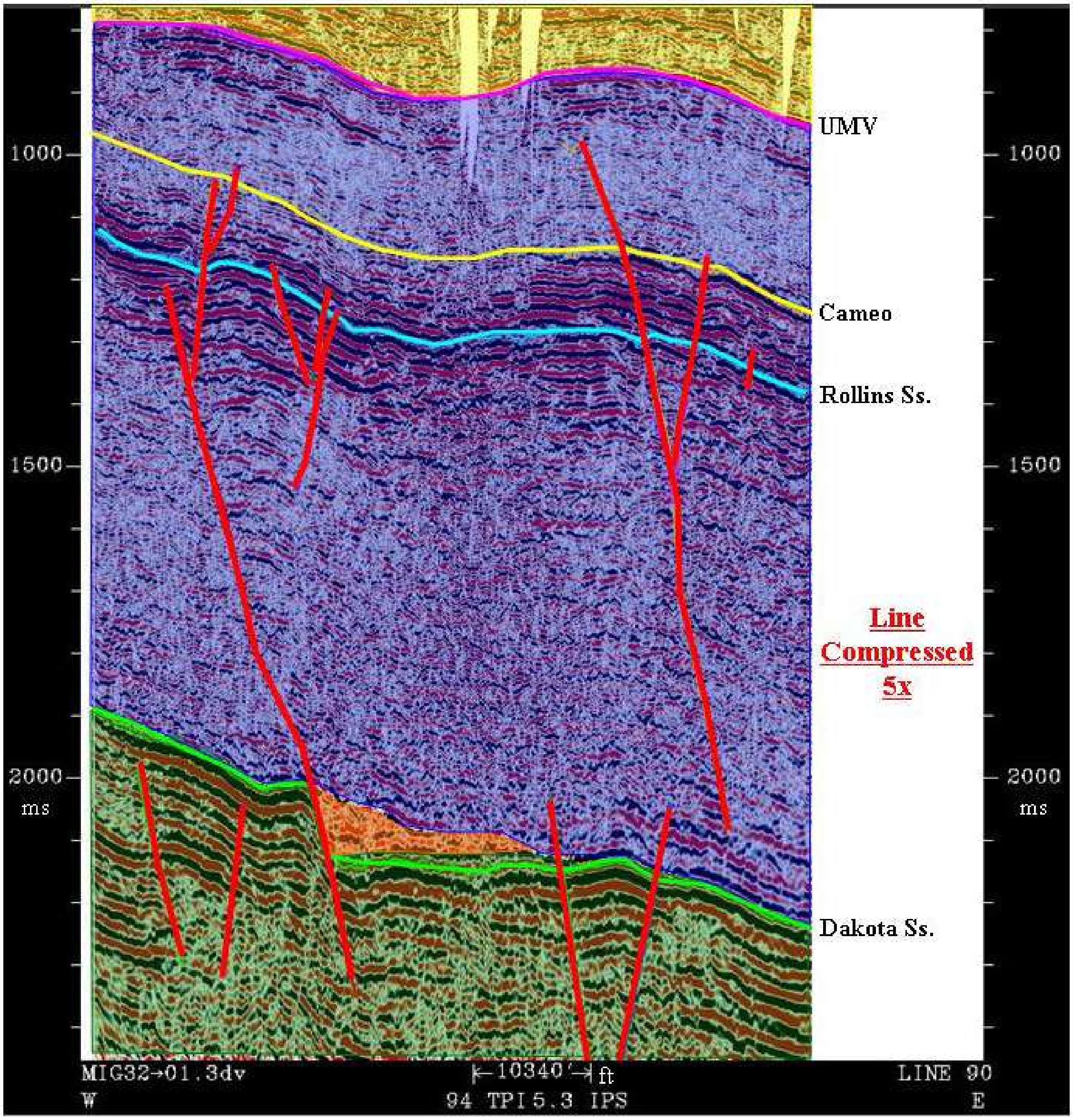

Figure 7.3 – Seismic line 90 from Seitel (2003) survey showing the colored interpretation.

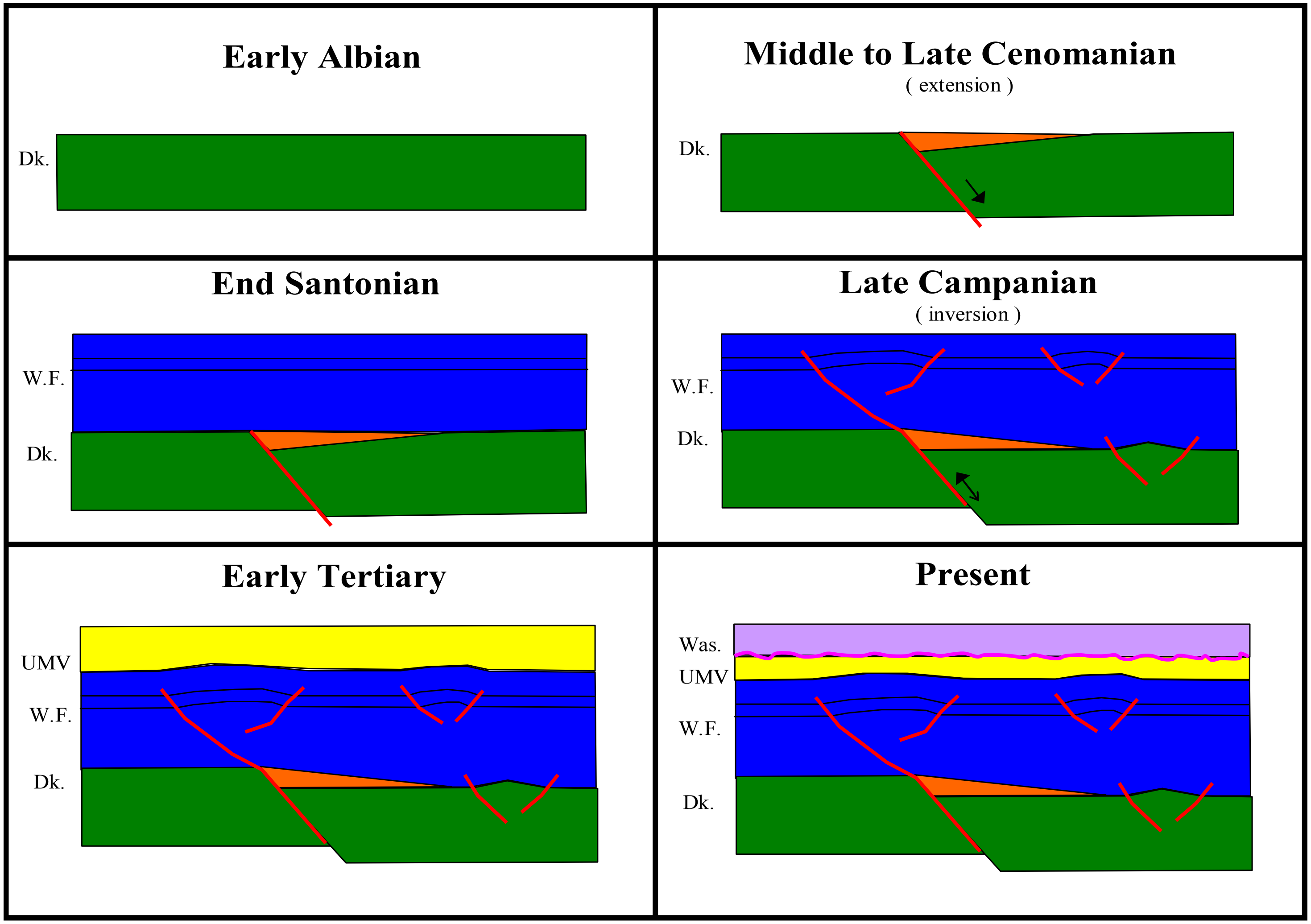

Figure 7.4 –Step evolution through time of line 90 from the Seitel (2003) survey. Dakota Sandstone (Dk.) Williams Fork (W.F.) UMV Shale (UMV) Wasatch (Was.). Pink line in last slide is an unconformity. Red lines are faults.

Reservoir Fault Blocks

The Seitel (2003) survey covers a very large area. It covers the western edge of the Rulison field as well as the eastern edge of the Parachute field. Using the above described interpretation of Chapter 3, and the fault model described in Chapter 7.1 it is apparent that the two fields are composed of these large pop-up blocks. The larger pop-up blocks are composed of smaller blocks. The combination of structural strain from the numerous faults within the large blocks is the likely cause of the increased permeability zones within the reservoir.

RCP Fault Block

At the Cameo Coal and Rollins Sandstone level are a series of reverse faults that lie within the RCP study area. These faults create a small pop-up structure within the study area. Figure 7.5 shows these faults in map view as well as side view. These faults are example of the idea that smaller blocks have formed outside the larger fault block structures. This block separates the RCP study area from the rest of the survey. The faults bounding the RCP block may make the RCP area have different reservoir characteristics. These faults might separate the block from the surrounding reservoir when we look at reservoir pressures, fracture densities, etc.

This reservoir block is also confined to the brittle Williams Fork and Iles formations. It also lies outside of the larger fault block structure in the Rulison Field area. It is an example of tectonic structures created by Laramide tectonics that are not related to deeper pre-existing features.

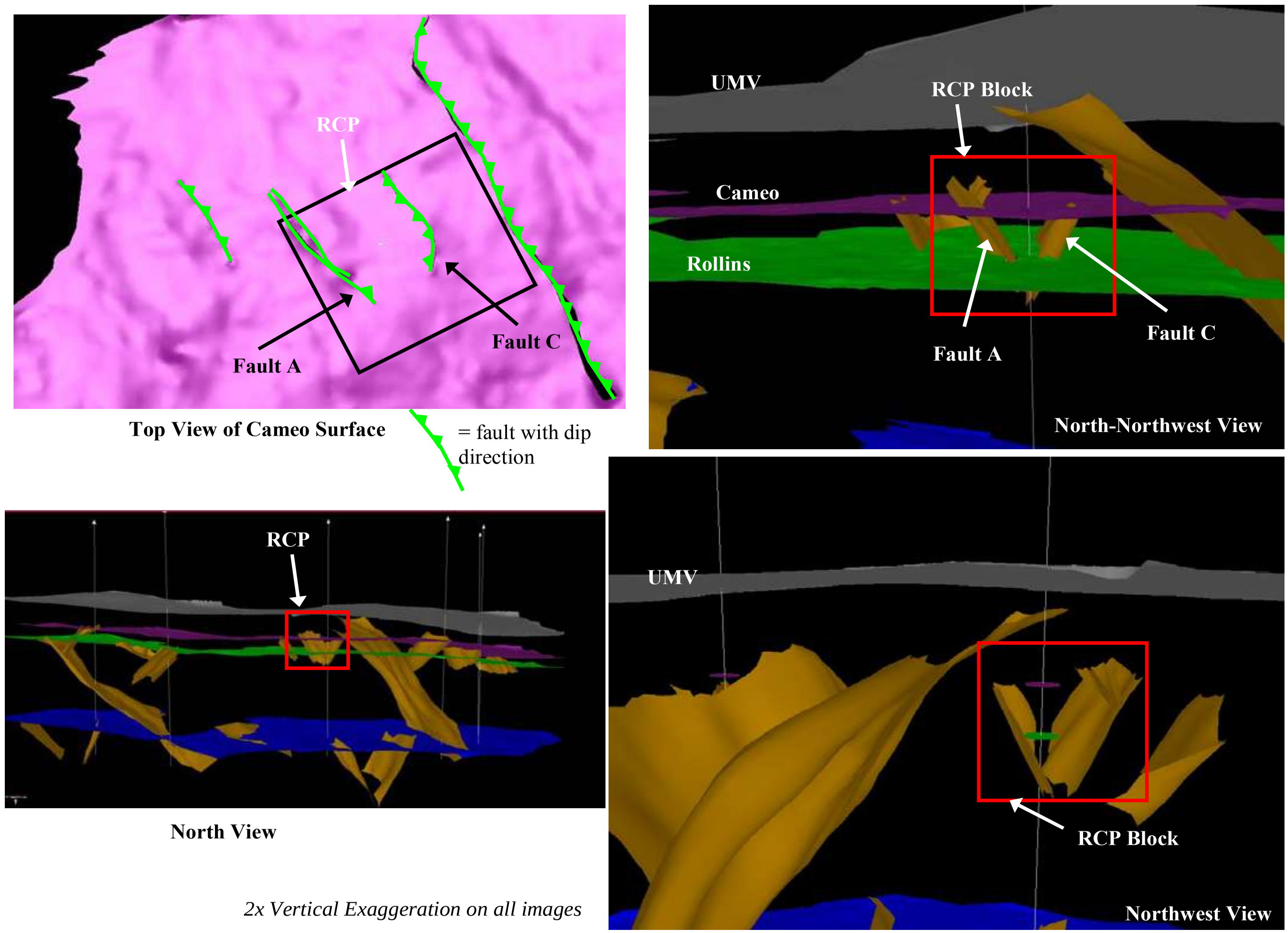

Figure 7.5 – Upper left is a top view of the Cameo Coal horizon. Bottom left is a north view of the model. Bottom right and upper right are close ups of the RCP block.

7.2 Fault Zone Characteristics

From the calculations completed in Chapters 4 and 5 a number of the fault zone characteristics are known. These include estimates of how much clay has been caught up in the fault zones, as well as the tendency of specific fault and fracture orientations to be dilated. With this information we can now predict how the characteristics of the faults and fractures are affecting the gas migration in the reservoir.

Shale Gouge in the Fault Zone

The Shale Gouge Ratio (SGR) is a quantitative way of assessing the composition of the fault zone. Yielding (2000) discusses analyses completed by Foxford et al. (1998) and how SGR calculations relate to those at the outcrop level, as well as the validity of those calculations. The SGR algorithm assumes a complete mixing of the wall-rock components in any throw interval (Yielding, 2000). Yielding (2000) also states that if the wall rock is incorporated into the fault zone in the same proportions as it is present in the wall rock, then the SGR is an estimate of the fault zone composition. With this in mind, I used the SGR calculations to predict the composition of fault zones. However, this method has a caveat that must be kept in mind. It is only valid if the proportion of shale and sand is greater then 15 to 20 percent (Yielding, 2000), as this allows for the formation of continuous smears along the fault zone. In Rulison, I made the assumption that the reservoir interval had proportions greater then 15 to 20 percent shale and sand because of the meandering fluvial system that comprises the reservoir interval. Without this assumption the SGR values can not be used with great confidence.

From the SGR calculations along the faults we can make a conclusion based on the input lithology of the reservoir. The data show that many of regional faults appear to have an overall sealing capacity based on the high SGR values along the faults, (Figure 7.6). This supports the interpretation that the faults, bounding and within the fault blocks discussed in Chapter 7.1, are sealing faults. However, a few of the faults show the potential to leak in certain places. This outcome suggests that the faults in Rulison may leak at some locations within the reservoir interval, and may not be 100% sealing, (Figure 7.7). At these locations the reservoir is interpreted to be leaking hydrocarbons into the fault zone. With the general sealing capacity of the fault zones in mind, we can make a case for the compartmentalization of the reservoir based on calculated SGR values.

The SGR could also be used as a way of constraining fault zone permeability. If pressure and production data are incorporated into the model we could derive fault transmissibility multipliers (Yielding, 2000). However, in the case of Rulison, production data were not readily available and therefore the fault permeability was not determined.

The SGR present along the faults that bound the RCP block show similar characteristics to the other regional faults. The SGR values of the faults in the RCP block can be seen in Figures 4.12 and Figure 7.7. Figure 7.7 shows the potential leak points of faults in and near the RCP fault block.

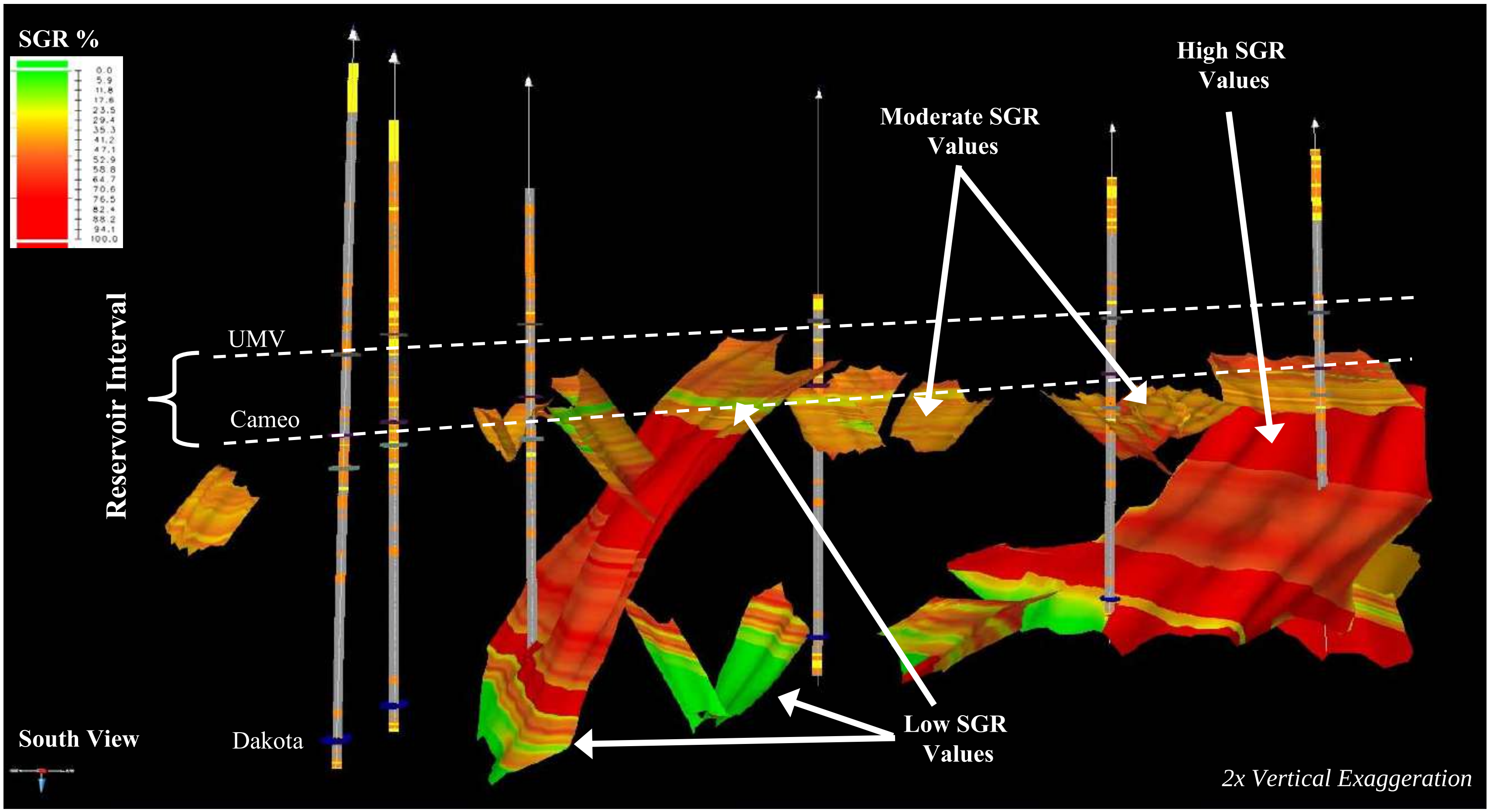

Figure 7.6 – The Shale Gouge Ratios mapped out on the regional faults. The dark red and orange values indicate a high sealing potential. The green is areas of low sealing potential. The reservoir interval has a high capacity to be sealing with a few areas of potential non sealing or leakage.

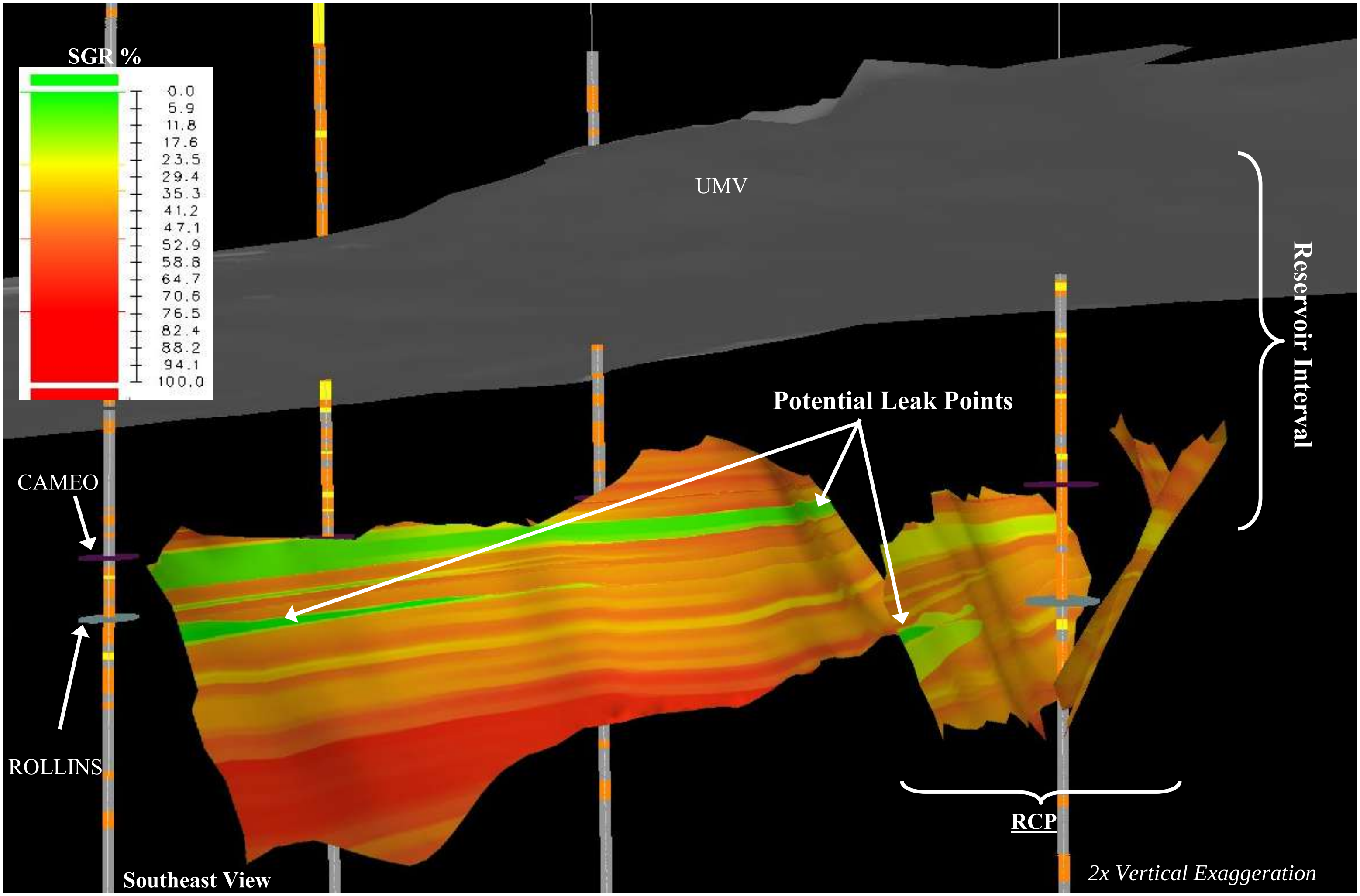

Figure 7.7 – The Shale Gouge Ratios mapped out in the RCP study area. The green areas within the reservoir interval are places where hydrocarbons may to leak into the fault zone.

Dilation of Fault Zones

The dilation tendency of the faults is a qualitative analysis based on the in-situ stress present in the reservoir. The results of this analysis show which orientation of faults, as well as fractures are more likely to be dilated. If a fault or fracture is dilated it will allow fluids to flow more easily, therefore increasing permeability. This result is purely independent of the orientations of the faults and fractures; it is a function of the stress field. The stress field, as defined by Higgins (2006), shows that faults and fractures with an orientation of N10˚E (azm. 010 degrees) have a higher tendency to be dilated than faults and fractures with other orientations, (Figure 7.8). From the seismic mapping, of the Seitel (2003) survey discussed in Chapter 3, the majority of the faults have strikes of N35˚W (azm. 325 degrees). Figure 7.9 is a rose diagram of the faults mapped at each horizon overlain on the dilation tendency hemisphere of Figure 7.8. This figure suggests that segments exist along the faults that have orientations that correspond to high dilation tendencies. This dilation would allow hydrocarbons to flow along the fault zones. Unfortunately, in the Rulison study area there has not been any work correlating to the exact percentage of dilation that leads to gas flow along the faults.

Figures 5.6 and 5.7 from Chapter 5 have the dilation tendency mapped out on the faults themselves. From these figures we are able to see regions of the fault zones that might allow more fluid flow. Figure 5.6 is a view south of all of the regional faults. Figure 5.7 is the faults that are in the RCP study area. From these calculations we can assume that if gas is able to flow into the fault zone at a specific point, then that gas should be able to flow along the fault zone away from where it entered the fault zone.

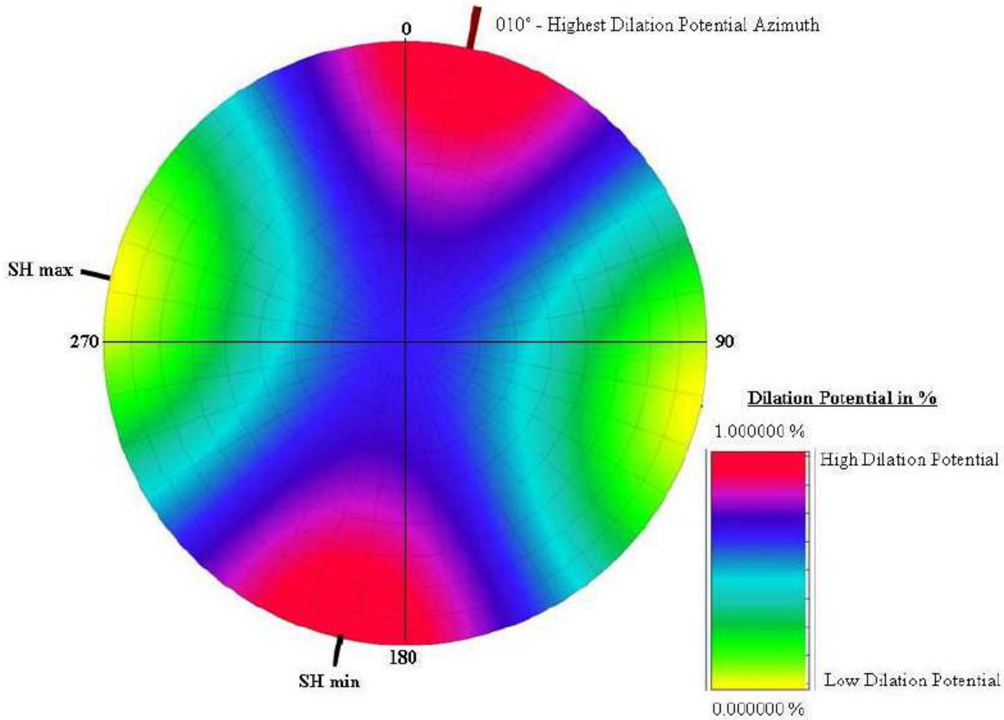

Figure 7.8 – Dilation tendency mapped out on the lower hemisphere of a stereonet.

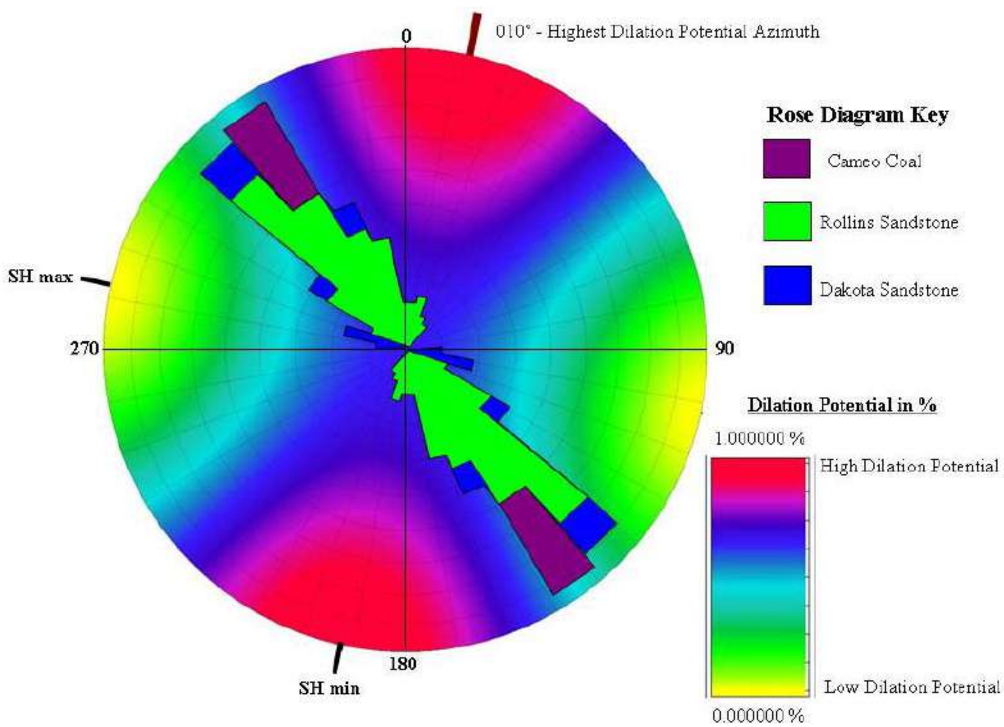

Figure 7.9 – Rose diagram of fault strikes at each horizon mapped out on the dilation tendency stereonet hemisphere. The fault orientations suggest that they are dilated.

7.3 Compartmentalization and Fluid Migration

Compartmentalization within a reservoir often controls the effectiveness of draining the reservoir. The tight gas sands of the Piceance Basin are considered to be continuous throughout the Williams Fork Formation (Cumella and Ostby, 2003). Knowing where depletion and other pressure barriers are located is essential information for understanding field compartmentalization. From the modeled SGR results it is apparent that the regional faults have created some compartmentalization of the reservoir interval, because of the high SGR values along the faults, (Figure 7.6). While some of the faults may leak slightly, most appear to be sealing along their strike, given a sufficient amount of throw.

This idea of compartmentalization needs to be interpreted care however. The volume shale logs used to calculate the SGR were smoothed, and this smoothing took away a portion of the log detail that might be crucial in calculating the SGR values of low throw faults that offset small sand bodies.

More evidence for compartmentalization of the reservoir interval comes from micro seismic tests. Riley (2007) analyzed several hydraulic fracture jobs completed in the RCP study area. These fracture jobs used a micro seismic test to determine how the fracture jobs were propagating in the reservoir. Riley (2007) found that at several intervals in well RWF 541-20 (hydraulically fractured in the Mesaverde Formation)the hydraulic fractures did not propagate as far in one direction as they did in the other. He hypothesized that the fracture job was encountering a barrier that was not allowing the fracture to propagate. The high SGR values of the faults zones could be creating one of these barriers that the fracture job encountered. Using the fault pop-up block model discussed in Chapter 7.1 Riley (2007) plotted out potential fracture barriers for well RWF 541-20, (Figure 7.10).

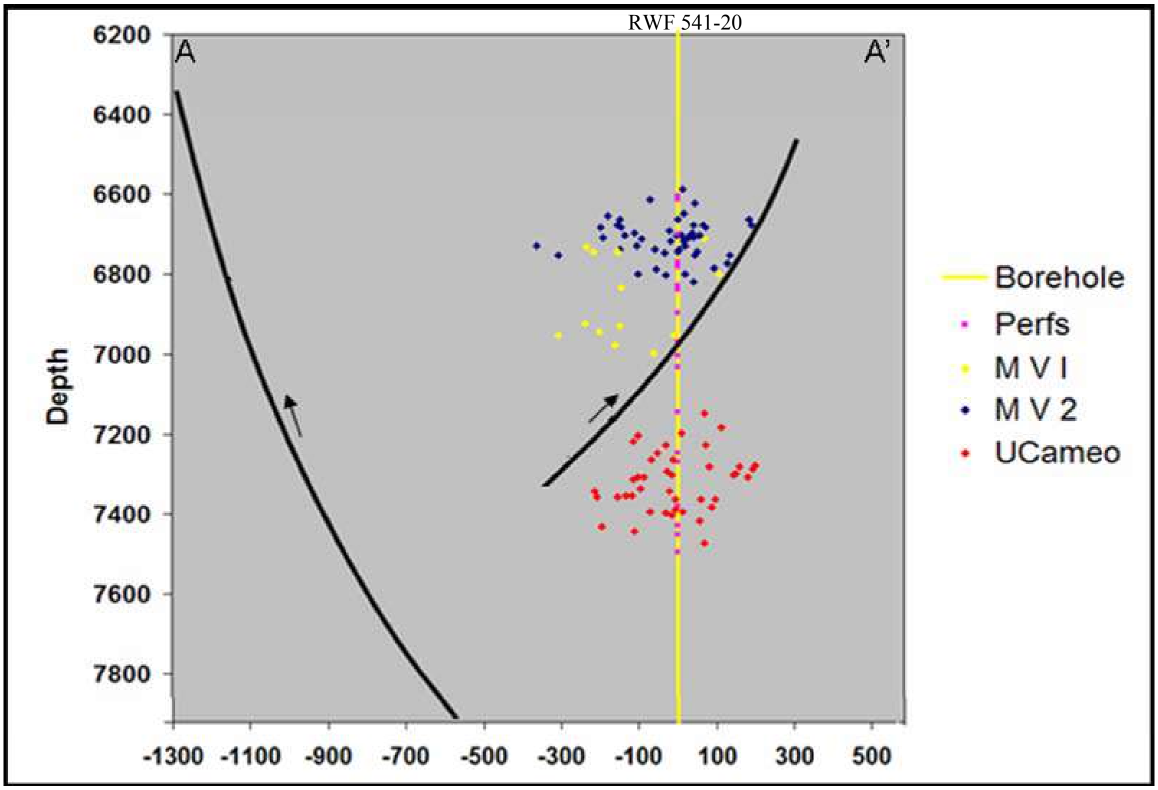

Figure 7.10 – Micro seismic results of a hydraulic fracture job completed in well RWF-541-20. Riley (2007) hypothesized that a fault was acting as a barrier to the fractures in the Mesaverde (MV 1 and MV 2), modified from Riley (2007).

Fluid Migration

Several authors (Cumella and Ostby, 2003 and Cumella, 2006) have broken the reservoir interval in the Piceance Basin up in to two main zones, a continuous gas zone and a transition zone above that, (Figure 7.11). The continuous gas zone has very little producing water, while the transition zone produces significantly more water (Cumella 2006). The reason for the two zones is that gas generated deep in the basin during maximum burial created enough pressure to fracture the rock allowing the gas to migrate up these natural fractures (Cumella, 2006). Cumella (2006) also suspects that the faults are acting as migration pathways for the gasses in the continuous gas zone to migrate in to sand bodies in the transition zone.

The fault dilation tendency calculations I performed support the fluid migration theory, Figures 5.6 and Figure 5.7. The current in-situ stress regime suggests that the faults and fractures within the reservoir are dilated, (Figure 7.9). The current stress regime matches that of the stress regime present during Laramide tectonics, (Higgins, 2006) therefore the faults and fractures during Laramide tectonism were also dilated.

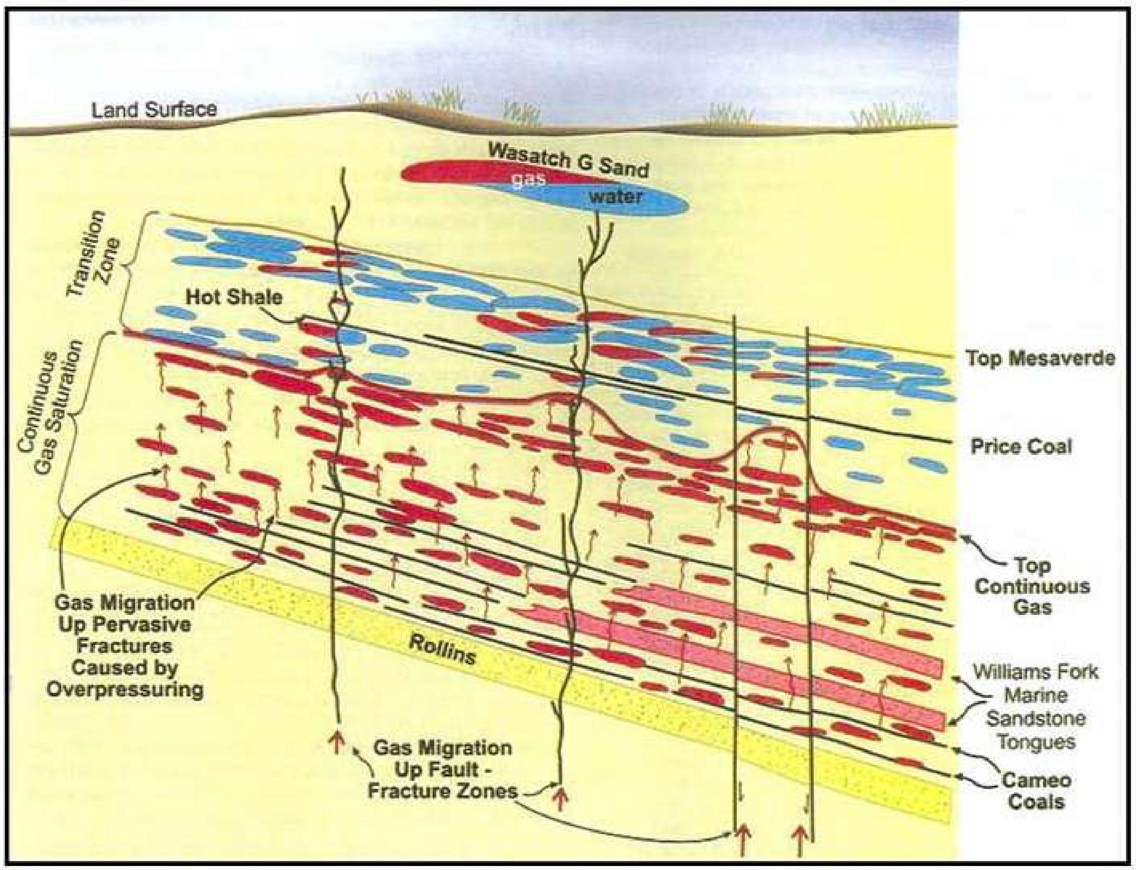

Figure 7.11 – The gas migration model of Cumella (2006). This model shows gas migrating from deeper in the basin along faults and fractures.

7.4 3-D Fracture Model

The elastic dislocation modeling predicted locations of where a higher density of fractures might exist. The modeling also produced the orientation and failure type of some of the predicted fractures caused by the regional faults.

Fracture Density Maps

The MCSS is a way of measuring the potential shear failure that a rock body has undergone. Shear failure can be directly related to the density of fractures as discussed in Chapter 6.2.2. Figures 6.4 to 6.8 show the results of the MCSS calculations I completed on the four mapped horizons and an arbitrary plane. One notable result of the modeling is that a few of the faults do not have consistent MCSS values along their strike. This is counter- intuitive when we would usually expect the most fractures nearer to faults. An example of this can be seen in Figure 7.12. Figure 7.12 is a close up of the Cameo deformation surface over the RCP study area. In this figure the black arrow locates a portion near Fault C with low MCSS values, due to the fault having less throw in this area. These low throw areas are regions that are not fractured enough according to the model and should be avoided if we are looking for regions of densely packed fractures.

The MCSS maps also show areas of the survey that have been deformed by faults that do not cut the horizon seismically. This is especially visible at the UMV horizon, (Figure 6.8). None of the mapped faults can be seen intersecting the UMV Shale. However, the model predicts that the horizon should be deformed to a degree. This deformation at the UMV is related to several of the faults at the Cameo level propagating upwards towards the UMV level. With this in mind we can expect each of the faults to act in a similar fashion in all directions creating deformation halos around them. Figure 7.13 and Figure 6.7 represent the vertical plane cut through the survey showing deformation extending away from the faults. Figure 7.14 is a close up of the RCP study area representing both the Cameo deformation plane as well as the vertical deformation plane with the MCSS values mapped out on them.

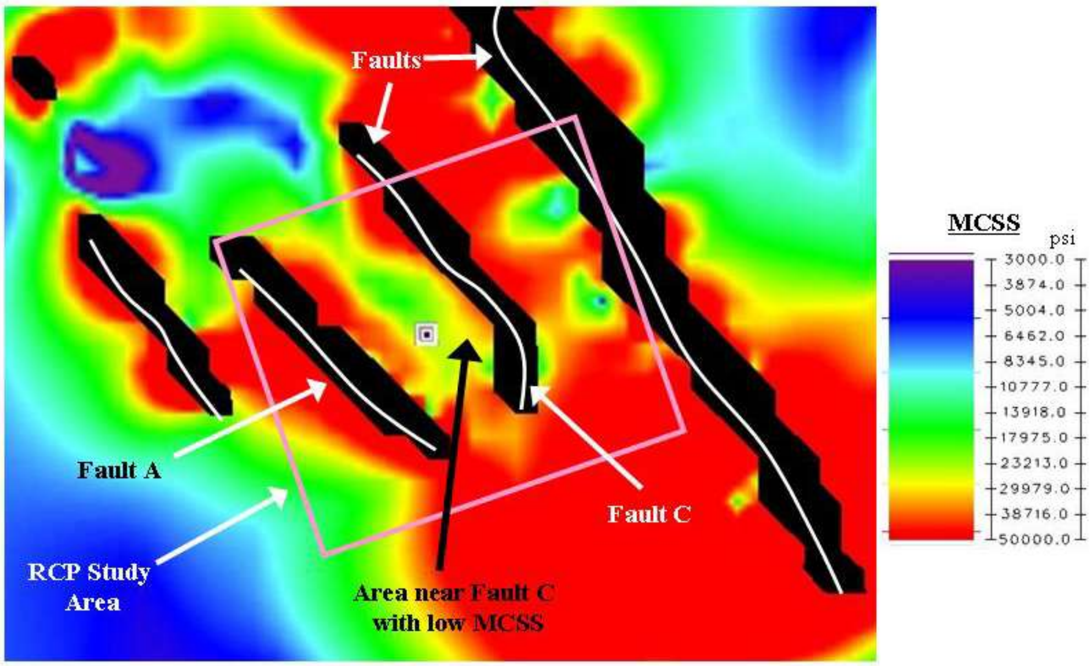

Figure 7.12 – The Maximum Coulomb Shear Stress (MCSS) at the Cameo deformation surface near the RCP study area. Areas near Fault C have low MCSS values. These low MCSS areas relate to portions of the Fault C that have small throws.

The mapped MCSS values the model predicts need to be used with caution. The values of MCSS are estimates based on the shear failure Higgins (2006) determined in her modeling. While the greater the MCSS, the more fractures we can expect there is no quantification as to what value of MCSS directly relates to a specific number of fractures. These results only indicate the areas in which we should expect more fractures.

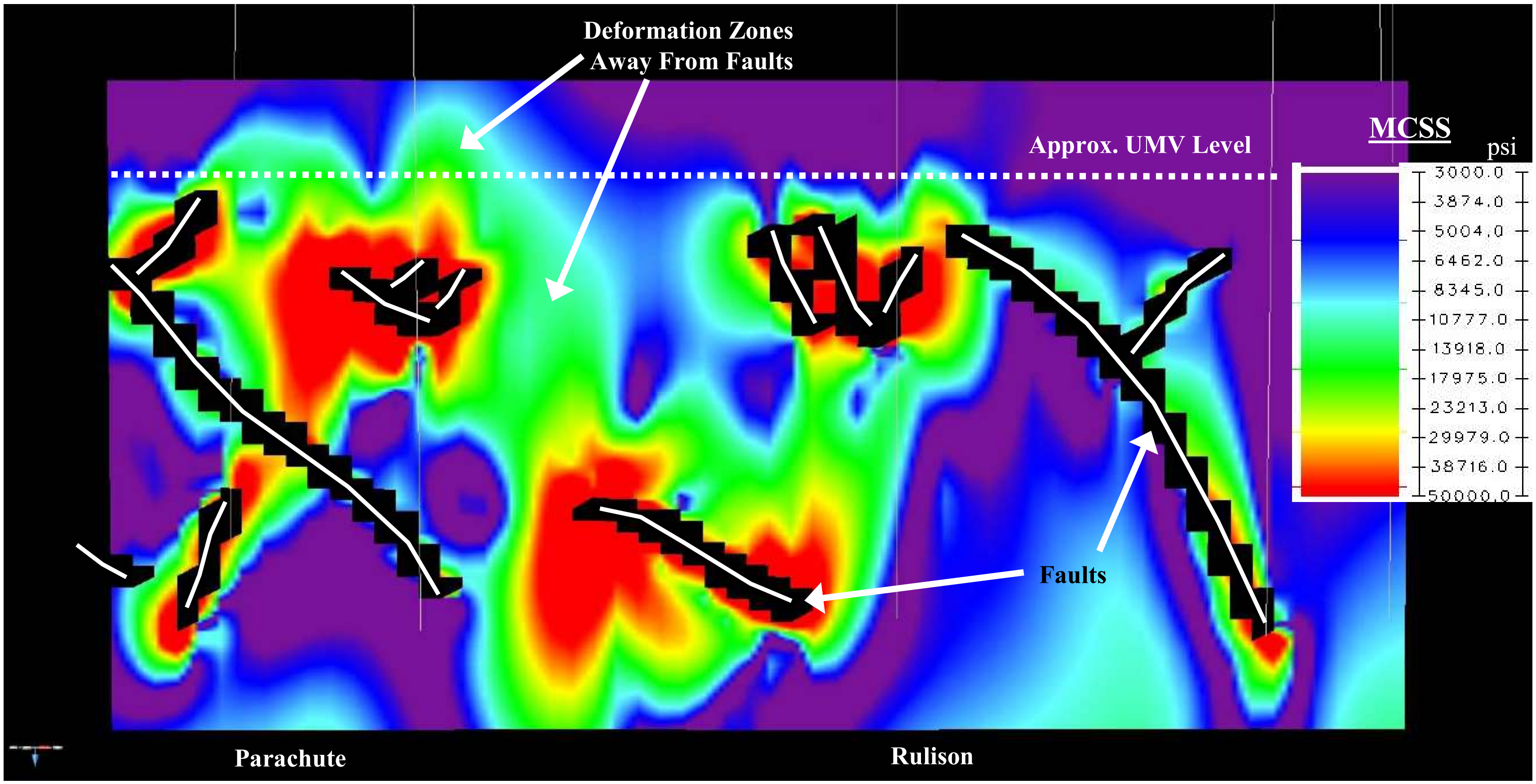

Figure 7.13 – Maximum Coulomb Shear Stress (MCSS) mapped out on the vertical plane cut through the survey. Deformation from the faults extends out from the various faults. The deformation event extends up to the UMV level where no faults are mapped seismically.

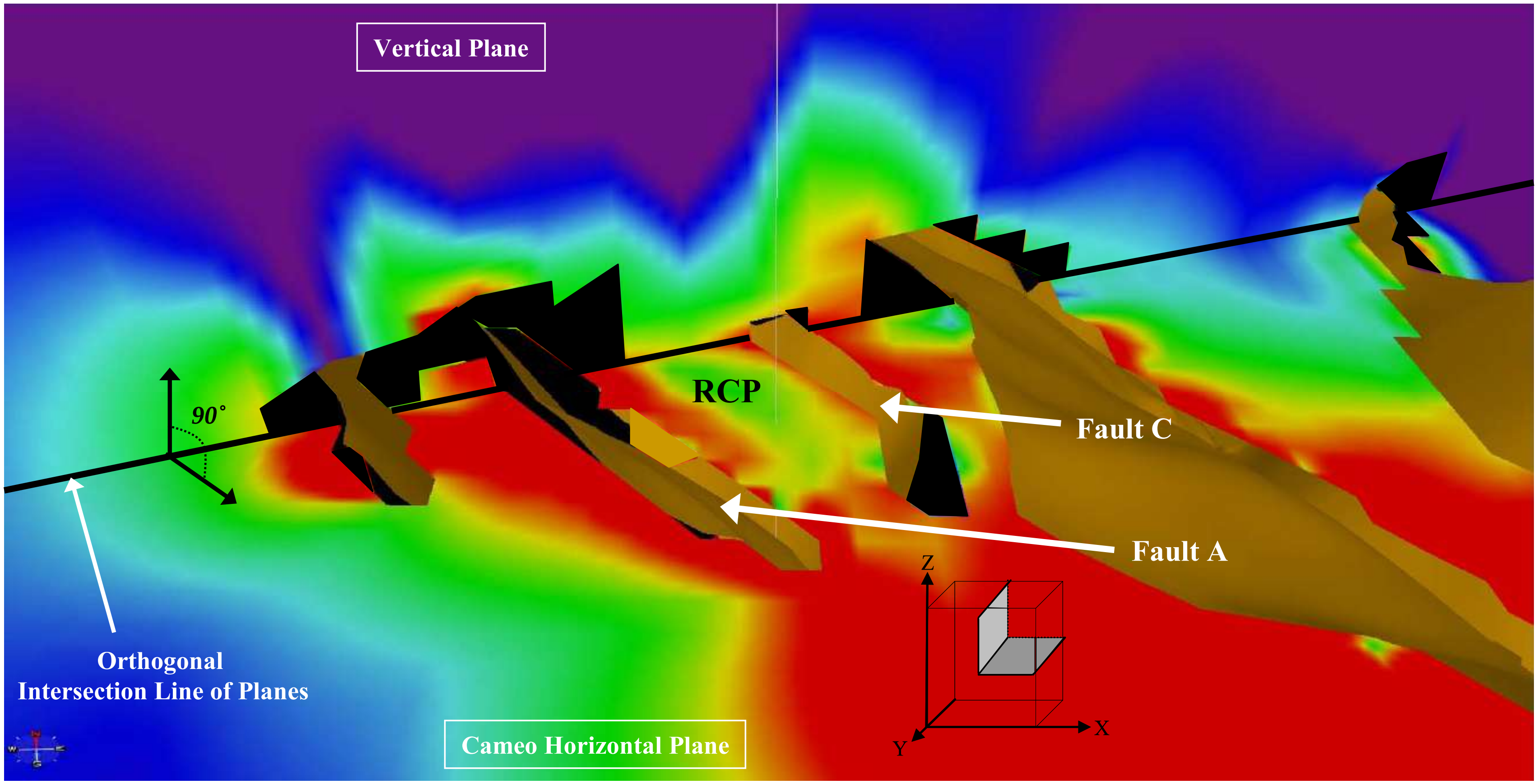

Figure 7.14 – A view of the RCP study area with the MCSS mapped out on two deformation planes; the vertical plane and the Cameo horizontal plane. This image also shows the 3D halo affect of the deformation around the faults.

Fracture Orientation

For the discussion of the fracture orientations predicted by the elastic dislocation modeling I will focus on the RCP study area. The orientations of the fractures and the fracture types can be seen at a larger scale in Figures 6.11, 6.12, 6.13, 6.14, and 6.15. Please keep in mind that this elastic dislocation model assumes that a uniform sand is covering the entire survey at that depth. This model only predicts how a sand body might deform if located at that position.

In the RCP study area, the predicted fractures of the reservoir interval vary in fracture type as well as fracture strike. Figure 7.15 is a close up of the Cameo deformation surface with the failure plane types mapped out on it. From this figure, the various strikes of the different failure planes can be seen. The dominate strike of the failure planes is roughly to the N50W (azm. 310). This is offset by about 30 degrees from the natural fracture set strike of N80W (azm. 280). The strike also varies based on closeness to faults that intersect the plane, as well as when multiple faults intersect the plane. The more faults that intersect the plane the more fault panels affect that node and cause the resulting failure type to be the product of a complex faulting system. This problem might be resolved by decreasing the node spacing to a distance less then 500 ft (152.4 m). Figure 7.16 is the vertical plane through the survey. This plane shows similar results to that of the Cameo plane.

One reason for the failure plane strikes to be offset by 30 degrees is possibly related to the lack of regional strain being included in the modeling. Incorporating regional strain might cause the predicted failure planes to be in a more east-west direction. Some possible regional strain sources would include the weight of the Grand

Hogback and the White River Uplift and differential loading and unloading of the basin sediments through time. Currently the failure planes orientations are controlled by the fault strikes only. This is why the failure planes are in a more northwest orientation. All of the failure planes generated in the modeling on each of the deformation surfaces in other areas of the Seitel (2003) survey have similar results to those described above.

The modeled fractures have strikes that are good representations of the actual fractures in the reservoir. The exact failure type predicted by the model may be suspicious due to the complex nature of the intersecting fault tips.

7.5 Hydrocarbon Significance of Study

Applying the previously described results to the production data of the RCP study area shows some interesting correlations. I hesitate to make any definitive statements about correlations to production because of the numerous variables that go into the production of gas in a well. However, these results may help obtain a better idea of the reservoir's production characteristics.

Decline Curves, MCSS, and EUR

The signature of a production decline curve can aid in determining the source of production in a well. When a well draws gas out of the surrounding reservoir, it first pulls the gas out of fractures, and then it pulls the gas from the matrix of the reservoir sands. A decline curve for a well can be used to determine when fracture depletion stops and when matrix depletion begins. The decline curve with fracture production will have two distinct slopes (J. L. Miskimins, 2007, Personal Communication).

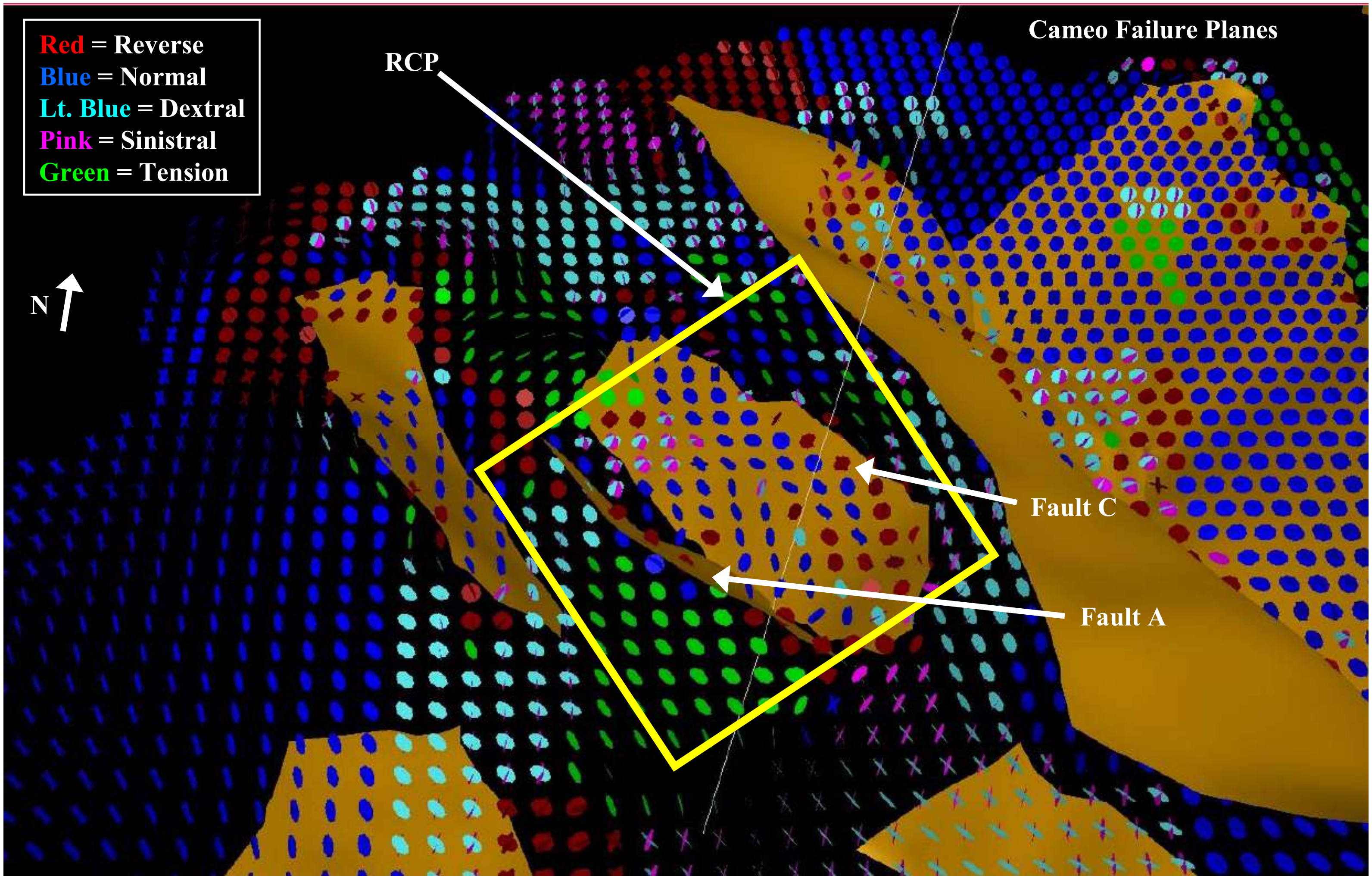

Figure 7.15 – Failure types mapped out on the Cameo deformation plane. The failure planes have strikes similar to that of the faults.

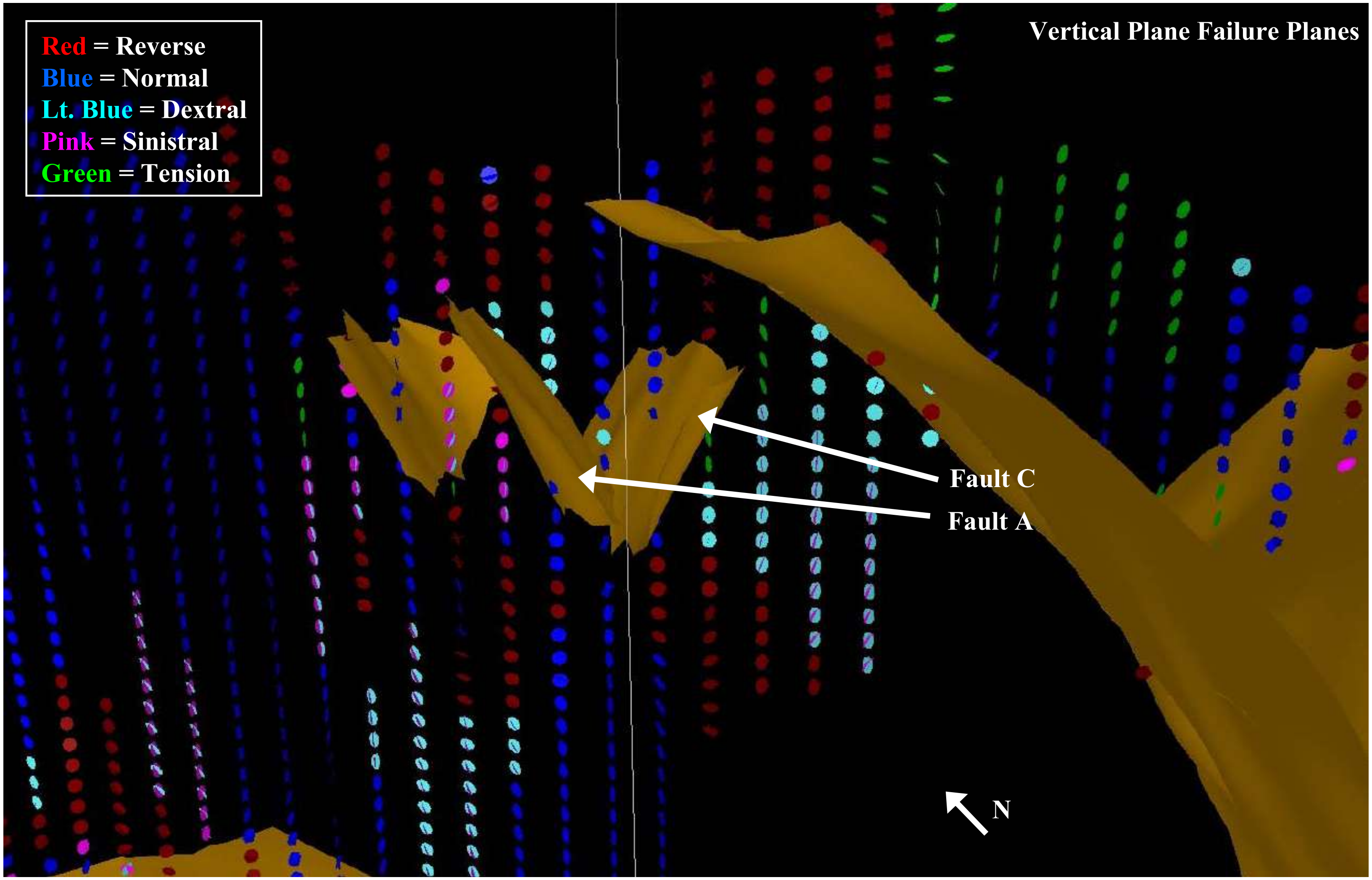

Figure 7.16 – Failure types mapped out on the vertical deformation plane near the RCP study area. The failure planes have strikes similar to that of the faults.

Production from fractures is relatively fast and drops off quickly in a well. Production from the reservoir matrix is slow and lasts a lot longer. If a decline curve has two distinct slopes we can assume that natural fractures are aiding in production of the well. Using decline curves of four wells in the RCP study area, I can show that areas that have been mapped with high MCSS values correlate to wells that have fracture production.

I picked four wells drilled between January 2000 and December 2006, normalized them, and examined the decline curves. Figure 7.17 shows the four normalized decline curves. Two decline curves, (RMV 60-17 and RMV 136-21) show fracture production while the other two do not. Figure 7.18 is a location map of the four wells. The map shows the predicted MCSS value at each well. The two wells that show fracture production sit in high MCSS areas (RMV 60-17 and RMV 136-21). Well RMV 92-29 sits in a low MCSS area and does not show fracture production. Well RMV 241-21 has a decline curve with a hyperbolic decline. This well also sits in a high MCSS area, but because of the wells hyperbolic decline it is difficult to determine if there are natural fractures affecting the production. This correlation suggests that the MCSS map could be used to predict where wells will have fracture production and where they will not.

The Estimated Ultimate Recovery (EUR) of each of the four wells also shows a similar correlation to the one described above. Figure 7.19 shows the decline curves with the MCSS as well as the EUR indicated for each of the four wells. The relationship between the EUR and the MCSS suggests that the higher fractured areas will have a higher EUR. However, RMV 241-21 is still an anomaly, with high MCSS and a a moderate EUR.

Figure 7.20 shows the results of the MCSS calculation mapped with the Estimated Ultimate Recovery (EUR) for all wells drilled in the RCP study area between January 2000 and January 2006. The relationships described above hold true for these data as well. However, in Figure 7.17 we can also see the affects of faults on EUR. The figure shows that near the faults, where the MCSS has not been modeled statistically there is a higher EUR, suggesting the faults might be conduits for gas or have locally highly fractured wall rocks.

There are a number of potential pitfalls that need to be considered before we can fully believe this relationship. The first has to do with the Cameo surface modeled and the number of intervals in the well that were completed. The second deals with the amount of reservoir quality sand available. Lastly, what does the MCSS surface really represent in the reservoir?

The Cameo surface modeled in this study represents one interval in the well. When an operator completes a well they complete the well at multiple intervals. Evidence for this can be seen in Figure 7.10 where four different intervals were hydraulically fractured in one well. Each well has different numbers of intervals as well as different depth intervals completed. The mapped EUR is for all of these intervals and does not necessarily represent the Cameo interval. It is very difficult, if not impossible to know which interval is producing the gas in the wells. Therefore, relating all of the production from the well to the MCSS mapped during modeling of the Cameo horizon cannot be done with a great degree of confidence.

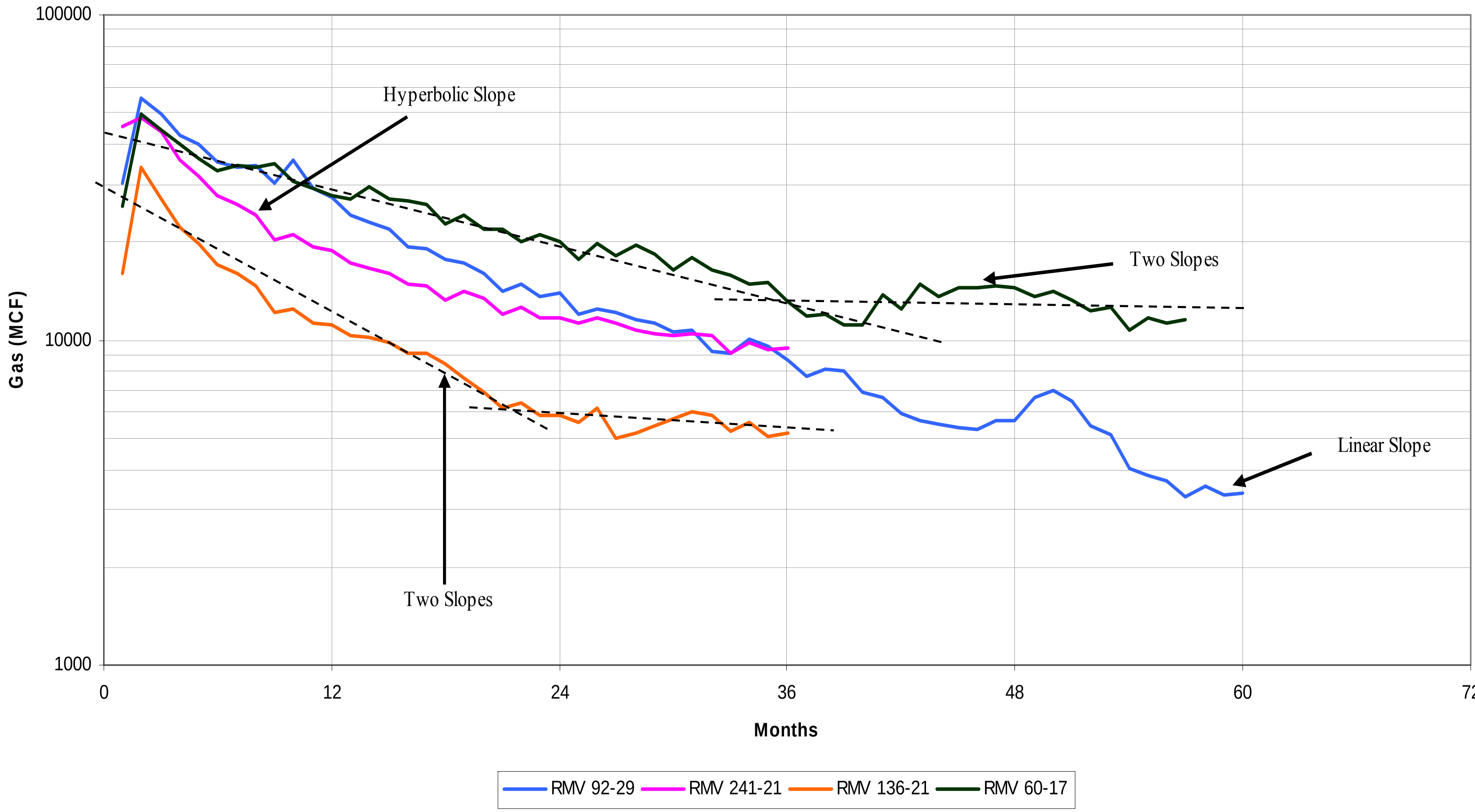

Figure 7.17 – Normalized decline curve slope analysis. Curves with two separate slopes are suggestive of natural fracture production. Curves with linear slopes have little to no natural fracture production.

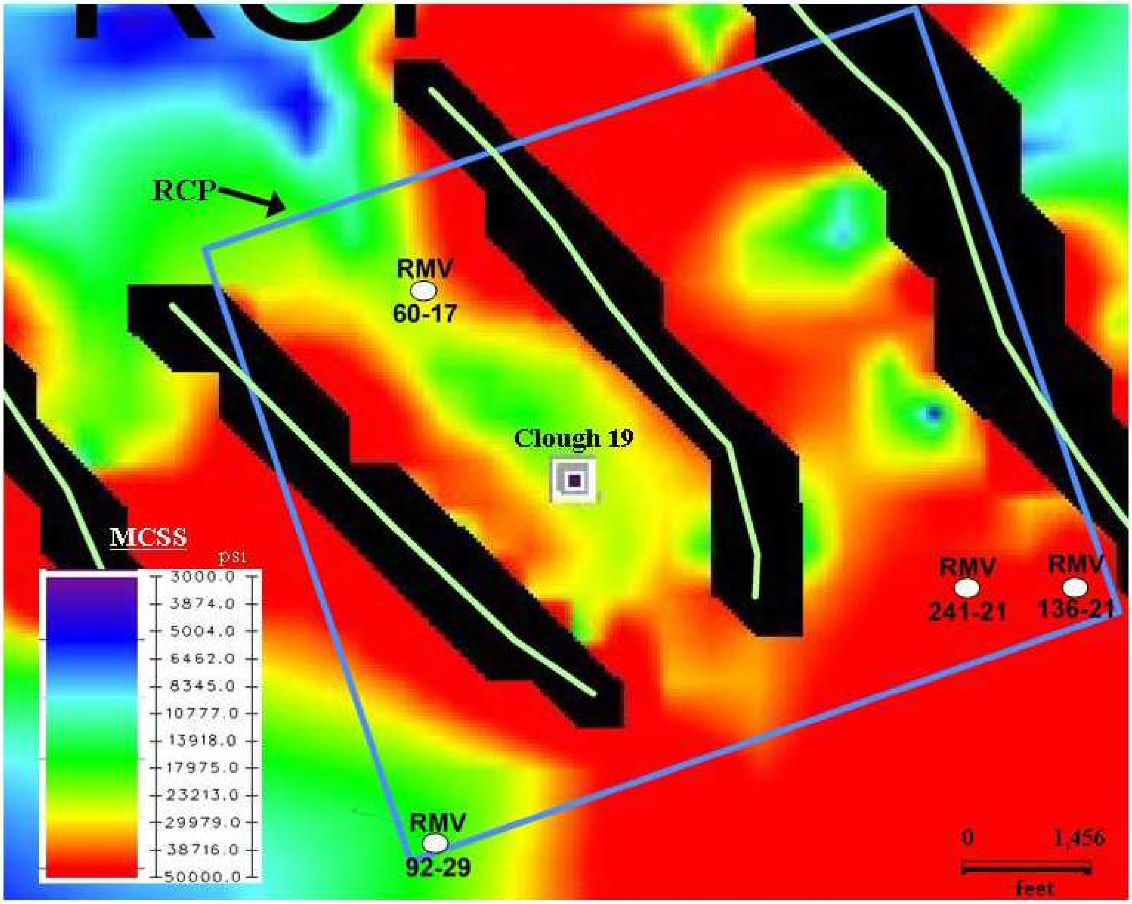

Figure 7.18 – The Maximum Coulomb Shear Stress (MCSS) at the Cameo deformation surface near the RCP study area mapped out with the four wells used in the decline curve analysis.

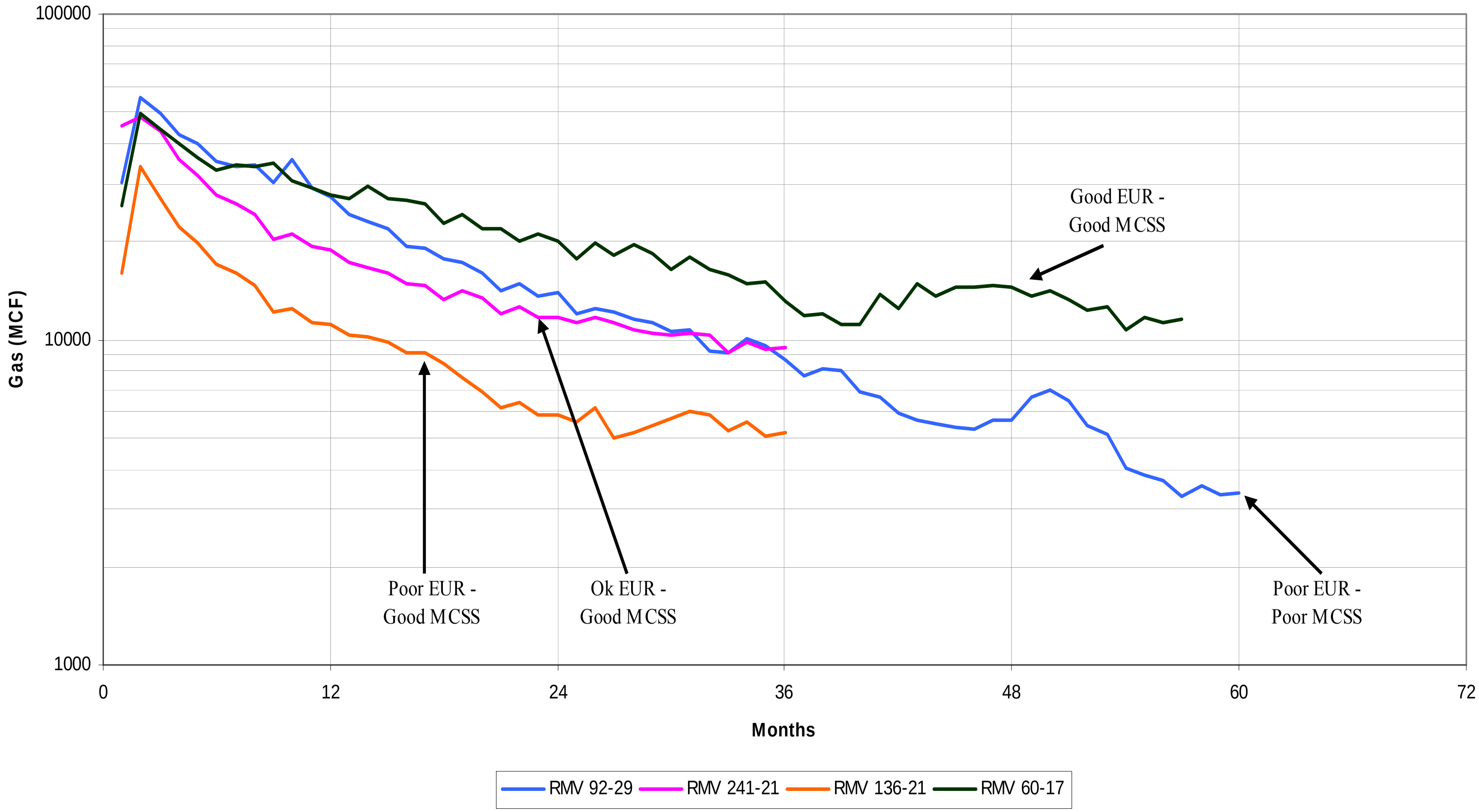

Figure 7.19 – The normalized decline curves with indicators of their respective EUR and MCSS values.

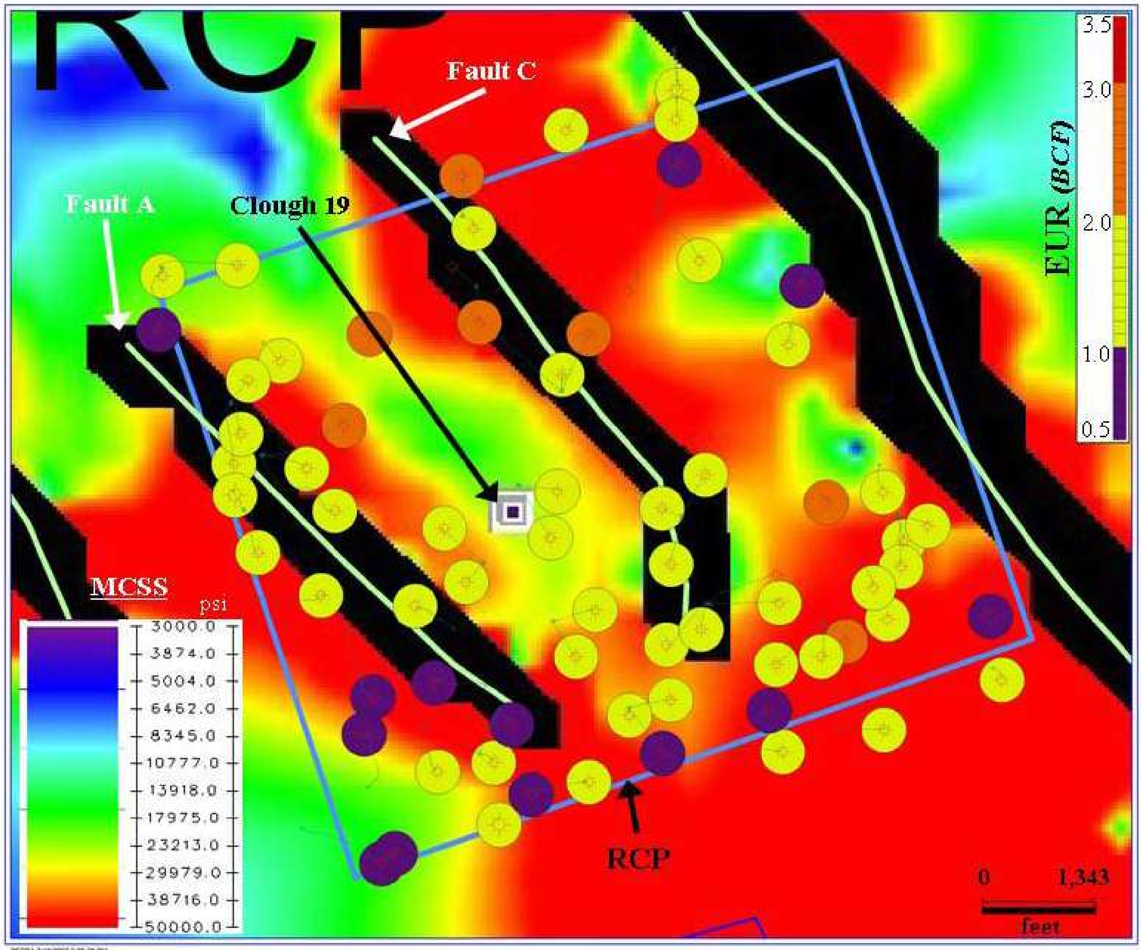

Figure 7.20 – The Maximum Coulomb Shear Stress (MCSS) at the Cameo deformation surface near the RCP study area and the Estimated Ultimate Recovery (EUR) of wells drilled after 1/1/2000. The EUR is the numerous colored circles. The faults are the thin green lines. High EUR seems to be related to high MCSS.

The amount of sand present in the reservoir and the quality of that sand is a pitfall that can be mitigated. While sands can be determined in a well log as in Figure 4.5 and Figure 4.6 (or 4.6a, see Appendix A) the lateral continuity of those sands in the reservoir should be suspected because of the fluvial nature of the system. The amount of reservoir sand present is also going to affect the EUR of the well and the number of completion intervals.

The calculated MCSS values on the modeled surfaces are those of reservoir sands with certain physical properties. The surface represents how sands present might be deformed. A better understanding of the stratigraphic relationship of the reservoir is needed before a definite correlation can be made between the deformation surface and the EUR values.

Other Model Benefits

There are two other benefits of the modeling. The first is possible useful information for drilling engineers. Drilling mud is often lost to the natural fracture system. The three-dimensionality of the fracture prediction results could be used to give engineers an idea of depths and areas where they may start to lose their drilling mud. The second benefit of the model relates to the future prospectivity. Exploration of the Dakota Sandstone is a future possibility. With the aid of the MCSS calculations any future drilling of the Dakota or other horizons could be high graded into lower risk areas with potential natural fracture systems aiding permeability using images similar to those of Figures 6.14 and 6.15.

CHAPTER 8

CONCLUSIONS AND RECOMMENDATIONS

8.1 Conclusions

I have shown that regional structural modeling is a tool that can be used to aid in reservoir characterization. From this research I have contributed twelve results related to the regional scale structures as well as reservoir scale structures.

(1) There were two structural styles active during the structural evolution of the Rulison Field area. The initial extensional phase was followed by reactivation of deeper structures during a later compressional phase.

(2) Laramide related compressional structural features probably occurred during the Late Campanian stage.

(3) The reservoir interval is dominated by reverse fault bounded pop-up blocks.

(4) The RCP study area has one of these distinct pop-up blocks in the reservoir interval.

(5) Shale Gouge Ratios (SGR) calculated on the regional faults suggest a tendency for the fault zones to be dominated by sealing. However, there are locations along the faults at the reservoir depth that may by be leaking gas into the fault zones.

(6) The current in-situ stress regime has dilated the regional faults and fractures, which have strikes of N35˚W (azm. 325 degrees).

(7) The high Shale Gouge Ratios within the reservoir interval supports the idea that the reservoir interval is compartmentalized.

(8) The faults and fractures, dilated by the current in-situ stress field, in the Rulison area are migration pathways to shallower reservoir intervals as long as the gas is able to leak into the fault zone.

(9) Maximum Coulomb Shear Stress (MCSS) maps show that not all of the regional faults have high density of fractures near the fault plane. The density is a function of the amount of throw on the fault.

(10) The regional faults have created deformation halos for long distances away from the fault surfaces.

(11) Modeled fracture orientations vary greatly the more complex the faulting. However, they have an average strike that is similar to that of the natural fracture in the reservoir.

(12) There is a qualitative correlation between the MCSS and the EURs, the higher the MCSS the higher the EUR.

8.2 Recommendations for Future Research

Using structural concepts to define key aspects of a reservoir is an essential step to taking theoretical ideas back to the rocks themselves. Simple structural concepts can also aid in characterizing the reservoir. I feel that the work presented here is an initial first step in the structural characterization of the reservoir in the Rulison Field area. Future work is needed to further understand the reservoir is described below.

Geologically, a stratigraphic correlation of the Williams Fork and Iles formations needs to be completed over the survey area. This correlation should relate back to core samples taken within the seismic survey itself. This correlation would allow better Shale

Gouge Ratios to be calculated. It will also allow the timing of faulting to be detailed to an exact degree.

I would also suggest that the interval below the Rollins Sandstone be drilled in the survey. This would test the feasibility of deeper reservoir sands at the Dakota level, and also test the potential of the Mancos to produce shale gas. These deeper tests would fill in the pseudo interval attached to the well logs used and more accurately model the stratigraphy of the Rulison Field area.

Seismically, several things are needed. The first is that a higher fold p-wave survey or a multi component survey should be shot over the original Seitel (2003) survey. This would allow a greater detail of mapping of the reservoir as well as the application of concepts put forth by other RCP students. I also feel that while I have created a first pass depth conversion of the Seitel (2003) survey using well logs in the RCP study area, a velocity model needs to be created that covers the Seitel (2003) survey. The Seitel (2003) survey also needs to have curvature calculations to be completed over its entirety. Curvature could be used to look for possible sub seismic features but could be compared to the MCSS calculations to try and find a relationship between them.

On a geomechanical standpoint of the future work to be done, I feel that a relationship between the amount of stress that a rock has undergone and the number of fractures generated by that stress should also be determined.

This is by far not the only research that needs to be completed in the Rulison area. I have just scratched the surface of possible work. However, these few items would aid in understanding the structural complexity of the reservoir in Rulison.

REFERENCES

Badley, 2006, TrapTester Reference Manual: version 5.351, Badley Geoscience Limited, North Beck House, Lincolnshire, UK.

Blakey, R.C., 2003, Paleogeography Through Geologic Time: GIF image from http:j//an.ucc.nau.edu/~rcb7/global_history.html.

COGCC, 2006, Information Database: Colorado Oil and Gas Conservation Commission, http://oil-gas.state.co.us/, (accessed November 2006).

Cole, R. D., R. G. Young, and G. C. Willis, 1997, The Prairie Canyon Member, a new unit of the Upper Cretaceous Mancos Shale, west-central Colorado and east-central Utah: Utah Geological Survey, Miscellaneous Publication 97-4, 23 p.

Cumella, S. P., 2006, Overview of a Giant Basin-Centered Gas Accumulation, Mesaverde Group, Piceance Basin, Colorado: The Mountain Geologist, Vol. 43, Mo.3 (July 2006), p 219-224.

Cumella, S. P. and D. B. Ostby, 2003, Geology of the basin-centered gas accumulation, Piceance Basin, Colorado: Piceance Basin Guidebook, Rocky Mountain Association of Geologists, p. 171-193.

Currie, B. S., 2002, Structural Configuration of the Early Cretaceous Cordilleran Foreland-Basin System and Sevier Thrust Belt, Utah and Colorado: The Journal of Geology, v.110, p. 697-718.

Foxford, K. A., J. J. Walsh, J. Watterson, I. R. Garden, S. C. Guscott, and S. D. Burley, 1998, Structure and content of the Moab Fault Zone, Utah, USA, and its implications for fault seal prediction: *in* G. Jones, Q. J. Fisher, and R. J. Knipe, eds, Faulting, Fault Sealing and Fluid Flow in Hydrocarbon Reservoirs: Geological Society of London, Special Publication no. 147, p. 87-103.

Gomes, L., J.F.W. Gale, S.E. Laubach, S. Cumella, 2003, Quantifying fracture intensity: an example from the Piceance Basin: Piceance Basin Guidebook, Rocky Mountain Association of Geologists, p. 96-113.

Grout, M. A., & E. R. Verbeek, 1992, Fracture history of the Divide Creek and Wolf Creek anticlines and its relation to Laramide basin-margin tectonism, South Piceance Basin, Northwestern Colorado: U.S. Geological Survey Bulletin 1787-Z, P. 32.

Gutierrez, G., 2007, Analysis of Faults and Fractures, and their Impact on a Tight Gas Sand Resource Play in the Uinta Basin: Masters Thesis, Colorado School of Mines, Golden, Colorado, 175 p.

Hemborg, H. T., 2000, Gas production characteristics of the Rulison, Grand Valley, Mamm Creek, and Parachute Fields, Garfield County, Colorado: Turning Marginally Economic Basin-Centered Tight-Gas Sands into Profitable Reservoirs in the Southern Piceance Basin, Resource Series 39, Colorado Geological Survey, Denver, 30 p.

Hettinger, R. D., and M. A. Kirschbaum, 2002, Stratigraphy of the Upper Cretaceous Mancos Shale (upper part) and Mesaverde Group in the southern part of the Uinta and Piceance basins, Utah and Colorado: Unites States Geological Survey, Geological Investigations Series I-2764.

Higgins, S. M., 2006, Geomechanical Modeling as a Reservoir Characterization tool at Rulison Field, Piceance Basin, Colorado: Masters Thesis, Colorado School of Mines, Golden, Colorado, 151 p.

Hoak, T. E., and A. L. Klawitter, 1997, Prediction of fractured reservoir production trends and compartmentalization in the Piceance Basin, Western Colorado, Fractured Reservoirs: Characterization and Modeling Guidebook, Rocky Mountain Association of Geologists, p. 67-102.

Jansen, K., 2005, Seismic Investigation of Wrench Faulting and Fracturing at Rulison Field, Colorado: Masters Thesis, Colorado School of Mines, Golden, Colorado, 121 p.

Johnson, R. C., T. M. Finn, and S. B. Roberts, 2004, Regional Structural Setting of the Maastrichtian Rocks in the Central Rocky Mountain Region, in J. W. Robinson and K. W. Shanley, eds.: AAPG Studies in Geology 52 and Rocky Mountain Association of Geologists 2004 Guidebook, p. 21-35.

Johnson, R. C., 1989, Geologic history and hydrocarbon potential of Late Cretaceous-Age, low-permeability reservoirs, Piceance Basin, Western Colorado: United States Geological Survey Bulletin 1787-E, 51 p.

Kellogg, H. E., 1997, Geology and petroleum of the Mancos B Formation, Douglas Creek Arch area, Colorado and Utah, *in* H. K. Veal, ed., Exploration frontiers of the central and southern Rockies: Rocky Mountain Association of Geologist Symposium, p. 167-179.

Kusuma, M, 2005, Analysis of time-lapse P-wave seismic data from Rulison Field, Colorado: Masters Thesis, Colorado School of Mines, Golden, Colorado, 210 p.

Kuuskraa, V.A., D. Decker, and H. Lynn, 1997, Optimizing technologies for detecting natural fractures in tight sands of the Rulison Field, Piceance Basin: Advanced Resources International, DOE File NG6-3, 29 p, Retrieved at: http://www.netl.doe.gov/publications/proceedings/97/97ng/ng97_pdf/NG6-3.PDF.

Lorenz, J. C., 1997, Heartburn in predicting natural fractures: The effects of differential fracture susceptibility in heterogeneous lithologies, Fractured Reservoirs: Characterization and Modeling Guidebook, Rocky Mountain Association of Geologists, p. 57-66.

Lorenz, J. C., and S. J. Finley, 1991, Regional fractures II: Fracturing of Mesaverde reservoirs in the Piceance Basin, Colorado: AAPG Bulletin, V. 75, No.11, p. 1738-1756.

Matesic, M., 2007, Structural and Stratigraphic Control on Mesaverde Reservoir Performance: Rulison Field, Garfield County, Colorado: Masters Thesis, Colorado School of Mines, Golden, Colorado, 169 p.

Okada, Y, 1992, Internal deformation due to shear and tensile faults in a half-space: Bulletin of the Seismological Society of America, v. 82 no. 2, p 1018-1040.

Picha, F., 1986, The influence of preexisting tectonic trends on geometries of the Sevier orogenic belt and its foreland in Utah: AAPG Memoir, v. 41, p. 309-320.

Pittman, J. K., C. W. Spencer, and R. M. Pollastro, 1989, Petrography, mineralogy, and reservoir characteristics of the Upper Cretaceous Mesaverde Group in the east-central Piceance Basin, Colorado: Unites States Geological Survey Bulletin 1787-G.

Riley, B., 2007, Combined Micro-Macro Seismic Monitoring of a Hydraulic Fracture Stimulation, Rulison Field, *in* K. Wikel, ed., Reservoir Characterization Project, Spring 2007 Sponsor Meeting, April 12th and 13th : Colorado School of Mines, Golden Colorado, p. 66-81.

Ryer, T. A., J .J. McClurg, and M. M. Muller, 1987, Dakota-Bear River paleoenvironments, depositional history and shoreline trends—implications for foreland basin paleotectonics, southwestern Green River basin and southern Wyoming overthrust belt, *in* W. R. Miller, ed., The thrust belt revisited, 38th Field Conference Guidebook: Casper Wyoming Geological Association, p. 179-206.

Tayler, R., A. R. Scott, W. R. Kaiser, H. S. Nance, R. G. McMurry, C. M. Tremain, and M. J. Mavor, 1996, Geologic and hydrologic controls critical to coalbed methane producibility and resource assessment: Williams Fork Formation, Piceance basin, Northwest Colorado: Gas Research Institute report GRI-95/0532, 397 p.

Yielding, G., 2000, Shale Gouge Ratio—calibration by geohistory: *in* A. G. Koestler and R. Hunsdale, eds., Hydrocarbon Seal Quantification: Norwegian Petroleum Society (NPF), Special Publication no. 11, p. 1-15.

APPENDIX A

(see attached CD)

APPENDIX B

(see attached CD)

APPENDIX C

C.1 Nomenclature of the Depth Conversion Equations

Depth Conversion Equations:

$$CumulativeVelocity = \sum_{n} \{(1/DT) * 1{,}000{,}000\} \qquad (4.1)$$

$$VelocityAverage = \frac{CumulativeVelocity}{n} \qquad (4.2)$$

$$Depth = 6.7431 \times Time - 0.7252 \qquad (4.3)$$

Where:

n = the number of sample points to that depth (unitless)
DT = the sonic log reading at that depth (microseconds / foot)
CumulativeVelocity (feet / second)
VelocityAverage = Vav (feet / second)
Depth (feet)
Time (milliseconds)

C.2 Nomenclature of the Volume Shale Equation

$$Vsh = \frac{GammaRayCount - SandValue}{ShaleValue - SandValue} \qquad (4.4)$$

Where: GammaRayCount = the gamma ray count at depth (api)
SandValue = the minimum gamma ray count in the well (api)
ShaleValue = the maximum gamma ray count in the well (api)
Vsh = volume of shale at that depth (%)

C.3 Nomenclature of the Shale Gouge Ratio Equation

$$SGR = \sum \frac{(Vsh, \Delta z)}{t \times 100\%} \tag{4.5}$$

Where: SGR = Shale Gouge Ratio
Vsh = Volume of Shale in Δz (%)
Δz = thickness of bed (ft)
t = amount of throw that the bed has undergone (ft)

C.4 Nomenclature of the Dilation Tendency Equation

$$DT = \frac{(\sigma 1 - \sigma n)}{(\sigma 1 - \sigma 3)} \tag{5.1}$$

Where: DT = the Dilation Tendency
$\sigma 1$ = the vertical stress or σ V (psi)
σn = the stress normal to the fault plane (psi)
$\sigma 3$ = the maximum horizontal stress or σH (psi)